AD/A-002 245

ROCKET CHAMBER TEMPERATURE MEASUREMENTS BY MICROWAVE TECHNIQUES

James L. Hou, et al

Utah University

Prepared for:

Department of Defense

1 July 1974

DISTRIBUTED BY:

NTIS

National Technical Information Service
U. S. DEPARTMENT OF COMMERCE

AD/A002 245

BIBLIOGRAPHIC DATA SHEET	1. Report No.	2.	3. Recipient's Accession No.

4. Title and Subtitle
"Rocket Chamber Temperature Measurements by Microwave Techniques"

5. Report Date
July 1, 1974

6.

7. Author(s)
James L. Hou and Richard W. Grow

8. Performing Organization Rept. No. UTEC MD 74-055

9. Performing Organization Name and Address
Microwave Device and Physical Electronics Laboratory
Department of Electrical Engineering
University of Utah
Salt Lake City, Utah 84112

10. Project/Task/Work Unit No.
Task 4

11. Contract/Grant No.
Partially completed on
F44620-68C-0022

12. Sponsoring Organization Name and Address
Partially supported by Department of Defense, Project Themis.
Primarily supported by University of Utah

13. Type of Report & Period Covered
Final -- October 1,1970 to March 31, 1974

14.

15. Supplementary Notes

16. Abstracts

Microwave attenuation techniques are used to find the combustion chamber temperature of a solid rocket motor, and the predicted value calculated by a theoretical specific impulse computer program and the value calculated with the microwave measurements agree within three percent. The propellants used in this investigation were seeded with five percent potassium perchlorate by weight to furnish enough electrons in the plasma to cause measurable attenuation. The propellants were also seeded with 5 to 10 percent aluminum to produce suspended metallic particles in the plasma.

The temperature profile inside the combustion chamber is determined for a distance of two inches away from the burning surface by scanning the focused microwave signal transverse to the combustion chamber and by utilizing the motion of the burning surface with respect to the antennas. The experimental and theoretical results for the temperature gradient have a maximum angular difference of 25 degrees for 5 percent aluminized propellant and 18.5 degree for 10 percent aluminized propellant.

The acoustic oscillation inside a cylindrical end burner is theoretically derived and experimentally observed. The oscillation frequencies observed range from 3.2 to 4.4 kHz, whereas the theoretical oscillation frequencies range from 2.98 to 5.13 kHz for various oscillation modes.

Acoustic gain and loss expressions are derived and applied to the rocket firings. The results show that for a stable system, the acoustic loss exceeds the acoustic gain for some value of A_b^r, the real component of burning surface admittance, and for an unstable system, the acoustic gain exceeds the loss for the same value of A_b^r.

17. Key Words and Document Analysis. 17a. Descriptors
Rocket chamber temperature measurements
Microwave plasma temperature measurements

17b. Identifiers Open-Ended Terms

17c. COSATI Field/Group

18. Availability Statement	19. Security Class (This Report)	21. No. of Pages
Distribution of this document is unlimited.	UNCLASSIFIED	157
	20. Security Class (This Page) UNCLASSIFIED	22. Price

FORM NTIS-35 (REV. 3-72) USCOMM-DC 14952-P72

UTEC MD 74-055

ROCKET CHAMBER TEMPERATURE MEASUREMENTS BY MICROWAVE TECHNIQUES

J. L. Hou and R. W. Grow

July 1, 1974

DDC
RECEIVED
DEC 23 1974
D

Microwave Device and Phyaical Electronics Laboratory
University of Utah
Salt Lake City, Utah

DISTRIBUTION STATEMENT A
Approved for public release;
Distribution Unlimited

ABSTRACT

Microwave attenuation techniques are used to find the combustion chamber temperature of a solid rocket motor, and the predicted value calculated by a theoretical specific impulse computer program and the value calculated with the microwave measurements agree within three percent. The propellants used in this investigation were seeded with five percent potassium perchlorate by weight to furnish enough electrons in the plasma to cauae measurable attenuation. The propellants were also seeded with 5 to 10 percent aluminum to produce suspended metallic particles in the plasma.

The temperature profile inside the combustion chamber is determined for a diatance of two inches away from the burning surface by scanning tne focused microwave signal transverse to the combuation chamber and by utilizing the motion of the burning surface with respect to the antennas. The experimental and theoretical results for the temperature gradient have a maximum angular difference of 25 degrees for 5 percent aluminized propellant and 18.5 degrees for 10 percent aluminized propellant.

The acoustic oscillation inside a cylindrical end burner is theoretically derived and experimentally observed. The oscillation frequencies observed range from 3.2 to 4.4 kHz, whereas the theoretical oscillation frequencies range from 2.98 to 5.13 kHz for varioua oscillation modes.

Acoustic gain and loss expressions are derived and applied to

the rocket firings. The results show that for s stable system, the acoustic loss exceeds the acoustic gain for some value of A_b^r, the real component of burning surfsce admittsnce, and for an unstable system, the acoustic gsin exceeds the loss for the same value of A_b^r.

TABLE OF CONTENTS

LIST OF ILLUSTRATIONS AND TABLES

I. INTRODUCTION

Temperatures of a hot, multispecies, confined plasma are difficult to measure with thermocouples and other pyrometers. The idea of determining the temperature of hot gases from their radiation is at least as old as the century. Optical methods of gas pyrometers, using visible[1] and infrared[2,3] radiation, were used in the early 1900's. More complex spectroscopic methods for gas temperature measurement were developed with the advance in quantum theory and its interpretation of atomic and molecular spectra. Much literature is available on these methods.[4-7] The usefulness of these spectroscopic methods heavily depends upon the understanding of what to measure and how to interpret the results. This is mainly due to the complexity of gas radiation.[8]

In 1964, Jones, Johnson, and Grow[9] developed a microwave attenuation measurement technique which was applied to the plume of rocket exhausts. Propagating microwave signals through the plasma and measuring the wave attenuation and phase shift provide information about the plasma temperature, pressure, and electron density. Olsen and Grow[10] further applied this technique to the study of temperature inside the rocket combustion chamber for the burning of solid propellant of various electron concentrations.

Metallic particles are often added to solid propellant to increase the specific impulse of the engine or to stabilize the combustion process or both. The presence of metal additives produces graybody radiation from the particle cloud in the flame in addition to the spectral

bands. These properties enable the fast spectral-scanning pyrometer to measure the temperature of solid propellant flame containing suspended solid particles by the two-color method,[11] and Tourin[12] has noted that only a sooty flame is sufficiently gray for the two-color method to be applicable. Tourin[12] also noted that most gases are not gray.

Part of the present investigation is to study the applicability of using microwave measurement techniques to determine the combustion chamber temperature of solid propellant with various amounts of aluminum seeding. By measuring the chamber pressure and wave attenuation that is caused by a known number of free electrons in the plasma, the combustion chamber temperature of the rocket motor is determined accurately.

The localized plasma temperature can be measured by focusing the microwave signal to a few millimeter-beam radius and scanning it across the plasma. By using this method the temperature change away from the propellant burning surface is determined for a distance less than two inches.

Acoustic oscillation inside the rocket combustion chamber is a phenomenon associated with pressure oscillation at the frequencies corresponding to the acoustic frequencies of the chamber. In this investigation, the acoustic oscillation inside a cylindrical end burner is explored both theoretically and experimentally. To the author's knowledge, the oscillation phenomenon has never been observed for the cylindrical end burner rocket motor.

In Chapter II, the theoretical results obtained for electro-

magnetic wave impinging on a single electron source plasma will be discussed. The dispersion equation describing the propagation of the wave through the plasma region is first derived. These mathematical relations will describe the wave attenuation in terms of the frequency of the wave, the electron density of the plasma and the electron drift velocity.

In Chapter III, the oscillation of acoustic waves is discussed. From the equation of conservation of energy, conservation of momentum, and equation of continuity, the oscillatory pressure wave equation is derived. The oscillation frequency as well as acoustic gain and loss mechanism are also discussed.

In Chapter IV, the heat loss inside the combustion chamber is discussed from the thermodynamics aspect. The results are used as a comparison for the temperature profile measurement.

All the theories discussed previously are applied to the rocket motor designed for this investigation in Chapter V. The experimental setup and procedures are discussed in detail and the theoretical results are also presented.

Chapter VI contains all the experimental results and their interpretations.

The summary and conclusions are given in Chapter VII.

II. ELECTROMAGNETIC WAVE PROPAGATION THROUGH A HOT MULTISPECIES PLASMA

In this section, the phenomenon of microwave interaction with a high temperature, multispecies plasma, generated by the burning of solid rocket propellant, is investigated to determine the attenuation of the incident wave. The dispersion equation is derived from Maxwell's equation and Langevin's force equation, and the attenuation is found in terms of the frequency, electron density, and drift velocity. The mean electron drift velocity is shown to be a function of the species of the gas present, their electron collision cross section, gas pressure, temperature, and frequency.

The propellant used in this study contains five per cent potassium perchlorate to furnish enough electrons to swamp the random generation of free electrons and produce a measurable attenuation in the pressure range of interest. Metallic particles are very often added to propellant either to increase the specific impulse of the engine or to stabilize the combustion process or both. Various amounts of aluminum were "seeded" to produce a "metallic cloud" in the combustion chamber for the purpose of this study. The final form of the sttenuation expression is expressed in terms of the wave frequency, the composition of the gas, electron density, gas density, and temperature. Part of the following derivations were given by Jones, Johnson and Grow.[9]

2.1 Dispersion Equation

The propagation of electromagnetic wave through a confined conducting medium is governed by Maxwell's equation,[13]

$$\nabla \times \vec{H} = \vec{J}_T + \dot{\vec{D}} \tag{2.1}$$

$$\nabla \times \vec{E} = -\dot{\vec{B}} \tag{2.2}$$

where the total electronic current density, J_T, is defined by

$$J_T = \rho \vec{v} \tag{2.3}$$

The velocity, v, in Eq. 2.3 is the average drift velocity of the electron caused by the impressed field and is not the random thermal velocity of the medium. From the relations above, a wave equation may be developed for the electric field intensity given by

$$\nabla^2 E = \mu \rho \dot{v} + \mu \varepsilon \ddot{E} \tag{2.4}$$

This is a simple scalar equation which can be used from the geometry of the test rocket motor and the frequency of the applied signal. Looking ahead momentarily at this point, Fig. 2.1 shows the relative position of the horn antenna, dielectric lens, and rocket combustion chamber.

The operating frequency of the incoming signal is 23.6 GHz, which gives a free-space wavelength of 0.5004 inch. The quartz window aperture measured one by two inches. Although the plane wave approximation would be valid for $2L^2/\lambda = 50$ inches for a 2.5 inch aperture, the directivity of the horns is sufficiently high that transmission between the two lens-fitted horns is only 0.6 dB less than solid waveguide and transmission after insertion of the motor with quartz windows only decreases by an additional 1.0 dB (see Appendix III). These results give confidence in the plane wave assumption used in the theory.

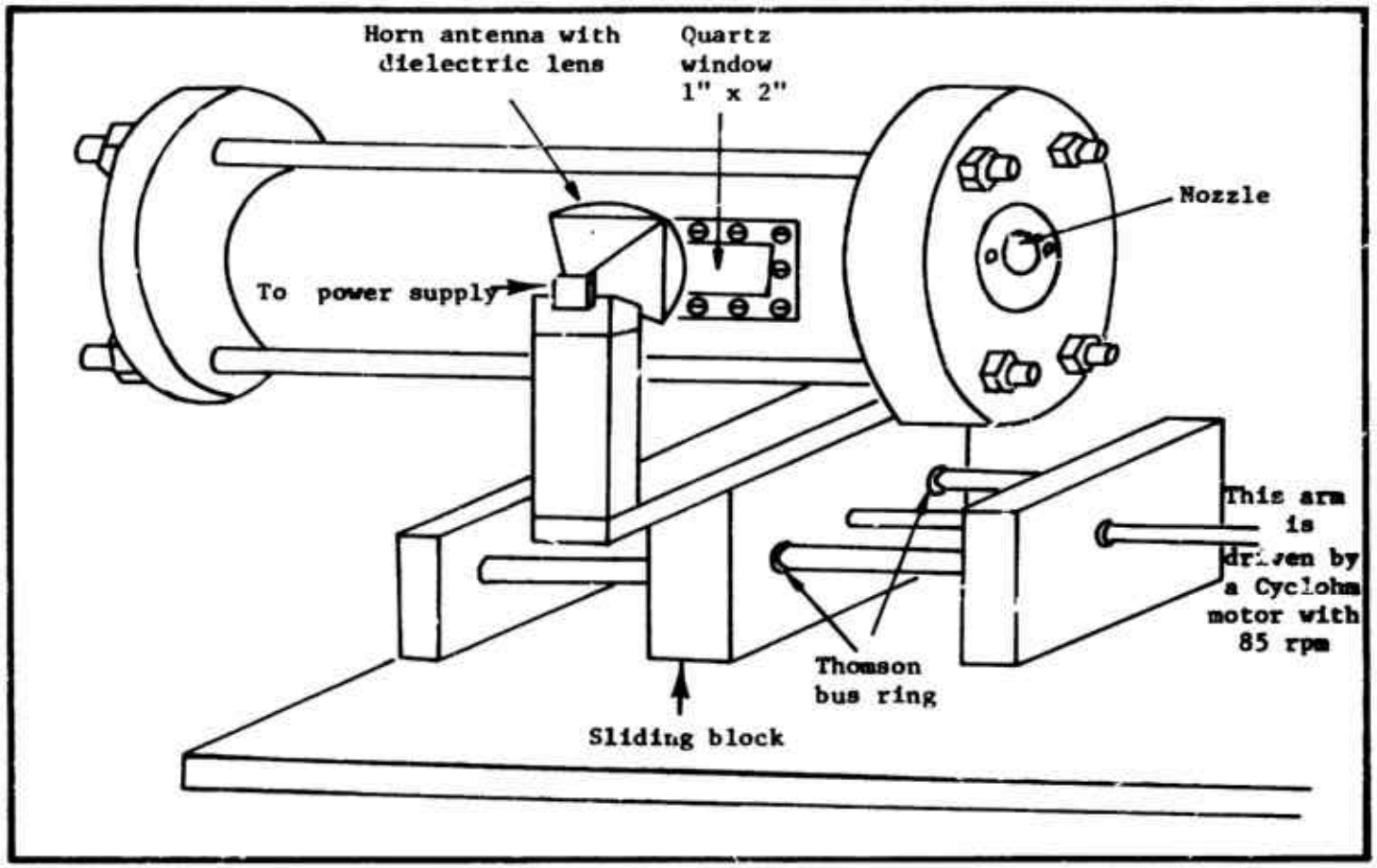

Fig. 2.1. Relative position of horn antenna, dielectric lens, and rocket combustion chamber.

To find the average drifting velocity, v, in a sufficiently high density gas molecule plasma, the Langevin force equation is used with a damping term to account for the energy loss due to collision.[14] Since the collision is random, it is necessary to write this equation for the average electron; that is, one that experiences one collision per mean-free-path length. Thus we have

$$\dot{v} + gv = \frac{e}{m} E \tag{2.5}$$

which, for a given harmonic time dependence, has a solution of

$$v = \frac{e}{m} \frac{E}{g + i\omega} \tag{2.6}$$

If the electric field has a one-dimensional space dependence given by

$$E = E_o e^{-\Gamma z} \tag{2.7}$$

then the simultaneous solution of the Langevin equation, Eq. 2.6, the wave equation, and Eq. 2.7 for the propagation conatant Γ, yields the diapersion equation,

$$\Gamma^2 + k^2 - k_p^2 \frac{i\omega}{g + i\omega} = 0 \tag{2.8}$$

where k is the propagation constant in free space and k_p is defined by

$$k_p = \frac{\omega_p}{c} \tag{2.9}$$

The quantity ω_p is the plasma frequency and is given by

$$\omega_p = \left(\frac{\rho_e e}{m\varepsilon_o}\right)^{1/2} \tag{2.10}$$

The quantity ρ_e is the electron charge density of the medium in Coulomb per unit volume, with the usual identification

$$\Gamma = \alpha + i\beta \tag{2.11}$$

where α is the attenuation constant in nepers per meter and β is the phase constant in radians per meter.

The parameter g in the Langevin equation has the dimension of frequency. For a simple plasma where g is independent of electron[15] velocity, it reduces to the collision frequency of the electrons. The rocket combustion chamber plasma assumed constitutes a very hot, dense mixture of gases and, under this condition, the quantity g may be complex and unequal to the collision frequency. In order to allow for this possibility, the solution to Langevin's equation may be written as

$$v = \frac{eE}{m}(B - iD) \tag{2.12}$$

using Molmud's notation.[16] The conductivity, σ, is defined by the equation

$$J = \sigma E \tag{2.13}$$

Combining Eqs. 2.3, 2.10, 2.12, and 2.13 yields Eq. 2.14,

$$\sigma = \omega_p^2 \varepsilon_o (B - iD) \tag{2.14}$$

From Eq. 2.14 it is clearly seen that "B" and "D" are directly related to the conductivity of the plasma. Using this relation the resultant determinantal equation is given by

$$\Gamma^2 + k^2 - ik_p^2 \omega B - k_p^2 \omega D = 0 \tag{2.15}$$

Substituting Γ from Eq. 2.11 and collecting real and imaginary parts of Eq. 2.15, we have

$$\alpha = \frac{k}{\sqrt{2}} \left\{ \left(\frac{\omega_p^2}{\omega^2} \omega D - 1 \right) + \left[\left(\frac{\omega_p^2}{\omega^2} \omega D - 1 \right)^2 + \frac{\omega_p^4}{\omega^4} \omega^2 B^2 \right]^{1/2} \right\}^{1/2} \tag{2.16}$$

$$\beta = \frac{k}{\sqrt{2}} \left\{ \left(1 - \frac{\omega_p^2}{\omega^2} \omega D \right) + \left[\left(\frac{\omega_p^2}{\omega^2} \omega D - 1 \right)^2 + \frac{\omega_p^4}{\omega^4} \omega^2 B^2 \right]^{1/2} \right\}^{1/2} \tag{2.17}$$

From these equations α and β are functions of wave frequency, plasma frequency, which is related to electron density, and the complex drift velocity terms, B and D.

2.2 Investigation of the Drift Velocity

In order to complete the derivation of attenuation and phase constants in terms of physical parameters, the functional dependence

of drift velocity must be investigated. The velocity term described in Eq. 2.12 is an average velocity of all electrons in the gas and is in the same direction as the electric field. If a coordinate system is assumed so that the electric field is in the z-direction, then the velocity given by Eq. 2.12 is actually the average velocity in the z-direction. Using Maxwell's law of the velocity distribution, the average drift velocity is written as

$$\bar{v}_z = \frac{\int_0^\infty v_z f d\tau}{\int_0^\infty f d\tau} \tag{2.18}$$

where the function f must satisfy the Boltzmann equation which is a mathematical relation that specifies the phase-space distribution function for a particular system of particles.[17]

$$\frac{e}{m} E \frac{\partial f}{\partial v} + \frac{\partial f}{\partial t} = \left(\frac{\partial f}{\partial t}\right)_c \tag{2.19}$$

Margenau[18] has shown that the solution to Eq. 2.19 has, as the first terms of its expansion,

$$f = f_o + \frac{eE}{m} v_z \left[f_1 \cos \omega t + g_1 \sin \omega t\right] \tag{2.20}$$

where f_o, f_1, and g_1 are coefficients of the expansion. Equation 2.18 may then be rewritten as

$$\bar{v}_z = \frac{\int_{\phi=0}^{2\pi}\int_{\theta=0}^{\pi}\int_{v=0}^{z} v_z\left[\left(f_1 \cos \omega t + g_1 \sin \omega t\right) v_z\right] v^2 dv \sin\theta d\theta d\phi}{\int_{\phi=0}^{2\pi}\int_{\theta=0}^{\pi}\int_{v=0}^{\infty} f_o\, v^2 dv \sin\theta d\theta d\phi} \tag{2.21}$$

Relations may be developed[18] between f_o, f_1, and g_1 such that Eq. 2.21 may be expressed in complex form as

$$\bar{v}_z = \frac{\int_{\phi=0}^{2\pi}\int_{\theta=0}^{\pi}\int_{v=0}^{z} \frac{eE}{m} v^4 dv \frac{\lambda m v}{v^2 + \omega^2\lambda^2} n\left(\frac{m}{2kT}\right)^{3/2}\left(1 - \frac{i\lambda\omega}{v}\right)\cos^2\theta \sin\theta d\theta d\phi}{\int_{\phi=0}^{2\pi}\int_{\theta=0}^{\pi}\int_{v=0}^{z} n\left(\frac{m}{2kT}\right)^{3/2} e^{-\frac{mv^2}{2kT}} v^2 \sin\theta d\theta d\phi dv} \tag{2.22}$$

where λ is the mean free path between collisions, and n is the electron density. If a change of variable is made such that

$$\nu = \frac{v}{\lambda} \tag{2.23}$$

and the θ and ϕ integrations are carried out, then Eq. 2.22 becomes

$$\bar{v}_z = \frac{8\pi}{3}\frac{eE}{m}\int_o^{\infty} \beta\left(\frac{\beta}{\pi}\right)^{3/2} \frac{v^4 e^{-\beta v^2} dv}{i\omega + \nu} \tag{2.24}$$

where

$$\beta = \frac{m}{2kT} \tag{2.25}$$

For most cases ν is a velocity dependent function. For ao-called Maxwellian gas, in which the potential between electrona and neutral molecules varied as r^{-4}, ν is not a velocity dependent function. A mixture of frequency is found from thc average electron-molecule collision cross section, Q_{ave}, given by

$$Q_{ave} = \sum m_i Q_i \tag{2.26}$$

where the m_i's are the mole fraction averaging factors of each species of gas present, since the collision frequency of the electrons and a particular neutral gas is given by

$$\nu_i = \rho v Q_i \tag{2.27}$$

where ρ is the gas particle density. The sverage collision frequency for a given electron velocity is

$$\nu_{avg} = \rho v Q_{avg} \tag{2.28}$$

Substitution of Eq. 26 in Eq. 28 gives

$$\nu_{avg} = \rho v \sum m_i Q_i \tag{2.29}$$

The average drift velocity of electrons due to the incident microwave signal as given in Eq. 2.24 is now a function of the frequency of the wave, the mole fraction of each gas species, and each collision cross section. Rewriting Eq. 2.24 we get

$$\bar{v} = \frac{8\pi}{3} \frac{eE}{m} \beta \left(\frac{\beta}{\pi}\right)^{3/2} \int_0^\infty \frac{v^4 e^{-\beta v^2} dv}{i\omega + \rho v \sum m_i Q_i} \tag{2.30}$$

To obtain useable expressions for the cross-section terms in the summation in Eq. 2.30, a power series approximation of the collision cross sections will be used. This approximation is valid for only a limited range of velocity; however, it is known that the variation in the combustion gas temperature for pressures between 20 psia and 100 psia is only about 100° K out of an equilibrium temperature of 2600° K, indicating that the thermal energy of the electrons actually changes very little over the entire pressure range considered. It will be shown in a later section that the significant collision species in the plasma are water, hydrogen chloride, carbon dioxide, carbon monoxide, diatomic hydrogen, and diatomic nitrogen. Abundant information exists about the dependence of the collision cross section on electron energy for these substances.[19-21] Using the fact that the thermal energy of the plasma electrons is of the order of 0.22 electron volts and varies only a few percent from that value, the following expressions represent good approximations to the collision cross sections for the given gaseous species:

$$Q_{H_2O} = \frac{5.90 \times 10^{-8}}{v^2} \tag{2.31}$$

$$Q_{HCl} = \frac{1.835 \times 10^{-8}}{v^2} \tag{2.32}$$

$$Q_{CO_2} = \frac{7.16 \times 10^{-14}}{v} \tag{2.33}$$

$$Q_{CO} = 2.65 \times 10^{-20} + \left(2.08 \times 10^{-25}\right) v \tag{2.34}$$

$$Q_{H_2} = 8.92 \times 10^{-20} + \left(1.464 \times 10^{-25}\right) v \tag{2.35}$$

$$Q_{N_2} = \left(2.70 \times 10^{-25}\right) v \tag{2.36}$$

where v is the thermal velocity of the plasma electrons. It is seen that the summation in Eq. 2.29 contains terms of the form

$$Qv^r = \text{const.} = c_r \tag{2.37}$$

where the value of r is 2, 1, 0, and -1. Equation 2.30, when written so that the constants of Eq. 2.37 appear, becomes

$$\bar{v} = \frac{8\pi}{3} \frac{eE}{m} \beta \left(\frac{\beta}{\pi}\right)^{3/2} \int_o^\infty \frac{v^5 e^{-\beta v^2} dv}{i\omega v + m_2 c_2 \rho + m_1 c_1 \rho v + m_o c_o \rho v^2 + m_{-1} c_{-1} \rho v^3} \tag{2.38}$$

Making the change of variable such that

$$y = \beta^{1/2} v \tag{2.39}$$

and substituting Eqs. 2.39 and 2.12 into Eq. 2.38 gives

$$B - iD = \frac{8}{3\sqrt{\pi}} \int_0^\infty \frac{\beta y^5 e^{-y^2} dy}{i\omega\beta y + m_2 c_2 \rho \beta^{3/2} + m_1 c_1 \rho \beta y + m_o c_o \rho \beta^{1/2} y^2 + m_{-1} c_{-1} \rho y^3} \tag{2.40}$$

Upon rationalizing the denominator, it is seen that

$$B = \frac{8}{3\sqrt{\pi}} \int_0^\infty \frac{\left(m_2 c_2 \rho \beta^{3/2} + m_1 c_1 \rho \beta y + m_o c_o \rho \beta^{1/2} y^2 + m_{-1} c_{-1} \rho y^3\right) \beta y^5 e^{-y^2} dy}{(\omega \beta y)^2 + \left(m_2 c_2 \rho \beta^{3/2} + m_1 c_1 \rho \beta y + m_o c_o \rho \beta^{1/2} y^2 + m_{-1} c_{-1} \rho y^3\right)^2} \tag{2.41}$$

and

$$D = \frac{8}{3\sqrt{\pi}} \int_0^\infty \frac{\omega \beta^2 y^6 e^{-y^2} dy}{(\omega \beta y)^2 + \left(m_2 c_2 \rho \beta^{3/2} + m_1 c_1 \rho \beta y + m_o c_o \rho \beta^{1/2} y^2 + m_{-1} c_{-1} \rho y^3\right)^2} \tag{2.42}$$

With the determination of B and D as functions of the incident wave frequency, gas composition, and temperature, the propagation constants of Eqs. 2.16 and 2.17 are determined except for the value of the plasma frequency. Once the electron density is known for the plasma of a given propellant, the wave attenuation is completely determined and can be theoretically predicted for a given geometry.

2.3 Investigation of the Electron Density

In this derivation of the propagation constants for the incident electromagnetic wave, the temperature contained in the expressions thus far is the temperature of the electrons and was introduced through

the mean velocity expression, Eq. 2.12. When the electrons are in thermal equilibrium with the gas molecules, the temperature in α and β can be equated to the gas temperature, which in turn relates to the gas density through the perfect gas law,

$$\rho = \frac{N_o p}{RT} \tag{2.43}$$

where N_o is Avogadro's number, R is the gas constant, and p is the pressure. The perfect gas law then allows the expression of density in terms of temperature provided the pressure is known. The equilibrium electron density then may be derived from the thermal state of the gas. It will be assumed that the source of electrons is the seeded potassium perchlorate and that the mechanism of free electron production is thermal ionization. There are two ways of considering the production of electrons; they are:

1. Assuming that no sinks for electrons exist in the gas.
2. Assuming that chlorine acts as a sink for electrons.

2.3.1 Assuming No Electron Sinks

For the simple reaction

$$K \rightarrow K^+ + e^- \tag{2.44a}$$

$$Al \rightarrow Al^+ + e^- \tag{2.44b}$$

Saha's equation[21] may be written as

$$\frac{X^2 N}{1 - X} = \left(\frac{\sqrt{2\pi k m_e}}{h}\right)^3 T^{3/2} e^{-\frac{eI}{kT}} \tag{2.45}$$

where N is the total number density per unit volume of potassium and aluminum, X is the fraction of those atoms ionized, k is Boltzmann's constant, h is Plank's constant, m_e is the electronic mass, e is the electronic charge, and I is the ionization potential.[22] For a given temperature, the number density for electrons per unit volume is simply

$$n_e = XN \tag{2.46}$$

and the plasma frequency defined in Eq. 2.10 becomes

$$\omega_p^2 = \frac{(n_e e)e}{n_e \varepsilon_o} \tag{2.47}$$

2.3.2 Consideration of Electron Sinks

When electron recombination is taken into account, not only the number density of the electron source, but also the number density of the electron sink must be known. Chlorine will be assumed to be the only effective electron sink because it is the only constituent present in substantial amounts in the propellant that has an electron affinity of the order of the low ionization potential of potassium.

With the following two reactions considered, the chlorine electron sink is defined as

$$K \rightarrow K^+ + e^- \tag{2.48a}$$

$$Al \rightarrow Al^+ + e^- \tag{2.48b}$$

$$Cl + e^- \rightarrow Cl^- \tag{2.48c}$$

The chemical equilibrium constants for this pair are given by

$$\frac{[Al^+][e^-]}{[Al]} + \frac{[K^+][e^-]}{[K]} = \alpha_1 \tag{2.49a}$$

$$\frac{[Cl][e^-]}{[Cl^-]} = \alpha_2 \tag{2.49b}$$

When the bracketed quantities denote concentrations in number per unit volume, the equilibrium constants may be written as

$$\alpha_1 = \left(\frac{\sqrt{2\pi km}}{h}\right)^3 T^{3/2} \left[e^{-\frac{eI_K}{kT}} + e^{-\frac{eI_{Al}}{kT}}\right] \tag{2.50a}$$

and

$$\alpha_2 = 4\left(\frac{\sqrt{2\pi km}}{h}\right) T^{3/2} e^{-\frac{eD_{Cl}}{kT}} \tag{2.50b}$$

where I_K and I_{Al} are the ionization potential of potassium and aluminum, respectively, and D_{Cl} is the electron affinity of chlorine.[23]

Defining the total quantities of the reacting elements by the following equations:

$$A_1 = [K] + [K^+] + [Al] + [Al^+] \tag{2.51a}$$

and

$$A_2 = [Cl] + [Cl^-] \tag{2.51b}$$

it is possible to combine Eqs. 2.49 and 2.51 with the neutrality condition,

$$[e^-] + [Cl] = [K^+] + [Al^+] \tag{2.52}$$

to form a cubic equation in electron density,

$$n^3 + An^2 + Bn + C = 0 \tag{2.53}$$

where

$$n = [e^-] \tag{2.54}$$

and the coefficients are given by

$$A = \alpha_1 + \alpha_2 + A_2 \tag{2.55a}$$

$$B = \alpha_1(A_2 - A_1 + \alpha_2) \tag{2.55b}$$

$$C = -\alpha_1\alpha_2A_1 \tag{2.55c}$$

The determined value then establishes the plasma frequency through Eq. 2.40.

With the presence of aluminum in the solid propellant, considerable amounts of aluminum oxide particles are present in the plasma. The amount of Al_2O_3 at various conditions is listed in Appendix I.

Each aluminum oxide particle in the plasma can be considered as an isolated positive-charged particle since the average separation distance is about 7 microns, as reported by Richardson.[24] Compared to the 1 micron particle radius,[25] the interaction particles can be negiected. Each isolated particle is surrounded by a thin sheath of electrons with a potential ϕ as a function of distance r given by Jones.[16]

$$\phi = B \frac{e^{-\left[\frac{2\rho_o e}{\varepsilon_o kT}\right]^{1/2} r}}{r} \qquad (2.56)$$

where B is an arbitrary constant and ρ_o is the charge density.

An exact determination of the charge density profile has been reported by Johnson and Bullock.[26] They concluded that the electrons contained in the thin sheath are not contributing to the average electron density in the plasma. Thus, this effect can be negiected in the calculation of microwave attenuation when propagating through the plasma.

2.4 Plasma Temperature from the Attenuation Constant

To relate the attenuation of a microwave beam in a plasma to the temperature, consider that a plane wave normally impinges upon a

plasma region and passes through the plasma into free space as illustrated in Fig. 2.2. At plane I in the figure, due to differences in the characteriatic impedance of the plasma and free space, a reflection coefficient may be defined in terms of the two impedances by

$$R = \frac{Z_1 - Z_o}{Z_1 + Z_o} \tag{2.57}$$

where Z_o is the characteristic impedance of free space and Z_1 is that of the plasma. If it is assumed that the reflection coefficient is small compared to unity, then the amplitude of the transmitted wave, an infinitesimal distance to the right of plane I, will be essentially equal to the amplitude of the free space wave. If the transmitted amplitude of the electric field is designated as E_p and the incident wave by E_o, then the amplitude of the electric field within the plasma is given by

$$E_p = E_o e^{-\Gamma z} \tag{2.58}$$

where z is measured to the right of the plasma boundary I. If the assumption of a small reflection coefficient ia again made at plane II, then the electric field amplitude at plane II designated by E_T is given by

$$E_T = E_o e^{-\Gamma L} \tag{2.59}$$

The attenuation of the transmitted wave in decibels by definition is

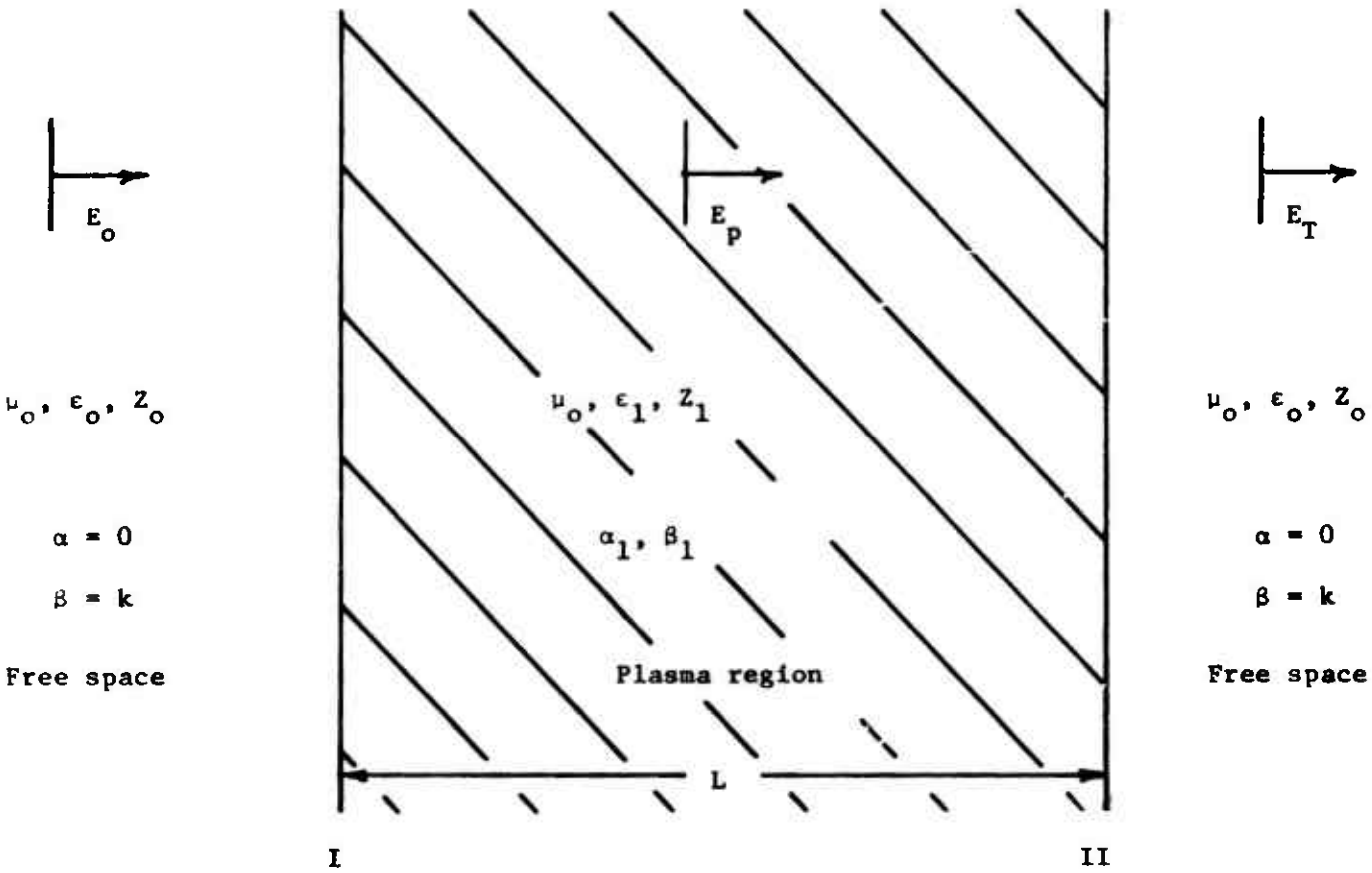

Fig. 2.2. Diagram of the assumed electromagnetic field geometry.

$$A = 20 \log_{10} \frac{E_T}{E_o} \tag{2.60a}$$

or

$$A = 20 \log_{10} e^{-\Gamma L} \tag{2.60b}$$

In terma of the magnitude of α of Eq. 2.16,

$$A = 20 \alpha L \log_{10} e \tag{2.61}$$

Substitution of Eq. 2.16 into Eq. 2.61 yielda

$$A = 10\sqrt{2}\ kL \log_{10} e \left[\left(\frac{\omega_p^2}{\omega^2} \omega D - 1 \right) + \left[\left(\frac{\omega_p^2}{\omega^2} \omega D - 1 \right)^2 + \left(\frac{\omega_p^2}{\omega^2} \omega B \right)^2 \right]^{1/2} \right]^{1/2} \tag{2.62}$$

It ia seen that one attenuation meaaurement through a specified path length of plaama of a known compoaition and pressure can yield the plasma temperature.

III. PRESSURE WAVE OSCILLATION INSIDE THE COMBUSTION CHAMBER

The equation describing preasure wave or acoustic wave oscillation inside the combuation chamber of a rocket motor ia derived from the continuity equation and the energy and momentum conaervation equations. Several valid and practical aaaumptiona are made to simplify the analysis. The equacion for the oscillation is then solved by Creen's function and perturbation methods. The final equations for both traveling and standing wavea are obtained in the lowest order of gas mean flow Mach number of cylindrical geometry.

The growth rate of acoustic waves is expreaaed in terms of the pressure wave, the flow velocity of the gas, and the acoustic admittance of the burning surface. The losa mechanism involved not only the nozzle size but also the damping effecta of solid particles.

Part of the derivationa can be found in Culick'a work.[27]

3.1 Ceneral Equation

The motion of a viscous, compressible, heat-conducting gas, as in the combustion chamber of a rocket motor, is given by the following equations:

Continuity equation:

$$-\frac{\partial P}{\partial t} + \nabla \cdot (\rho \underline{u}) = 0 \tag{3.1}$$

Conservation of momentum or Navier-Stokes equation:

$$\rho \frac{du}{dt} + \frac{\nabla P}{\gamma} = F_s + F_b \tag{3.2}$$

Conservation of energy:

$$\rho \frac{dT}{dt} - \frac{\gamma - 1}{\gamma} \frac{dP}{dt} = \text{a function of quantities that relate fluid viscosity to quantities such as fluid flow velocity, specific heat, thermal conductivity, and the boundary layer parameter.} \qquad (3.3)$$

Equation of state:

$$P = \rho T \qquad (3.4)$$

where the notations used are listed as follows:

F_s = viscous force

F_b = body force, related to the particle damping effects on the growth of the acoustic wave

ρ = density of the gas

$\underline{u}$ = velocity vector

γ = ratio of specific heat

P = amplitude of pressure

T = temperature

Equations 3.1 through 3.4 are written in terms of the dimensionless variables; i.e.,

$$P = \frac{P'}{P_o} \qquad \underline{u} = \frac{\underline{u}'}{a_o}$$

$$\rho = \frac{\rho'}{\rho_o} \qquad T = \frac{T'}{T_o} \qquad (3.5)$$

a_o is the average speed of sound, all "prime" superscripts refer to dimensional quantities, all "zero" subscripts refer to average (dimensional) conditions in the absence of waves.

With several crucial and valid assumptions, the work will be greatly simplified:

1. The linear burning rate is always small compared to the wave propagation speed. Generally speaking, the propellant used in the experiments always burned less than half an inch per second, whereas the speed of sound is around 3000 feet per second. Hence, the rate of recession of the surface can be ignored in a treatment of steady waves.
2. The combustion occurs within a very thin region on the order of 10^{-1} to 10^{-3} inches thick. So the coupling between the oscillations and the burning may be safely introduced as a boundary condition placed on the waves.
3. Mach number representative of the mean gas flow within the chamber at the burning surface is small;[27] i.e., the Mach number at burning surface is $M_b \sim 0.05$ and the Mach number at exit is $M_e \sim 0.2$ to 0.3.

Before using the perturbation method to solve these equations, we must also assume that the average Mach number of the acoustic disturbance, ε, is small, and the Mach number of the mean flow field at the burning surface where

$$\nu = \left(\frac{u'}{a_o}\right)_{\text{chamber wall}} \tag{3.6}$$

is also small.

The mean flow within the chamber is represented by

$$(\underline{u}) \text{ mean flow} = \nu \underline{U} \tag{3.7}$$

where $\underline{U}$ reflects the geometrical aspect of the mean flow pattern.

The effect of viscosity could be assumed to be confined to a thin layer of chamber walls, and the viscous terms are therefore dropped out from the governing equation. Thus we get

$$\frac{\partial \rho}{\partial t} + \nabla \cdot (\rho \underline{u}) = 0 \tag{3.8}$$

$$\rho \frac{\partial \underline{u}}{\partial t} + \frac{\nabla P}{\gamma} = F_b \tag{3.9}$$

$$\rho \frac{dT}{dt} - \frac{\gamma - 1}{\gamma} \frac{dP}{dt} = 0 \tag{3.10}$$

Differentiating Eq. 3.4 and combining with Eq. 3.10, we obtain

$$\frac{1}{\gamma} \frac{dP}{P} = \frac{d\rho}{\rho} \tag{3.11}$$

Hence we have $P = \rho^{\gamma}$ which indicates that the inviscid part of the flow may be regarded as isentropic. Using this result, Eq. 3.8 can be written as

$$\frac{\partial P}{\partial t} + \underline{u} \cdot \nabla P + \gamma P \nabla \cdot \underline{u} = 0 \tag{3.12}$$

$$\rho \frac{\partial \underline{u}}{\partial t} + \frac{\nabla P}{\gamma} = F_b \tag{3.13}$$

These equations are the governing equations for the inviscid chamber motion.

To apply the perturbation method, the following perturbation expansions are used:

$$P = 1 + \varepsilon P^{(1)} + \varepsilon^2 P^{(2)} + \ldots \tag{3.14a}$$

$$\rho = 1 + \varepsilon \rho^{(1)} + \varepsilon^2 \rho^{(2)} + \ldots \tag{3.14b}$$

$$T = 1 + \varepsilon T^{(1)} + \varepsilon^2 T^{(2)} + \ldots \tag{3.14c}$$

$$\underline{u} = \nu \underline{U} + \varepsilon \underline{u}^{(1)} + \varepsilon^2 \underline{u}^{(2)} + \ldots \tag{3.14d}$$

Substituting these values into Eqs. 3.12 and 3.9, we get

Order of ε:

$$\frac{\partial P^{(1)}}{\partial t} + \gamma \nabla \cdot \underline{u}^{(1)} = -\nu \left[\underline{U} \cdot \nabla P^{(1)} \right] \tag{3.15}$$

$$\frac{\partial \underline{u}^{(1)}}{\partial t} + \frac{\nabla P^{(1)}}{\gamma} = -\nu \left[\underline{U} \cdot \nabla \underline{u}^{(1)} + \underline{u}^{(1)} \cdot \nabla \underline{U} \right] + F_b^{(1)} \tag{3.16}$$

Order of ε^2:

$$\frac{\partial P^{(2)}}{\partial t} + \gamma \nabla \cdot \underline{u}^{(2)} = -\gamma P^{(1)} \nabla \underline{u}^{(1)} - \underline{u}^{(1)} \cdot \nabla P^{(1)} - \nu \left[\underline{U} \cdot \nabla P^{(2)} \right] \tag{3.17}$$

$$\frac{\partial \underline{u}^{(2)}}{\partial t} + \frac{\nabla P^{(2)}}{\gamma} = -\rho^{(1)} \frac{\partial \underline{u}^{(1)}}{\partial t} - \underline{u}^{(1)} \cdot \nabla \underline{u}^{(1)} - \nu \left[\underline{u}^{(2)} \cdot \nabla \underline{U} + \underline{U} \cdot \nabla \underline{u}^{(2)} + \rho^{(1)} \left(\underline{u}^{(1)} \cdot \nabla \underline{U} + \underline{U} \cdot \nabla \underline{u}^{(1)} \right) \right] + F_b^{(2)} \tag{3.18}$$

where

$\underline{U}$ is assumed to be steady and solenoidal; i.e., $\nabla \cdot \underline{U} = 0$

Differentiating Eq. 3.15 with respect to time, we obtain

$$\frac{\partial^2 P^{(1)}}{\partial t^2} + \gamma \frac{\partial}{\partial t} \left(\nabla \cdot \underline{u}^{(1)} \right) = -\nu \underline{U} \cdot \frac{\partial}{\partial t} \left(\nabla P^{(1)} \right) \tag{3.19}$$

Taking the divergence of Eq. 3.16, we get

$$\gamma \nabla \cdot \left(\frac{\partial \underline{u}^{(1)}}{\partial t} \right) + \nabla \cdot \left(\nabla P^{(1)} \right) = -\gamma \nu \left[\nabla \left(\underline{U} \cdot \nabla \underline{u}^{(1)} + \underline{u}^{(1)} \cdot \nabla \underline{U} \right) \right] + \gamma \nabla \cdot F_b^{(1)} \tag{3.20}$$

Combining these two equations, we get

$$\frac{\partial^2 P^{(1)}}{\partial t^2} - \nabla^2 P^{(1)} = -\gamma \nabla \cdot F_b^{(1)} + \gamma \nu \left[\nabla \cdot \left(\underline{U} \cdot \nabla \underline{u}^{(1)} + \underline{u}^{(1)} \cdot \nabla \underline{U} \right) - \underline{U} \cdot \frac{\partial}{\partial t} \left(\nabla P^{(1)} \right) \right] \tag{3.21}$$

In anticipation of oscillation, we assume:

$$p^{(1)} = \gamma p^{(1)} e^{jkt} \tag{3.22a}$$

$$\underline{u}^{(1)} = \underline{q}^{(1)} e^{jkt} \tag{3.22b}$$

$$F_b^{(1)} = \lambda \underline{f}^{(1)} e^{jkt} \tag{3.22c}$$

where k is the complex frequency and

$$k = \Omega + j\Lambda \tag{3.23}$$

The amplitudes of $p^{(1)}$, $\underline{q}^{(1)}$, and $\underline{f}^{(1)}$ may be complex.

With these relations, Eq. 3.21 can be written as

$$\nabla^2 p^{(1)} + k^2 p^{(1)} = \nu g^{(1)} \tag{3.24}$$

where

$$g^{(1)} = \left\{ jk\left(\underline{U} \cdot \nabla p^{(1)}\right) - \nabla \cdot \left(\underline{U} \cdot \nabla \underline{q}^{(1)} + \underline{q}^{(1)} \cdot \nabla \underline{U}\right) + \left(\frac{\lambda}{\nu}\right) \nabla \cdot \underline{f}^{(1)} \right\} \tag{3.25}$$

Now, introducing an admittance function, A,

$$A = A_r + jA_i \tag{3.26}$$

such that

$$\hat{n} \cdot \tilde{\underline{u}} = -\nu \left(\frac{\tilde{P}}{\gamma}\right) A \quad \text{burning surface} \tag{3.27}$$

where $\tilde{\underline{u}}$ a.. , $\tilde{P}$ are the complex velocity and pressure fluctuation at the wall. $\hat{n}$ is an outward pointing unit vector normal to the chamber wall.

Substituting Eq. 3.16 we get

$$\hat{n} \cdot \nabla p^{(1)} = \hat{n} \cdot \gamma\left[-jk\underline{q}^{(1)} - \nu\left(\underline{U} \cdot \nabla \underline{q}^{(1)} + \underline{q}^{(1)} \cdot \nabla \underline{U}\right) + \lambda f^{(1)}\right] \tag{3.28}$$

Also, using Eq. 3.27,

$$\hat{n} \cdot \underline{q}^{(1)} = -\nu A p^{(1)} \quad \text{at boundary} \tag{3.29}$$

where

$$A = \begin{cases} 0 & \text{at inhibited surfaces} \\ A_b & \text{at burning surface}^{28} \\ -\frac{\nu_n}{\nu} A_n & \text{at nozzle exits} \end{cases}$$

ν_n = Mach number of flow in nozzle entrance

A_n = nozzle admittance

So, the boundary condition can be expressed as

$$\hat{n} \cdot \nabla p^{(1)} = -\nu h^{(1)} \tag{3.30}$$

where

$$h^{(1)} = \left\{-jkAp^{(1)} + \hat{n} \cdot \gamma\left[\underline{U} \cdot \nabla \underline{q}^{(1)} + \underline{q}^{(1)} \cdot \nabla \underline{U} - \left(\frac{\lambda}{\nu}\right) f^{(1)}\right]\right\} \tag{3.31}$$

and A is the appropriate admittance function at the chamber boundary.

3.2 Solution by Green's Function Method

Equations 3.24 and 3.30 are nothing more than nonhomogeneous wave equations which satisfy the nonhomogeneous Newmann boundary condition.

Green's function method is used to solve this Helmholtz equation; the first order solution of Green's function aatiafies

$$\left(\nabla^2 + k^2\right) G\left(\vec{r}|\vec{r}_o\right) = \delta\left(\vec{r} - \vec{r}_o\right) \tag{3.32}$$

where $\delta\left(\vec{r} - \vec{r}_o\right)$ is the delta function representing an harmonic point source at the position $\vec{r}_o$; thus G representa the disturbance received at $\vec{r}$. The boundary condition chosen for G is that the normal component of its gradient vanishes on the entire bounding surface:

$$\hat{n} \cdot \nabla G\left(\vec{r}|\vec{r}_o\right) = 0 \qquad \text{for } \vec{r} = \vec{r}_s \tag{3.33}$$

where $\vec{r}_a$ is a vector defining poaition of pointa on the bounding surface.

Multiplying Eq. 3.24 by $G\left(\vec{r}|\vec{r}_o\right)$ and Eq. 3.32 by $p^{(1)}$, and subtracting the two equations, we get

$$G\left(\vec{r}|\vec{r}_o\right) \nabla^2 p^{(1)} - p^{(1)} \nabla^2 G\left(\vec{r}|\vec{r}_o\right) = \nu\left[G\left(\vec{r}|\vec{r}_o\right) g^{(1)}\right] - p^{(1)} \delta\left(\vec{r} - \vec{r}_o\right) \tag{3.34}$$

Integrating over the volume of the chamber -- $0 < r < 1$, $0 < z < L/R$, $0 < \phi < 2\pi$ in cylindrical coordinate where

R is the chamber radius

L is the characteristic length. For axial modes L is the chamber length; for tangential or radial modes, L is the chamber radius or the width.

hence

$$\int_V \left[G\nabla^2 p^{(1)} - p^{(1)}\nabla^2 G\right] dv = \nu \int_V G g^{(1)}\, dv - \int_V p^{(1)} \delta\left(\vec{r} - \vec{r}_o\right) dv \tag{3.35}$$

The last term is just $p^{(1)}$ evaluated at $\vec{r} = \vec{r}_o$ using symmetry property; i.e.,

$$G\left(\vec{r}|\vec{r}_o\right) = \left[G\left(\vec{r}_o|\vec{r}\right)\right]^* \tag{3.36}$$

where * denotes complex conjugate.

We get $p^{(1)}(\vec{r})$ in terms of G*:

$$p^{(1)}(\vec{r}) = \nu \int_V G^*\left(\vec{r}|\vec{r}_o\right) g^{(1)}\, dv - \int_V \left[G^*\nabla^2 p^{(1)} - p^{(1)}\nabla^2 G^*\right] dv \tag{3.37}$$

Using Green's theorem to convert volume integral to surface integral, we have

$$\int_V \left(G^*\nabla^2 p^{(1)} - p^{(1)}\nabla^2 G^*\right) dv = \int_S \left(G^*\nabla p^{(1)} - p^{(1)}\nabla G^*\right) \cdot \hat{n} ds \tag{3.38}$$

but

$$\hat{n} \cdot \nabla p^{(1)} = -\nu h^{(1)}$$

$$\hat{n} \cdot \nabla G^* = 0$$

over the boundary surface. Thus

$$p^{(1)}(r) = \nu \int_v G^*\left(\vec{r}|\vec{r}_o\right) g^{(1)}\, dv + \nu \int_a G^*\left(\vec{r}|\vec{r}_{oa}\right) h^{(1)}\, ds \quad (3.39)$$

where $\vec{r}_{os}$ refers to the value at points on the boundary surface.

A useful expression for $G\left(\vec{r}|\vec{r}_o\right)$ is the expansion in normal modes of the unperturbed wave equation. Assuming

$$G = \sum_\alpha A_\alpha \psi_\alpha(\vec{r}) \quad (3.40)$$

where

$$\left(\nabla^2 + k_\alpha^2\right) \psi_\alpha(\vec{r}) = 0 \quad (3.41)$$

with

$$\hat{n} \cdot \nabla \psi_\alpha = 0 \quad \text{for } \vec{r} = \vec{r}_s \quad (3.42)$$

and α stands for three indices: ℓ, m, and n.

The eigenfunctions must also be orthogonal; i.e.,

$$\left(\psi_\alpha, \psi_\beta\right) = \int_v \psi_\alpha^* \psi_\beta\, dv = 0 \quad \text{for } \alpha \neq \beta \quad (3.43)$$

The normalization factor E_α is

$$E_\alpha^2 = \int_v \psi_\alpha^* \psi_\alpha \, dv \tag{3.44}$$

Then Eq. 3.32 can be written as

$$\sum_\alpha A_\alpha \left(\nabla^2 \psi_\alpha + k^2 \psi_\alpha\right) = \delta\left(\vec{r} - \vec{r}_o\right) \tag{3.45}$$

From Eq. 3.41 we have

$$\nabla^2 \psi_\alpha(\vec{r}) = -k_\alpha^2 \psi_\alpha(\vec{r}) \tag{3.46}$$

so

$$\sum_\alpha A_\alpha \psi_\alpha(\vec{r}) \left(k - k_\alpha^2\right) = \delta\left(\vec{r} - \vec{r}_o\right) \tag{3.47}$$

Multiplying $\sum_\beta \psi_\beta^*(\vec{r})$ by Eq. 3.47 and intcgrating over volume v, we have

$$\int_v \sum_\beta \psi_\beta^*(\vec{r}) \, \delta\left(\vec{r} - \vec{r}_o\right) dv = \int_v \sum_\beta \psi_\beta^*(\vec{r}) \left[\sum_\alpha A_\alpha \psi_\alpha(\vec{r}) \left(k^2 - k_\alpha^2\right)\right] dv \tag{3.48}$$

Using orthogonal property and by the definition of δ function, we get

$$\sum_\alpha \psi_\alpha^*\left(\vec{r}_o\right) = \sum_\alpha A_\alpha \left(k^2 - k_\alpha^2\right) \int \psi_\alpha \psi_\alpha^* dv \tag{3.49}$$

$$\psi_\alpha^*\left(\vec{r}_o\right) = A_\alpha \left(k^2 - k_\alpha^2\right) E_\alpha^2 \tag{3.50}$$

Therefore,

$$A_\alpha = \frac{\psi_\alpha^*\left(\vec{r}_o\right)}{E_\alpha^2\left(k^2 - k_\alpha^2\right)} \tag{3.51}$$

Hence,

$$G\left(\vec{r}|\vec{r}_o\right) = \sum_\alpha \frac{\psi_\alpha(\vec{r})\ \psi_\alpha^*\left(\vec{r}_o\right)}{E_\alpha^2\left(k^2 - k_\alpha^2\right)} \tag{3.52}$$

with

$$E_\alpha^2 = \int_v \psi_\alpha^*\ \psi_\alpha\ dv$$

3.3 Solution to Zeroth Order in ν

Rewriting the governing equstions,

$$\nabla^2 p^{(1)} + k^2 p^{(1)} = \nu g^{(1)} \tag{3.24}$$

$$\hat{n} \cdot \nabla p^{(1)} = -\nu h^{(1)} \quad \text{at boundary} \tag{3.30}$$

From these two governing equations, $p^{(1)}$ csn be represented as a perturbation expansion with ν,

$$p^{(1)} = p^{(10)} + \nu p^{(11)} + \nu^2 p^{(12)} + \ldots \tag{3.53}$$

where the first element of the superscript refers to the order of ε

and the second refers to the order of ν. By the same token, since $g^{(1)}$ and $h^{(1)}$ are functions of $p^{(1)}$, we can also write

$$g^{(1)} = g^{(10)} + \nu g^{(11)} + \nu^2 g^{(12)} + \ldots \tag{3.54}$$

$$h^{(1)} = h^{(10)} + \nu h^{(11)} + \nu^2 h^{(12)} + \ldots \tag{3.55}$$

With these expansions substituted into Eqs. 3.24 and 3.30, we have

Order (0):

$$\nabla^2 p^{(10)} + k^2 p^{(10)} = 0 \tag{3.56}$$

$$\hat{n} \cdot p^{(10)} = 0 \quad \text{at the boundary} \tag{3.57}$$

Order (ν):

$$\nabla^2 p^{(11)} + k^2 p^{(11)} = g^{(11)} \tag{3.58}$$

$$\hat{n} \cdot \nabla p^{(11)} = -h^{(11)} \tag{3.59}$$

Note Eq. 3.56 is identical to the boundary value problem shown by Eq. 3.41. This simply demonstrates that the solution as it is unfolding is a perturbation on the classical acoustic solution. Thus, $p^{(10)}$ $_{,t}$, and it is proper to write

$$p^{(1)} = \psi_\alpha + 0(\nu) \tag{3.60}$$

where $0(\nu)$ is for higher order terms in ν. Solution of $p^{(1)}$ can be found in terms of Green's function where

$$p^{(1)} = \nu \int_v G g^{(1)} dv + \nu \int_s G^* h^{(1)} ds \tag{3.61}$$

$$G = \sum_\alpha \frac{\psi_\alpha(\vec{r})\ \psi_\alpha^*(\vec{r}_o)}{E_\alpha^2\left(k^2 - k_\alpha^2\right)} \tag{3.62}$$

So,

$$p^{(1)} = \nu \int_v g^{(1)} \sum_\alpha \frac{\psi_\alpha(\vec{r})\ \psi_\alpha^*(\vec{r}_o)}{E_\alpha^2\left(k^2 - k_\alpha^2\right)} dv + \nu \int_s h^{(1)} \sum_\alpha \frac{\psi_\alpha(\vec{r})\ \psi_\alpha^*(\vec{r}_o)}{E_\alpha^2\left(k^2 - k_\alpha^2\right)} ds$$

$$= \nu \sum_\alpha \frac{\psi_\alpha(\vec{r})}{E_\alpha^2\left(k^2 - k_\alpha^2\right)} \left\{ \int_v g^{(1)}\ \psi_\alpha^*(\vec{r})\ dv + \int_s h^{(1)}\ \psi_\alpha^*(\vec{r})\ ds \right\} \tag{3.63}$$

For a particulsr mode of oscillstion, say N,

$$p_N^{(1)} = \psi_N(\vec{r}) \left\{ \frac{\nu}{E_N^2\left(k^2 - k_\alpha^2\right)} \left[\int_v g^{(1)}\ \psi_N^*\ dv + \int_s h^{(1)}\ \psi_N^*\ ds \right] \right\}$$

$$+ \nu \sum_{\alpha \neq N} \frac{\psi_\alpha(\vec{r})}{E_\alpha^2\left(k^2 - k_\alpha^2\right)} \left[\int_v g^{(1)}\ \psi_\alpha^*\ dv + \int_s h^{(1)}\ \psi_\alpha^*\ ds \right] \tag{3.64}$$

To achieve Eq. 3.60, we need to have

$$\frac{\nu}{E_N^2\left(k^2 - k_\alpha^2\right)}\left[\int_v g^{(1)}\ \psi_N^*\ dv + \int_s h^{(1)}\ \psi_N^*\ ds\right] = 1 \qquad (3.65)$$

So,

$$k^2 = k_N^2 + \frac{\nu}{k_N^2}\left[\int_v g^{(1)}\ \psi_N\ dv + \int_s h^{(1)}\ \psi_N^*\ ds\right] \qquad (3.66)$$

As Eq. 3.23 shows,

$$k = \Omega + j\Lambda \qquad (3.23)$$

At this point, we can see Ω represents the frequency of the fluctuation, and Λ represents the rate of growth. Now if we write

$$\Omega = \Omega^{(10)} + \nu\Omega^{(11)} + \nu^2\Omega^{(12)} + \ldots \qquad (3.67)$$

$$\Lambda = \Lambda^{(10)} + \nu\Lambda^{(11)} + \nu^2\Lambda^{(12)} + \ldots \qquad (3.68)$$

expanding Eq. 3.66 in Taylor's series, we get

$$k = k_N + \frac{\nu}{2k_N E_N^2}\left[\int_v g^{(1)}\ \psi_N^*\ dv + \int_s h^{(1)}\ \psi_N^*\ ds\right] + O\left(\nu^2\right) \qquad (3.69)$$

and it is apparent that k has no imaginary part of order unity. Thus,

$$\Lambda^{(10)} = 0 \qquad (3.70)$$

$$\Omega^{(10)} = k_N \qquad (3.71)$$

Also,

$$\Omega^{(11)} = \frac{1}{2k_N E_N^2} R \left[\int_v g^{(10)} \psi_N^* \, dv + \int_s h^{(10)} \psi_N^* \, ds \right] \qquad (3.72)$$

$$\Lambda^{(11)} = \frac{1}{2k_N E_N^2} I \left[\int_v g^{(10)} \psi_N^* \, dv + \int_s h^{(10)} \psi_N^* \, ds \right] \qquad (3.73)$$

Equations 3.70 and 3.71 show that the frequency of the oscillations is the same as the acoustic frequency to zeroth order in the mean flow Mach number ν.

Now, back to Eqs. 3.56 and 3.57; the zeroth order in ν motion is given by

$$\nabla^2 p^{(10)} + \Omega^{(10)} \, p^{(10)} = 0$$

$$\hat{n} \cdot p^{(10)} = 0 \quad \text{at the boundary}$$

In cylindrical coordinates, these equations become

$$\frac{1}{r} \frac{\partial}{\partial r} \left(r \frac{\partial p^{(10)}}{\partial r} \right) + \frac{1}{r^2} \frac{\partial^2 p^{(10)}}{\partial \theta^2} + \frac{\partial^2 p^{(10)}}{\partial z} + \Omega^{(10)^2} \, p^{(10)} = 0 \qquad (3.74)$$

and

$$\frac{\partial p^{(10)}}{\partial r} = 0 \quad \text{on } r = R$$

$$\frac{\partial p^{(10)}}{\partial z} = 0 \quad \text{at } z = 0, \; z = \frac{R}{L} \qquad (3.75)$$

Here it is convenient to nondimensionalize the lengths, choosing R as characteristic length, nondimensionsl chamber radius and length are, respectively, 1 snd L/R. Then Eq. 3.74 can easily be solved. Hence wc get

$$p_{\alpha}^{(10)} = \begin{cases} J_m(k_{mn}\, r)\, \cos(m\theta)\, \cos(k_\ell z) & \text{standing wave} \quad (3.76) \\ J_m(k_{mn}\, r)\, e^{+im\theta}\, \cos(k_\ell z) & \text{traveling wave} \quad (3.77) \end{cases}$$

where

$\alpha = (\ell, m, n)$

+ is the sign for clockwise traveling waves

- is the sign for counterclockwise trsveling waves

To satisfy the boundary condition,

$$k_\ell = \ell\pi \left(\frac{R}{L}\right) \qquad \ell = 0, 1, 2 \ldots$$

k_{mn} is the root of $\left[\dfrac{d\, J_m(k_{mn}\, r)}{dr}\right]_{r=1} = 0$

For either traveling or stsnding waves, some values are listed in the following table ss given by Culick.[27]

Table 3.1. Frequency eigenvalues k_{mn} for cylindrical chamber.

m \ n	0	1	2
0	0	3.83	7.02
1	1.84	5.33	8.53
2	3.05	6.71	9.96

Values of the roots $\cdot \dfrac{d\, J_m(k_{mn}\, r)}{dr} = 0$

The frequencies are:

$$\Omega_{\alpha}^{(10)} = \sqrt{k_{\ell}^2 + k_{mn}^2} \tag{3.78}$$

and conversion to a dimensional form gives

$$f' = \frac{a_o}{2\pi R} \sqrt{k_{\ell}^2 + k_{mn}^2} \quad (Hz) \tag{3.79}$$

The normalization constants for either standing or traveling waves are:

$$E_{\alpha}^2 = \frac{L\pi}{2R} \left[1 + \frac{\sin \ell\pi}{\ell\pi}\right] \begin{cases} \left[J_o^2 (k_{on}) + J_1^2 (k_{on})\right] & m = 0 \\ \frac{1}{2}\left(1 - \frac{m^2}{k_{mn}^2}\right) J_m^2 (k_{mn}) & m \neq 0 \end{cases} \tag{3.80}$$

With Eqs. 3.22a, 3.53, and 3.76, we can easily write out a pressure wave equation in the form shown in Eq. 3.14d with the growth rate of acoustic wave, Λ, yet to be determined.

3.4 Growth of Acoustic Wave

In the previous section, the pressure wave equation in cylindrical chambers was derived. Rewriting these equations, we have

$$k = \Omega + j\Lambda \tag{3.23}$$

and Ω represents the oscillation frequency, Λ represents the growth or

decay of the oscillatory wave. We also derived

$$\Omega = \Omega^{(10)} + \nu\Omega^{(11)} + \nu^2\Omega^{(12)} + \ldots \tag{3.67}$$

$$\Lambda = \Lambda^{(10)} + \nu\Lambda^{(11)} + \nu^2\Lambda^{(12)} + \ldots \tag{3.68}$$

of which

$$\Lambda^{(10)} = 0 \tag{3.70}$$

$$\Omega^{(10)} = k_N \tag{3.71}$$

$$\Omega^{(11)} = \frac{1}{2k_n E_N^2} R\left[\int_v g^{(10)}\ \psi_N^*\ dv + \int_s h^{(10)}\ \psi_N^*\ ds\right] \tag{3.72}$$

$$\Lambda^{(11)} = \frac{1}{2k_N E_N^2} I\left[\int_v g^{(10)}\ \psi_N^*\ dv + \int_s h^{(10)}\ \psi_N^*\ ds\right] \tag{3.73}$$

with ψ_N representing the pressure wave. Substituting $\gamma p^{(10)}$ for ψ_N and for first order ν, we can write

$$k = \Omega^{(10)} + \nu\left[\Omega^{(11)} + j\Lambda^{(11)}\right] + 0\left[\nu^2\right] \tag{3.81}$$

where $0\left[\nu^2\right]$ represents higher order ν terms. Using Eqs. 3.72 and 3.73, we obtain

$$\Omega^{(11)} + \Lambda^{(11)} = \frac{(R + jI)}{2\Omega^{(10)} E_\alpha^2}\left[\int_v g^{(10)}\ p^{(10)*} dv + \int_s h^{(10)}\ p^{(10)*} ds\right] \tag{3.82}$$

So the determination of growth rate $\Lambda^{(11)}$ and the oscillation frequency $\Omega^{(11)}$ reduces to the evaluation of volume integral over the chamber and surface integral over the burning surface. To further simplify the integration, we recall that

$$g^{(1)} = \left\{ jk\left(\underline{U} \cdot \nabla p^{(1)}\right) - \nabla \cdot \left(\underline{U} \cdot \nabla q^{(1)} + q^{(1)} \cdot \nabla \underline{U}\right) + \left(\frac{\lambda}{\nu}\right) \nabla \cdot f^{(1)} \right\} \tag{3.25}$$

$$h^{(1)} = \left\{ jkAp^{(1)} + \hat{n} \cdot \gamma \left[\underline{U} \cdot \nabla q^{(1)} + q^{(1)} \cdot \nabla \underline{U} - \left(\frac{\lambda}{\nu}\right) f^{(1)} \right] \right\} \tag{3.31}$$

For the first integral of Eq. 3.82, substituting Eq. 3.25, we have

$$I_1 = \int_v g^{(10)}\, p^{(10)*} dv$$

$$= \int_v jk\left(\underline{U} \cdot \nabla p^{(10)}\right) dv - \int_v \nabla \cdot \left(\underline{U} \cdot \nabla q^{(10)} + q^{(10)} \cdot \nabla \underline{U}\right) p^{(10)*} dv$$

$$+ \int_v \left(\frac{\lambda}{\nu}\right) \nabla \cdot f^{(10)}\, p^{(10)*} dv$$

$$= \int_v jk \left(\underline{U} \cdot \nabla p^{(10)*} dv - \int_v \frac{j}{k_N} p^{(10)*}\, \nabla^2\, \underline{U} \cdot \nabla p^{(10)} \right) dv$$

$$+ \left(\frac{\lambda}{\nu}\right) \int_v p^{(10)*}\, \nabla \cdot f^{(10)} dv \tag{3.83}$$

Using Green's theorem, the second term can be expanded into the form

$$\int_v \frac{j}{k_N} p^{(10)*} \nabla^2 \left(\underline{U} \cdot p^{(10)} \right) dv = \int_v \frac{j}{k_N} \underline{U} \cdot \nabla p^{(10)} \nabla^2 \left(p^{(10)*} \right) dv$$

$$+ \int_s \frac{j}{k_N} \left\{ p^{(10)*} \nabla \left(\underline{U} \cdot \nabla p^{(10)} \right) - \left(\underline{U} \cdot \nabla p^{(10)} \right) p^{(10)*} \right\} \cdot \hat{n} \, ds \tag{3.84}$$

Recalling that

$$\nabla^2 p^{(10)} = -k_N^2 \, p^{(10)} \tag{3.56}$$

$$\hat{n} \cdot p^{(10)} = 0 \quad \text{at the boundary} \tag{3.57}$$

we have

$$I_1 = 2jk_N \int_v \left(p^{(10)} \right)^* \underline{U} \cdot \nabla p^{(10)} dv - \frac{j}{k_N} \int_s \left[\left(p^{(10)} \right)^* \nabla \left(\underline{U} \cdot \nabla p^{(10)} \right) \right] \cdot \hat{n} \, ds$$

$$+ \frac{\lambda}{\nu} \int_v \left(p^{(10)} \right)^* \nabla \cdot f^{(10)} \, dv \tag{3.85}$$

In similar fashion the second integral of Eq. 3.82 leads to

$$I_2 = \int_s h^{(10)} \, p^{(10)*} ds$$

$$= \int_s -jk_N A p^{(10)} \left(p^{(10)} \right)^* ds + \int_s \frac{j}{k_N} \hat{n} \cdot \nabla \left(\underline{U} \cdot \nabla p^{(10)} \right) \left(p^{(10)*} \right) ds -$$

$$- \left(\frac{\lambda}{\nu}\right) \int_s f^{(10)} \, p^{(10)*} \cdot \hat{n} \, ds \qquad (3.86)$$

Recall that A is an admittance function with real and imaginary parts as shown in Eq. 3.26. When applied to the burning surface, we can write A as $A = A_b^r + jA_b^i$.

Substituting Eqs. 3.85 and 3.86 into Eq. 3.82, again using Green's theorem, we get:

$$\Omega^{(11)} + \Lambda^{(11)} = \frac{R + jI}{E_\alpha^2} \left[j \int_v \left(p^{(10)}\right)^* \underline{U} \cdot \nabla p^{(10)} \, dv - j\left(A_b^r + jA_b^i\right) \right.$$

$$\left. \cdot \int_s \frac{p^{(10)} \, p^{(10)*}}{2} \, ds - \left(\frac{\lambda}{\nu}\right) \frac{1}{2k_N} \int_v f^{(10)} \cdot \nabla p^{(10)*} dv \right] \qquad (3.87)$$

The first term can be written as

$$\int_v p^{(10)*} \, U \cdot \nabla p^{(10)} dv = \int_v \underline{U} \cdot \frac{p^{(10)*} \, p^{(10)}}{2} \, dv$$

$$= \int_s \left[\frac{p^{(10)*} \, p^{(10)}}{2} \right] \underline{U} \cdot \hat{n} \, ds \qquad (3.88)$$

This represents the average convection of energy into the system by the mean flow, where the $\left(p^{(10)*} \, p^{(10)}\right)/2$ term is just a measure of energy per unit volume. The second term,

$$-j\left(A_b^r + jA_b^i\right)\int_s \frac{p^{(10)*}\, p^{(10)}}{2}\, ds \qquad (3.89)$$

represents the work input associated with the oscillatory combustion, and the last term reflects work done on the system by the body force or other additional forces.

Therefore the growth rate of the acoustic wave Λ can be expressed as:

$$\Lambda = \frac{\nu}{E_\alpha^2}\int_s \left[\underline{U}\cdot\hat{n} - A_b^r\right]\frac{p^{(10)*}\, p^{(10)}}{2}\, ds + \sum_{d=1}^{N}\Lambda_d \qquad (3.90)$$

where Λ_d is one of N damping factors including dissipation due to aluminum oxide particles, viscous losses, energy lost due to visco-elastic motion of propellant grain.

The term with the integral over the burning surface can be referred to as Λ_{gain} since it represents the source of driving energy for acoustic waves. In this term it includes the driving effects of combustion as represented by the admittance function, driving of wave motion by the mean flow, and dissipation due to flow of acoustic energy through the nozzle. It is important that all effects which drive oscillation be reduced to a surface integral over the combustion chamber. Thus, once the mode shapes, $p^{(10)}$, for the chamber have been determined, a simple integration is all that is required to determine the driving effects. Note that $\underline{U}\cdot\hat{n}$ is simply the flow velocity normal to the chamber surface; this quantity is readily calculated at

the burning surface in terms of propellant burning rate and is zero on inhibited surfaces.

3.4.1 Discussion of Acoustic Gain

From Eq. 3.90, the gain expression of acoustic waves can be written as:

$$\Lambda_{gain} = \frac{\nu}{E_\alpha^2} \int_S \left[\underline{U} \cdot \hat{n} - A_b^r \right] \frac{p^{(10)*} \, p^{(10)}}{2} \, ds \tag{3.91}$$

with E_α^2 defined as in Eq. 3.80.

To write pressure wave in its fundamental mode, i.e., $\alpha = (0, 0, 1)$, use Eqs. 3.76 and 3.77 to get

$$p^{(10)}_{(0,0,1)} = \cos\left(\frac{\pi R}{L} z\right) \tag{3.92}$$

R, L and z are all dimensionless quantities as defined on p. 41 shortly after Eq. 3.75. Also using the boundary conditions defined in Eq. 3.77, rewriting Eq. 3.80 with $m = n = 0$, $\ell = 1$, we have

$$\Lambda_{gain} = \frac{\nu 2R}{L\pi} \int_S \left[\underline{U} \cdot \hat{n} - A_b^r \right] \cos^2\left(\frac{\pi R}{L} z\right) ds \tag{3.93}$$

Since in cylindrical coordinates $ds = r dr d\phi$, carrying out the integral, we get

$$\Lambda_{gain} = \frac{\nu R}{L} \left(\underline{U} \cdot \hat{n} - A_b^r \right) \cos^2\left(\frac{\pi R}{L} z\right) \tag{3.94}$$

Now, if we summarize the derivation of time dependent preasure wave expresaion for the fundamental mode, we get

$$P_{(z,t)} = P_o + \varepsilon(P_o\gamma)\, e^{-\nu\Lambda^{(11)}t} \cos\left(\pi \frac{R}{L} z\right) \cos\left(\frac{\pi a_o}{L}\right) t' \tag{3.95}$$

where t is a dimensionless quantity and t' ia dimensional. Examining Eq. 3.95 we can see that the term $\left(\underline{U} \cdot \hat{n} - A_b^r\right)$ in Eq. 3.94 plays a very important role in determining the growth or decay of an acoustic wave inside the combustion chamber.

At the present time, the data for the calculation of A_r at the burning surface are very limited. Figure 3.1 shows some experimental results by Angelus[29] for doublebased propellant and the calculated curve by Culick[30] for hollow cylindrically caat propellant. Both results are for very high pressure compared to present work. However, for oscillation frequency on the order of kilohertz, the value of A_r is more than likely to be a small or even negative number.

3.4.2 Discussion of Acoustic Loss

The decrease of acoustic energy in the combustion chamber of a rocket motor can be ascribed either to losses in the medium or to losses occurring at the system boundaries. Various losses and their magnitudes were compiled by Buffman, Dehority, Slates, and Price.[31] Table 3.2 shows these results in terms of present notation.

From this table it is clearly seen that nozzle loss is the most important one. Also, in Buffman, et al., it is suggested experimentally

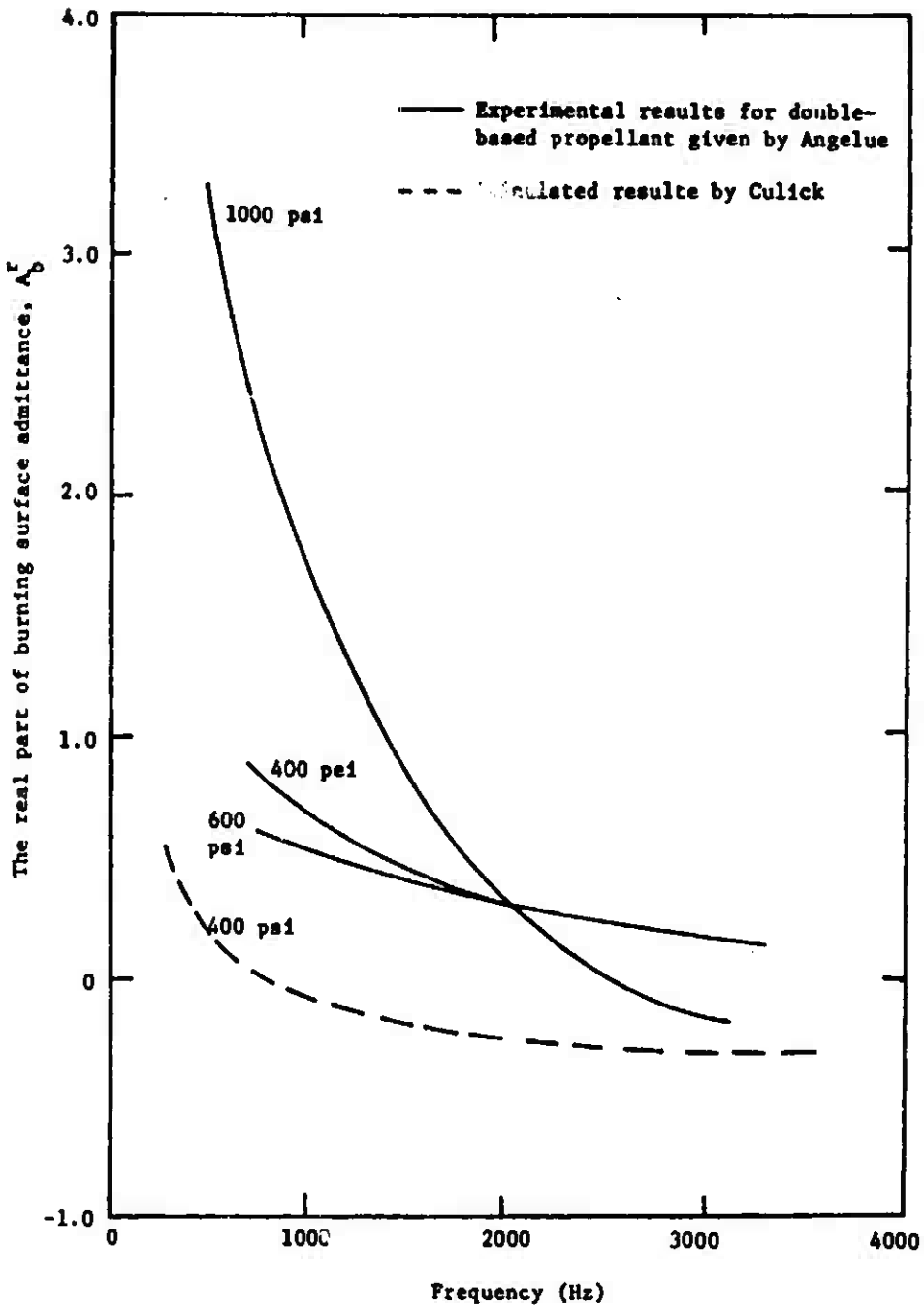

Fig. 3.1. Response of a burning propellant to steady pressure oscillations. (After F. E. C. Culick.)

Tsble 3.2. Mechanisms contributing to acoustic losses.

	$\nu\Lambda_d\left(\frac{a_o}{L}\right)\ (sec^{-1})$
Losses in the medium (or bulk losses):	
Viscous bulk losses Heat conduction bulk losses	<0.0014
Molecular relaxation bulk losses	<0.6
Inhomogeneous media bulk losses	~0
Losses at the system boundaries (or wall losses):	
Viscous wall losses Heat conduction wsll losses	~5
Acoustic radiation losses to the walls	~0
Absorption losses to the porous plste	~0
Transmission losses through the nozzle	50 to 600

that the longitudinal wave nozzle loss term can be written, in present notation, as:

$$\frac{\nu}{E^2_{(001)}} \int_{\text{nozzle}} \left[\underline{U} \cdot \hat{n} - A_r\right] \frac{p^{(10)*}\, p^{(10)}}{2}\, ds \simeq (1.58)\, J \qquad (3.96)$$

$$\alpha = (0,\ 0,\ 1)$$

of which

$$J = \frac{\text{nozzle throat area}}{\text{channel area at nozzle entrance}}$$

For a wave transverse to the chamber axis, Culick[27] proved that nozzle admittance may be taken to be identically zero.

Particle damping by aluminum oxide smoke is also an important loss mechanism and should be included in the calculation. Culick[27] adapted the work of Epstein and Carhart[32] to this problem and found:

$$\left[\Lambda_d\right]_{particles} = \begin{cases} \frac{4}{9}\,\delta_o \left(\frac{\rho_s}{\rho_o}\right)^2 \left(\frac{R_s^2\omega}{2\nu_o}\right)^2 & \text{for small particles, } \frac{\omega R_s^2}{2\nu_o} << \frac{9\rho_o}{4\rho_s} \\ \frac{9}{4}\,\delta_o & \text{for medium particles, } \frac{9\rho_o}{4\rho_s} << \frac{\omega R_s^2}{2\nu_o} << 1 \\ \frac{9}{4}\,\delta_o \left[\frac{R_s^2\omega}{2\nu_o}\right]^{1/2} & \text{for large particles, } 1 << \frac{\omega R_s^2}{2\nu_o} \end{cases} \tag{3.97}$$

where

$$\delta_o = \frac{\rho_o}{\rho_s} \frac{C_m \nu_o \Omega^{(\omega)}}{\omega R_s^2} .$$

and

ρ_o = average gas density

ρ_s = average solid density

C_m = mass fraction of solid particles (or liquid particles) in the combustion gases

ν_o = kinematic viscosity

ω = circular frequency of wave motion = $\Omega^{(10)}\left(a_o/L\right)$

R_s = average radius of solid particles

Other loss characteristics of potential importance were investigated during the past. Hart, McClure, and Bird[33] made a thorough study of the damping due to the viscoelastic motion of the chamber boundary. The interaction of acoustics with the burning propellant surface was studied by Hart and Cantrell.[34] Sound wave attenuation in a doublebased solid propellant was investigated by Nall.[35] For the present work, only losses due to nozzle and particle damping will be considered.

IV. HEAT LOSS INSIDE COMBUSTION CHAMBER

In this chapter, both conducting and radiating heat loss inside the combustion chamber of a rocket motor were investigated in a very primitive form. Due to the complexity of the combustion process and mass and heat transfer phenomena, several important assumptions were made to reduce the task to a workable form. These assumptions include the combustion system as well as some gas properties.

To theoretically predict the temperature profile away from the burning surface of solid propellant inside the rocket combustion chamber is almost impossible without some assumptions about the combustion system and the properties of the gas. In this study, the solid propellant is assumed to be burned uniformly and the burning surface is always normal to the longitudinal axis of the combustion chamber. At any cross section, the gas temperature is assumed to be constant from the center to the edge of the gas column. Considering the burning surface covers the entire cylinder, this assumption is a good one. Limited by the available data, some properties of the gas have to be assumed. These properties include the flow velocity, viscosity, specific heat ratio, heat transfer coefficient, and emissivity of the gas.

Consider a heat flow system with the fluid flow inside a heat-conducting cylindrical conduit. Assume the inside wall temperature is room temperature before the gas passes through, and the fluid temperature is much higher than the room temperature. The heat losses when fluid flows through the conduit are due to conduction as well as to radiation.

The conduction heat loss across the solid-fluid interface is dependent on the area of the interface and the temperature difference between them. Hence we can write the heat flow out of the fluid due to conduction, Q_c, as

$$Q_c = hA\Delta T \tag{4.1}$$

where h is the heat transfer coefficient, A is the interface area, and ΔT is the temperature difference. Rewriting Eq. 4.1 and referring to Fig. 4.1, we have

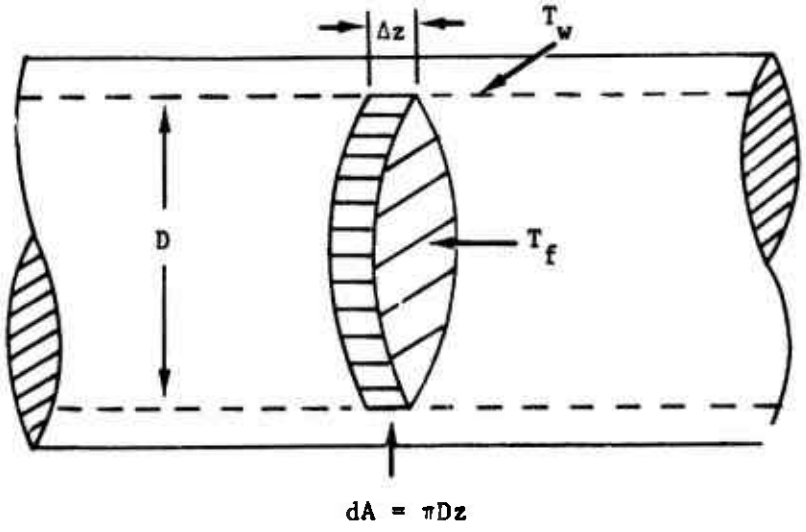

Fig. 4.1. Heat transfer in a circular tube.

$$dQ_c = h(\pi Ddz)\left(T_f - T_w\right) \tag{4.2}$$

T_f is the fluid temperature and T_w is the inside wall temperature of the conduit.

The gas generating rate, G, of burning propellant is defined as

$$G = \rho A \bar{U} \tag{4.3}$$

where ρ is the density of the solid propellant, A_b is the burning area, and $\bar{U}$ is the burning rate of the propellant.

As the gas travels down the conduit, the heat transfer phenomena can be described as

$$GC_p dT_f = \pi Dh \left(T_f - T_w\right) dz \tag{4.4}$$

where C_p is the specific heat at a constant pressure. Simplifying Eq. 4.4, we get

$$dT_f = \frac{4}{D} \frac{h}{[\rho \bar{U}]C_p} \left(T_f - T_w\right) \tag{4.5}$$

For the combustion chamber, a good average value for the term $h/[\rho \bar{U}]C_p$ was picked,[36] and Eq. 4.5 rewritten as

$$dT_f = \frac{4}{D} 0.023 \, N_{Re}^{-0.2} \left(T_f - T_w\right) dz \tag{4.6}$$

where N_{Re} is the Reynolds number which can be written as

$$N_{Re} = \frac{\rho \bar{U} D}{\mu} \tag{4.7}$$

where μ is the viscosity of the gas.

Besides the heat transferred by conduction to the rocket casing

from burned gas, heat also radiated into the solid steel chamber. This probably is a more important parameter to be considered. Unfortunately, due to the complicated gas composition, it is almost impossible for us to estimate the total emissivity of the gas. With a different amount of seeded aluminum, the emissivity should be considerably different. For a simple heat radiating case, as suggested by most transport phenomena books,[37] we can write

$$Q_r = \sigma \varepsilon A (\Delta T)^4 \tag{4.8}$$

where Q_r is the heat flow out of gas due to radiation, σ is Stefan-Boltzmann constant, ε is emissivity, and A is the interface area. ΔT is the temperature difference between fluid and wall. Since wall temperature is considerably lower than fluid temperature, it is reasonable to let $(\Delta T)^4 = T_f^4$.

Writing Eq. 4.8 in differential form, and also referring to Fig. 4.1, we have

$$GC_p dT = \sigma \varepsilon T_f^4 \pi D \, dz \tag{4.9}$$

Theoretically, we can combine Eqs. 4.6 and 4.9 to get the total temperature change as a function of distance; e.g.,

$$dT_f = \left[\frac{4}{D} 0.023 \, N_{Re}^{-0.2} \left(T_f - T_w \right) + \frac{\sigma \varepsilon \pi D}{GC_p} T_f^4 \right] dz \tag{4.10}$$

A simple integration will give us a linear relation between temperature and distance. The linear relation is more or less unrealistic.

This is due to the assumption that the wall temperature stays constant and becomes a lossy section only when gas passes through.

Another way to estimate the temperature change inside the combustion chamber is to consider the temperature difference between the chamber and nozzle exit. Assuming M is the Mach number at the nozzle, the ratio of chamber temperature T_f to the nozzle gas temperature, T^*, is derived as[38]

$$\frac{T_f}{T^*} = 1 + \frac{\gamma + 1}{2} M^2 \qquad (4.11)$$

where γ is the specific heat ratio. Knowing the chamber length and with the assumption that heat loss is uniformly distributed over the entire length of the combustion chamber, the heat loss due to a certain length section can be roughly decided.

V. APPLICATION OF THE THEORY

In Chapters II, III, and IV the wave attenuation equation, pressure wave oscillation equation, and heat loss equation were derived in a general form. In this chapter, each of the equations is applied to the rocket motor designed for this investigation. The test unit will be discussed first, since all the calculations and assumptions are based on it. Second, the gas composition inside the rocket chamber will be listed. With these data, the attenuation equation can be calculated. Following is the calculation of acoustic wave gain and loss term. The amplitude and frequency for a specific mode will be presented. Finally, the temperature profile away from the burning surface inside the combustion chamber will be calculated.

5.1 Test Unit

5.1.1 Experimental Setup

Figure 5.1 shows two photographs of the test rocket motor setup used in this investigation. The construction of the motor is shown in detail in Fig. 5.2. The system connection schematic is shown by the block diagram in Fig. 5.3.

The microwave portion of the test unit consisted of a klystron with its power supply. The klystron is connected to a horn antenna through an attenuator and frequency meter. A dielectric lens is inserted into the horn to focus the microwave output. After passing through the rocket motor, the K-band signal was then picked up by the antenna on the opposite side. Two separate channels were fed into the

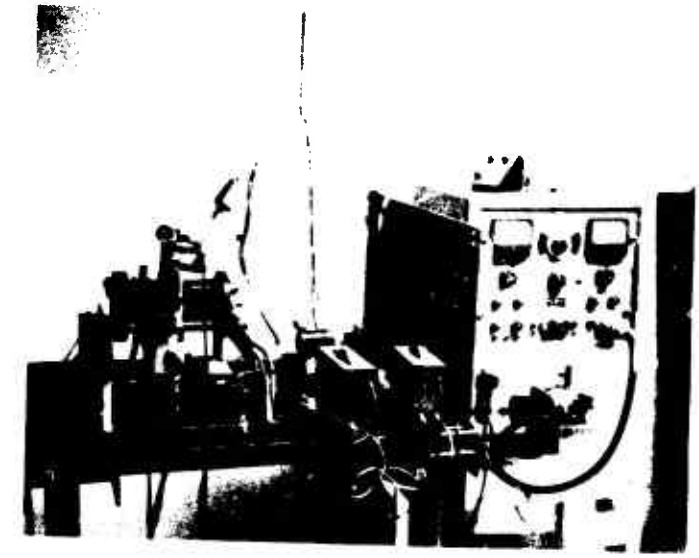

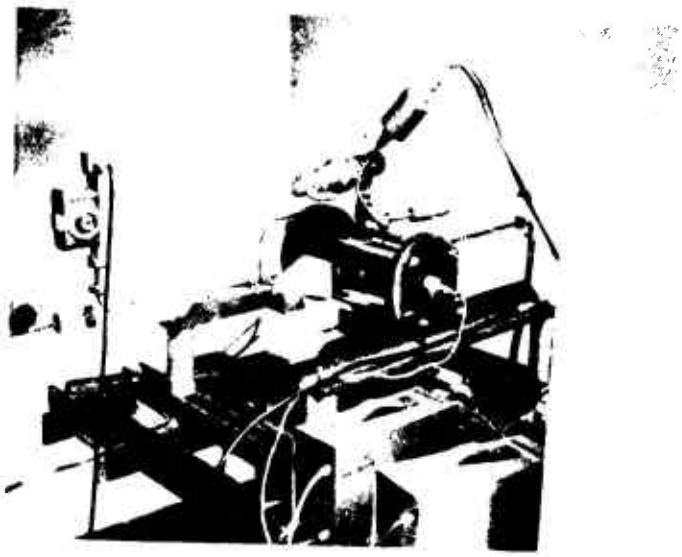

Fig. 5.1. Photographs of the test unit.

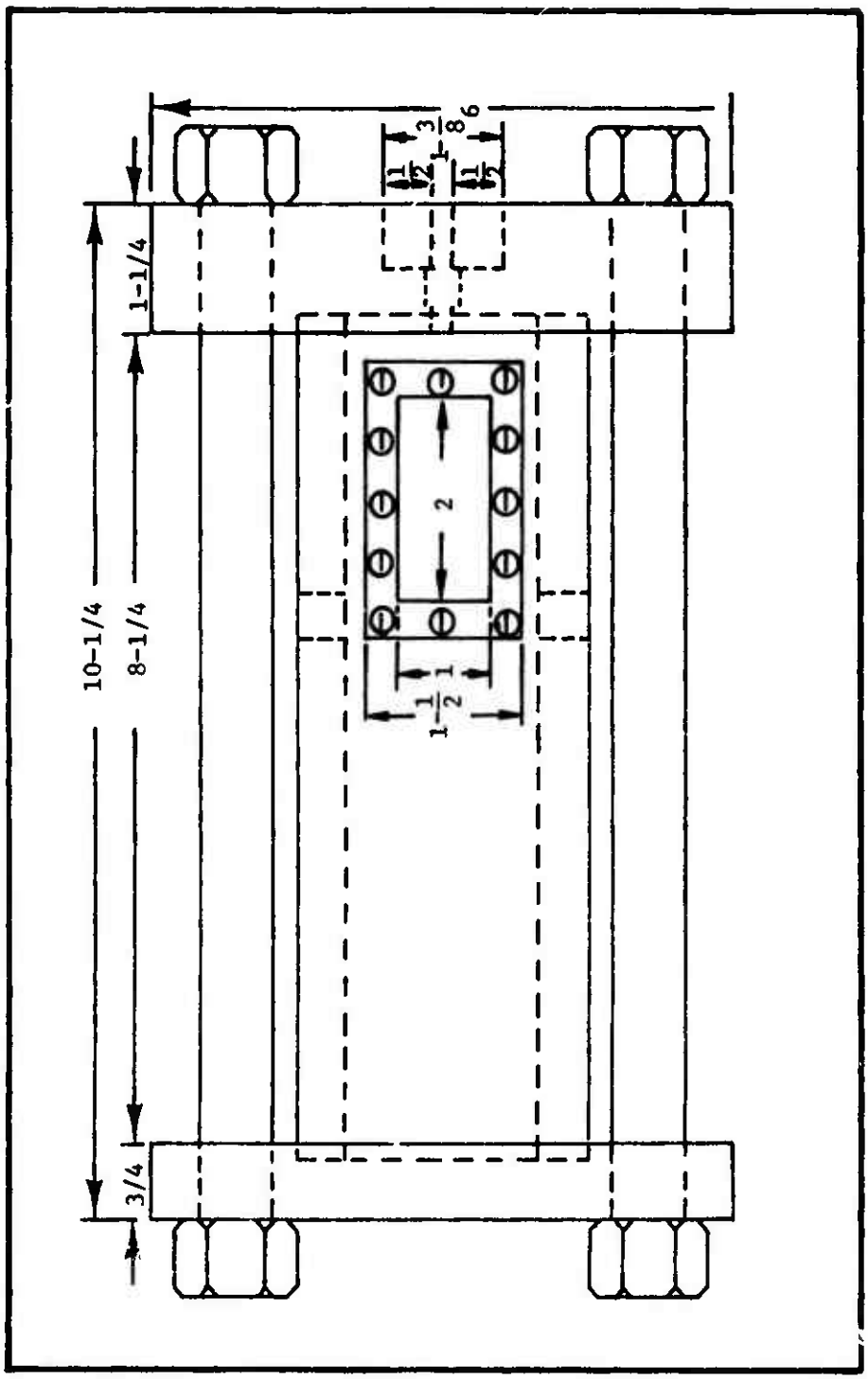

Fig. 5.2. Detail drawing of a rocket motor.

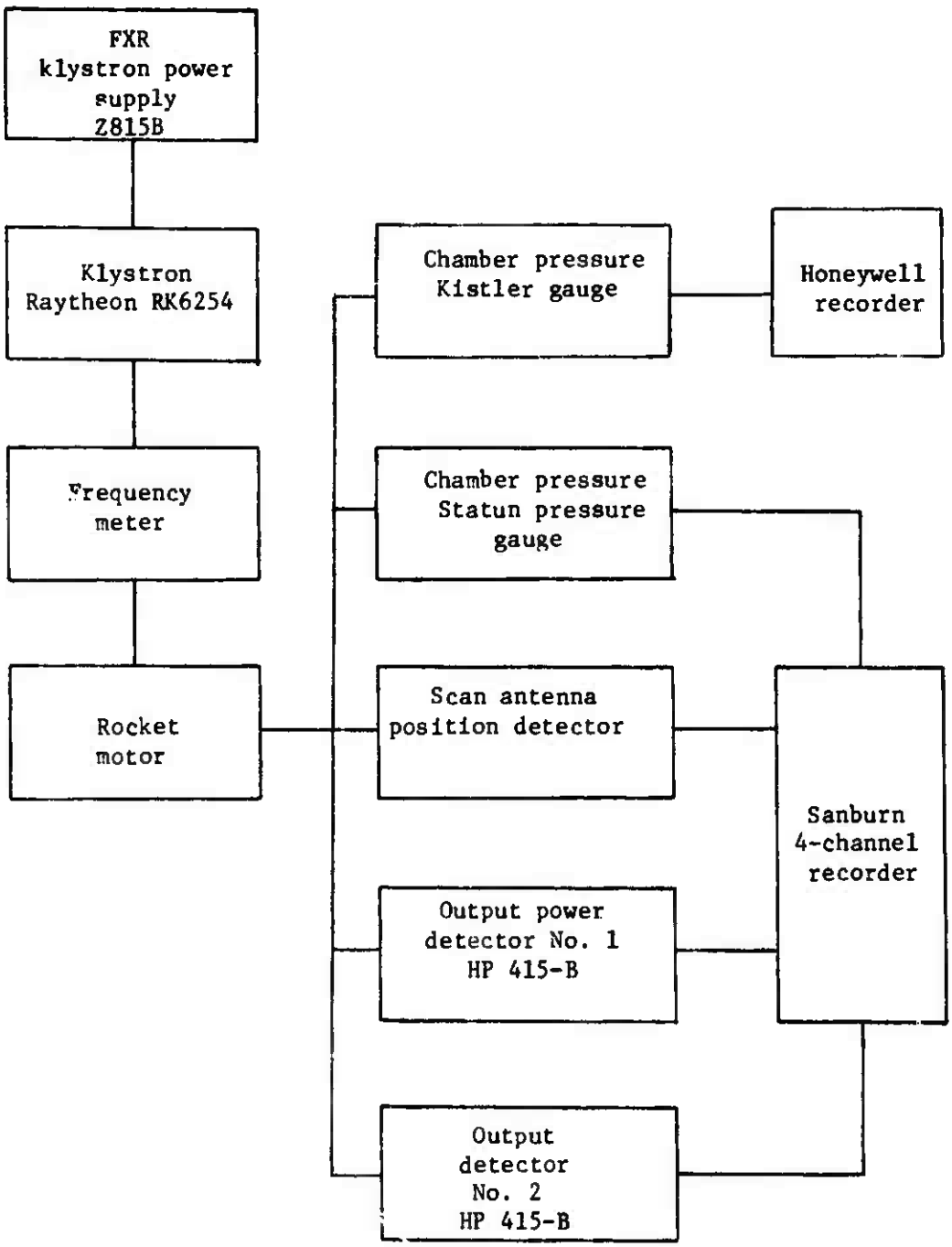

Fig. 5.3. Block diagram of experimental setup.

recorder to cover a rsnge of 0 to 38 dB attenuation. The recording signal was then registered on a four-chsnnel Sanborn strip recorder together with one channel of mean pressure and position of the antenna.

The mean pressure that wss fed into the Ssnborn recorder was detected by a Statun pressure gauge which was mounted on top of the rocket motor. A Kistler pressure gauge was mounted along with the Statun pressure gauge and fed into a Honeywell recorder as a back-up recorder in case of failure of the Statun gauge. These arrangements are shown in Fig. 5.1.

5.1.2 Dielectric Lens Design

Two polyethelene dielectric lenses were designed to fit into the horn antenna thst was originally designed by Hwang.[39] The lens gives a beam width of 4.32 mm in rsdius at the focsl point three inches away from the horn surface. The E-field rsdiation pattern is shown in Fig. 5.4. The theory psrt of the design was given by Hwang.[40] Physical dimensions of this lens are shown in Fig. 5.5.

5.1.3 Sample Prepsration

The propellant used in this investigation was prepared by the personnel of the Department of Chemical Engineering, University of Utah, Salt Lake City, Utah. The propellant was mixed and cast under the following specifications:

Mixing temperature	65° C
Mixing pressure	0.3" Hg

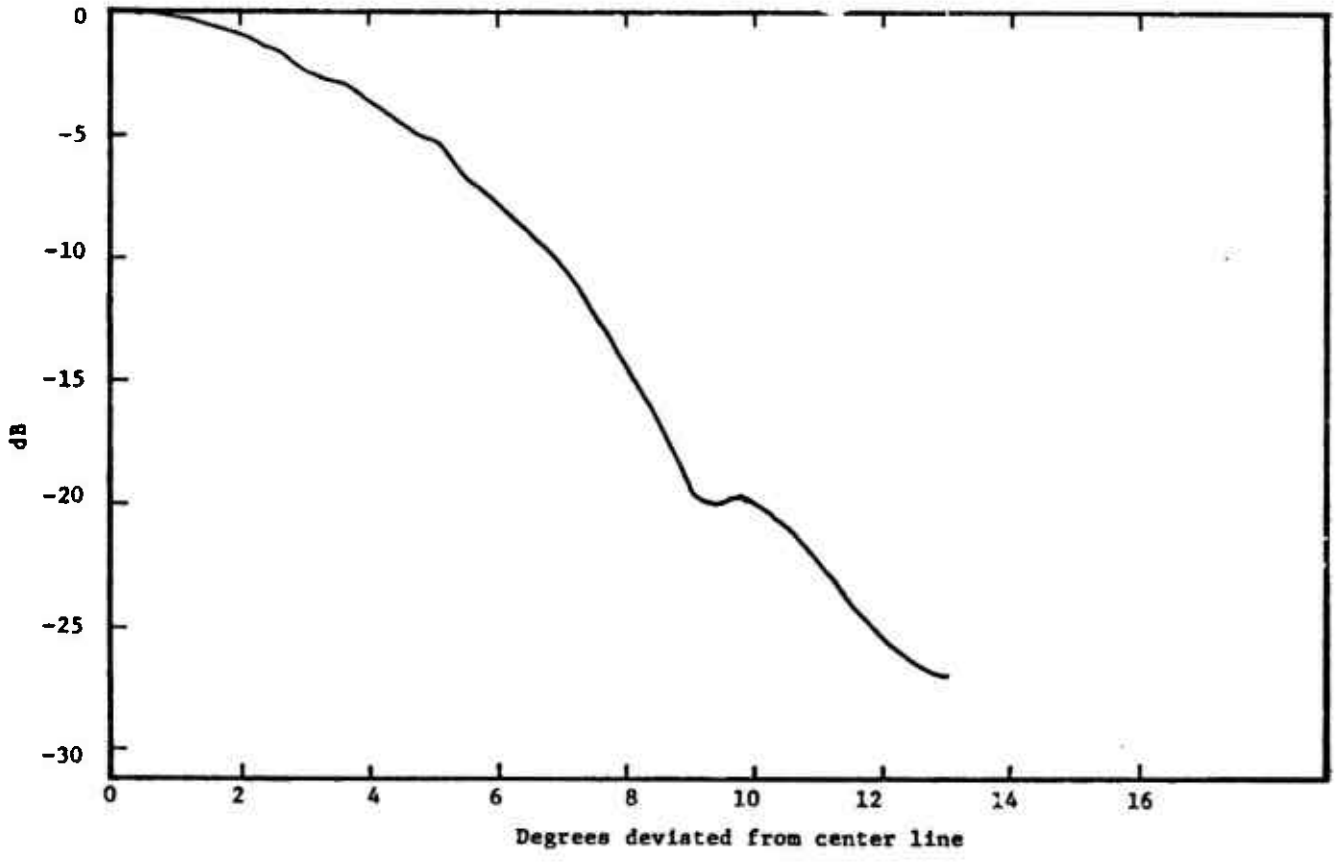

Fig. 5.4. E-field radiation pattern of horn antenna with dielectric lens.

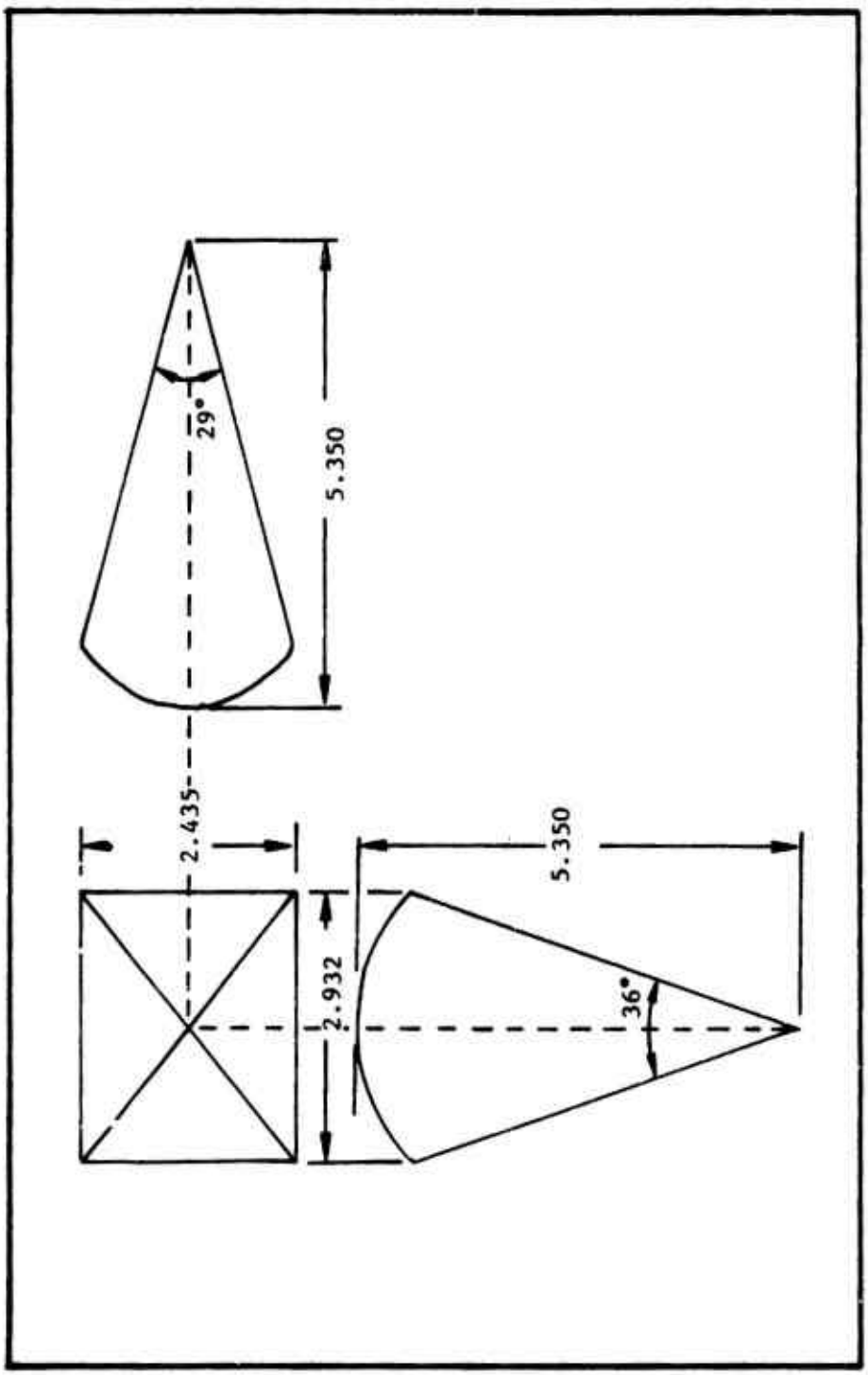

Fig. 5.5. Dielectric insert for horn antenna.

Mixing time	55 minutes
Casting preasure	0.3" Hg
Curing temperature	88° C
Curing time	7 days

The chemical composition of different propellants uaed in the experiment is listed in Table 5.1.

Table 5.1. Propellant composition (weight percentage).

Batch	Coarse[1] NH_4ClO_4	15 micron NH_4ClO_4	KP[2]	PBAA[3]	EPON282[4]	Al[5]
1	38.5	38.5	5	15.3	2.7	0
2	36.0	36.0	5	15.3	2.7	5
3	26.8	40.2	5	15.3	2.7	10
4	18.6	43.4	5	15.3	2.7	15

1 -- Coarse ammonium perchlorate particle size ~200 μ.

2 -- KP: potassium perchlorate particle size ~100 μ.

3 -- PBAA: polybutadiene-acrylic acid copolymer.

4 -- EPON282: epoxy resin.

5 -- Al: aluminum particle size ~5 μ.

The propellant was cast in the shape of a 2" diameter cylinder. Since the shrinkage from curing temperature to room temperature was 0.5 percent,[41] it fit in the 2" diameter rocket motor.[42] Moreover, because a uniform burning surface is desired, a thin layer of silicone

grease (Dow Corning Compound 11) was coated on the back and side of the grain to prevent burning. This also sealed the space between the propellant and the rocket motor.

5.2 Plasma Composition

The calculation of plasma composition is based on a computer program furnished to the University of Utah by the United States Air Force Rocket Propulsion Laboratory at Edwards Air Force Base in California. For a given chemical composition of propellant and combustion pressure, this program will print out all the equilibrium constants and chemical components of the resulting gases. For the propellant composition listed in Table 5.1, the gas composition is listed in Appendix I for various chamber pressures of interest. The equilibrium chamber temperature given by this program is listed in Table 5.2.

5.3 Computer Program for Calculating Wave Attenuation

The solution of the plasma attenuation equation was carried out on the Univac 1108 computer at the University of Utah Computer Center. The program listing is given in Appendix II. The program listing is divided into three major parts:

1. Initialization of constants representing a specific condition of gas and electron temperature.
2. Calculation of the mean velocity terms B and D, electron density, and attenuation.
3. Printing the calculated attenuation and other pertinent parameters of the plasma.

Table 5.2. Combustion chamber equilibrium temperature predicted.

Chamber Presaure psi	Aluminum Contained		
	5%	10%	15%
5	2569	2692	2764
10	2639	2744	2822
15	2663	2774	2856
20	2680	2794	2879
40	2717	2841	2934
60	2737	2867	2965
80	2750	2885	2986
100	2760	2898	3002
120	2767	2908	3014

5.3.1 Initialization of Constants

The initialization section definea physical constants such as frequency, velocity of light, etc., and then reada from the data deck the mole fraction concentrations of the important constituenta of the combustion. Values used for the representative mole fractiona were taken from a free energy analysis of the combustion. For the propellant compositions and chamber pressure described earlier in this report, more than 98 percent of the equilibrium mass is accounted for by six gaseous species:

1. Diatomic hydrogen
2. Water

3. Diatomic nitrogen

4. Carbon monoxide

5. Carbon dioxide

6. Hydrogen chloride

The mole fractions for these constituents were taken from the program printout and constitute the values in the summation of Eq. 2.29, which expression is used in the calculation of the mean velocity terms B and D.

After the data are read in, the temperature is initialized at 2000 degrees absolute. This temperature does not represent the equilibrium temperature of the gas predicted by the free energy analysis, but it merely serves as a starting reference temperature for attenuation calculations. During steady-state conditions of combustion, it can be assumed that the electrons and gas are in thermal equilibrium, yet it is conceivable that in a transient situation, the temperature could change from the equilibrium value and alter the attenuation. For this reason, a range of temperatures in a neighborhood about the equilibrium gas temperature is used; hence, for a given gas state, a number of attenuations will be calculated for a group of surrounding temperatures. Two other chemical concentrations are read from the data deck. These are the equilibrium amounts of potassium and chlorine, the assumed source and sink of electrons, respectively.

5.3.2 Calculation of Attenuation Quantities

After the physical constants of the plasma have been defined, it is necessary to calculate three quantities:

1. The mean velocity terms B and D.

2. The number denaity of electrona.

3. The theoretical attenuation itself.

First is the evaluation of the integrala of B and D from Eqs. 2.41 and 2.42. The integrands are continuous, positive functions, and the integrals are easily evaluated by a simple trapezoidal method.

The number density of free electrons is next determined from Eq. 2.53 using a subroutine to solve for the roots of the cubic equation. It must be ststed that for some outlying temperatures, the coefficients of the cubic equation were such that round-off error in the cubic calculations gsve no positive real roots. This fact is equivalent to the obviously nonphysical situation of assuming a temperature far away from the equilibrium value. The relatively large amount of chlorine compared to potassium rendered the cubic equation root locus sensitive to lower than equilibrium temperatures. The occurrence of no positive solutions was not felt important because the temperatures giving no roots were alwaya more than one hundred degrees from the indicated equilibrium value.

Early in the experiments of this investigation, it was seen that the assumption of no electron sinks gave predicted attenuations that were much larger than those observed in the test motor; therefore, the use of Saha's equation will be assumed incorrect, and the computer program uses only the cubic expression to determine the electron density.

5.3.3 Theoretical Reaulta

From the calculated attenuations of the computer program and the equilibrium temperatures predicted by the Air Force program, three plasma attenuation characteristics may be derived. One set of curves represents nonequilibrium states of the plasma and is a graph of attenuation versus temperature over a temperature range about equilibrium. The other two graphs are for an assumed equilibrium state, predicted by the Air Force program; one shows attenuation versus temperature for the various compositions of propellant, and the other shows attenuation versua pressure for different amounts of aluminum contained.

Figures 5.6 through 5.9 are plots of the nonequilibrium states of the plasma taken directly from the values printed by the attenuation program for the different concentration of aluminum. From these graphs, it is seen that the predicted attenuation is a strong function of both the aluminum content and pressure. Also these graphs clearly show how much attenuation is to be expected for a given K-band signal incident upon a 3.975-inch cross section of homogeneous plasma of assumed composition at a certain pressure.

Figure 5.10 shows the theoretical attenuation versus temperature for the equilibrium condition. From the lines of constant pressure that are shown, it is again seen that the attenuation is a strong function of pressure and aluminum contained.

Also in Fig. 5.10, the pressure range lowered to 5 psi to show that wave attenuation peaks up in the vicinity of one atmosphere

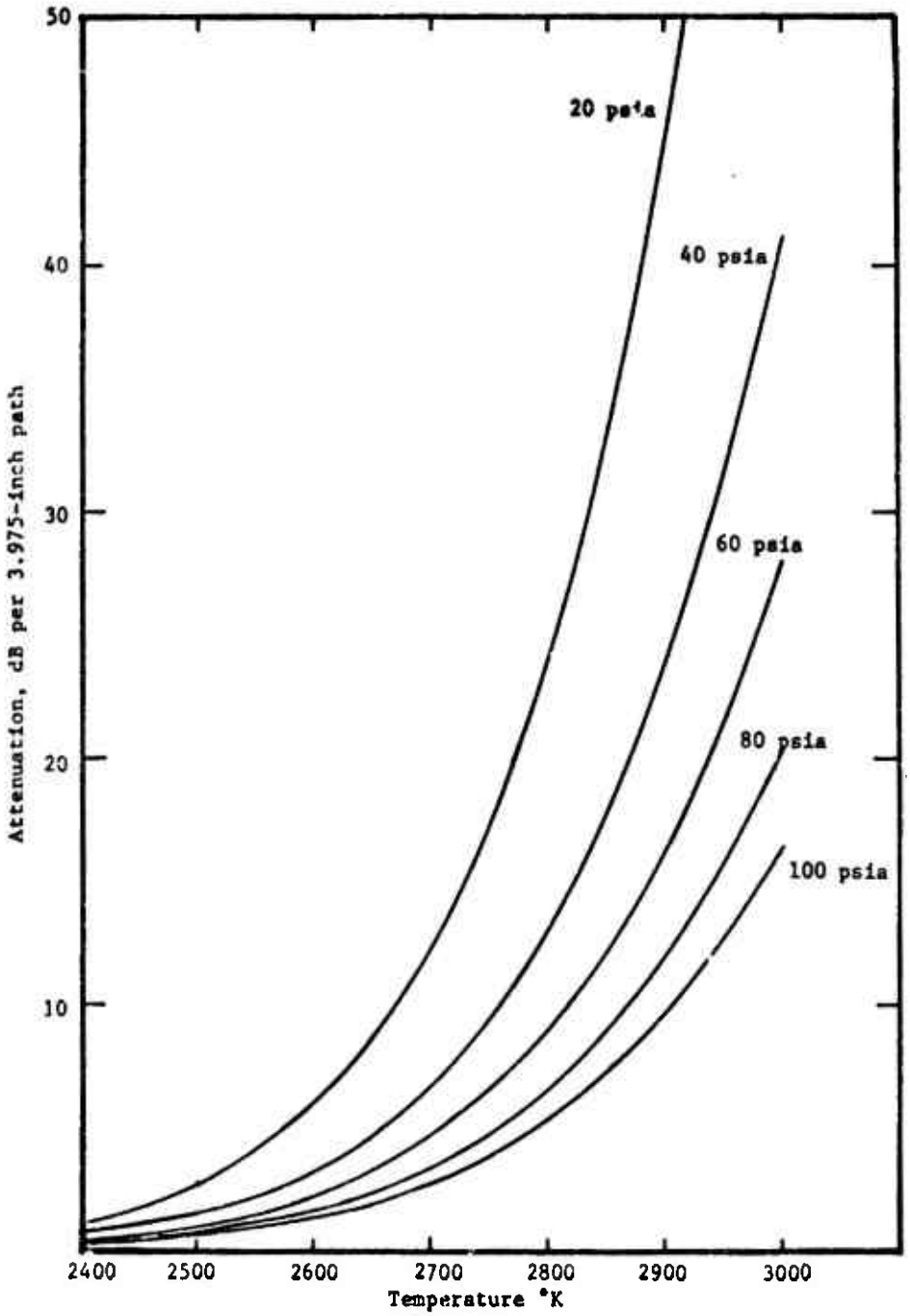

Fig. 5.6. Theoretical attenuation versus temperature and pressure for a seeding of 5 percent potassium perchlorate and 0.0 percent aluminum.

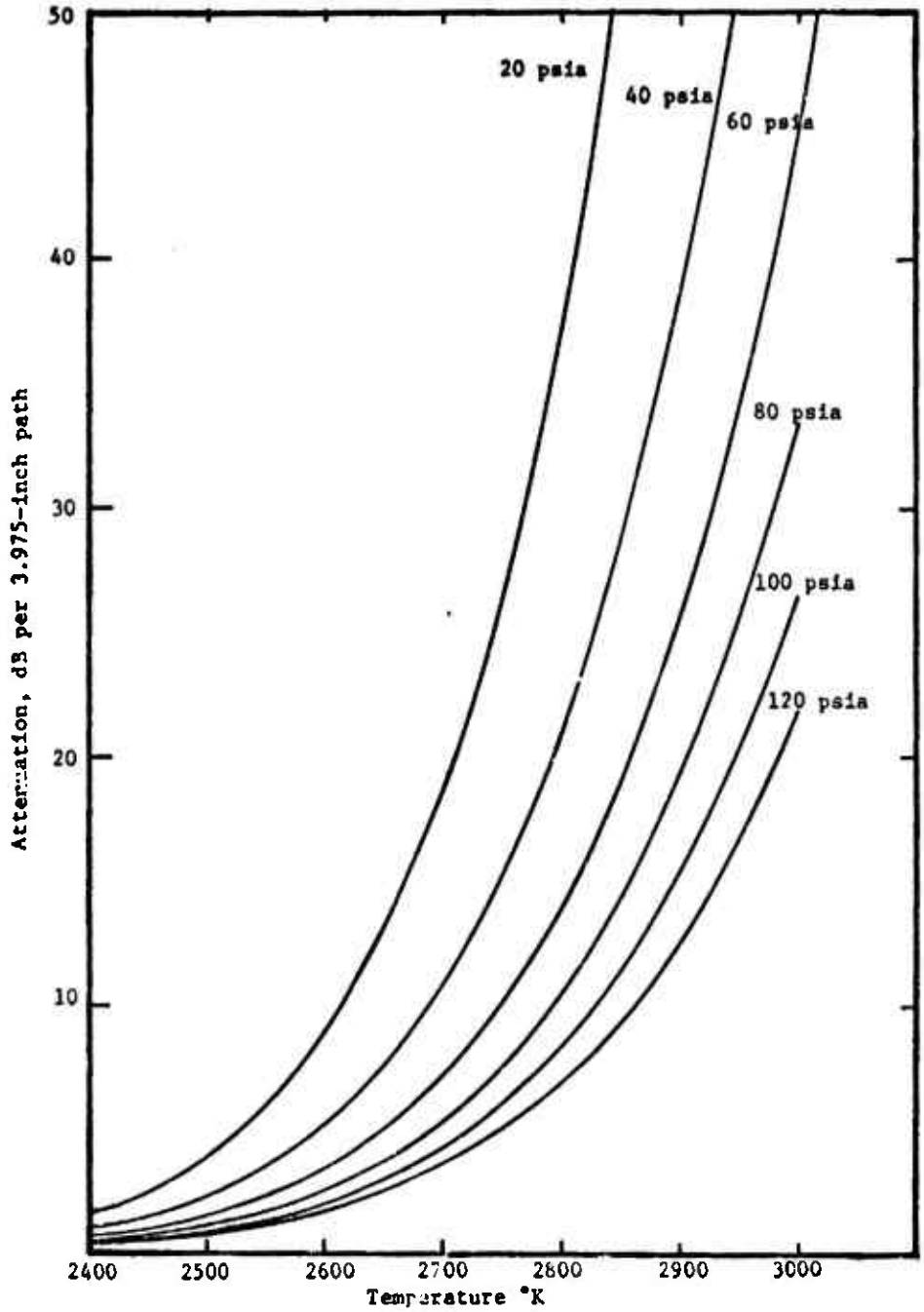

Fig. 5.7. Theoretical attenuation versus temperature and pressure for a seeding of 5.0 percent potassium perchlorate and 5.0 percent aluminum.

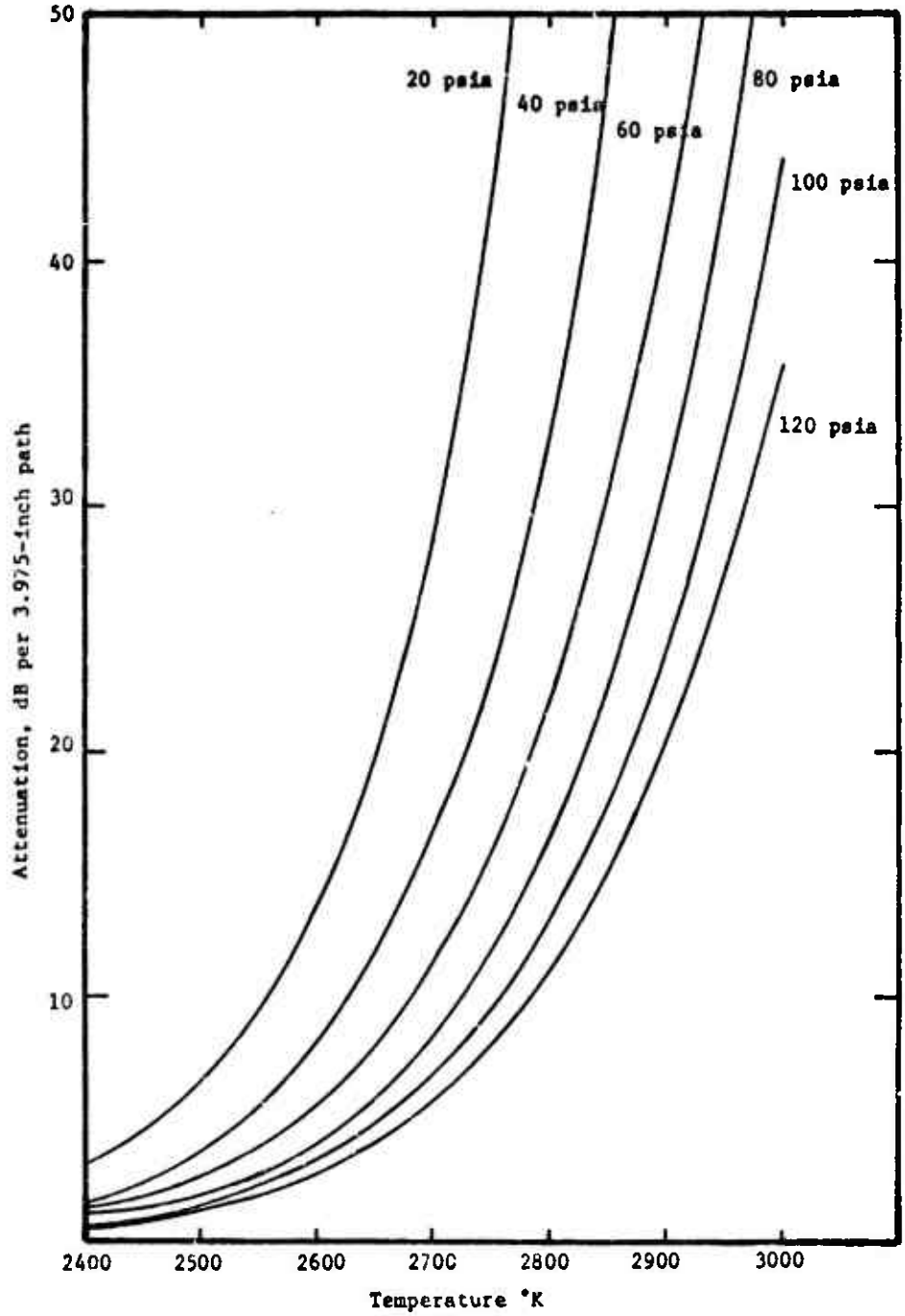

Fig. 5.8. Theoretical attenuation versus temperature and pressure for a seeding of 5 percent potassium perchlorate and 10 percent aluminum.

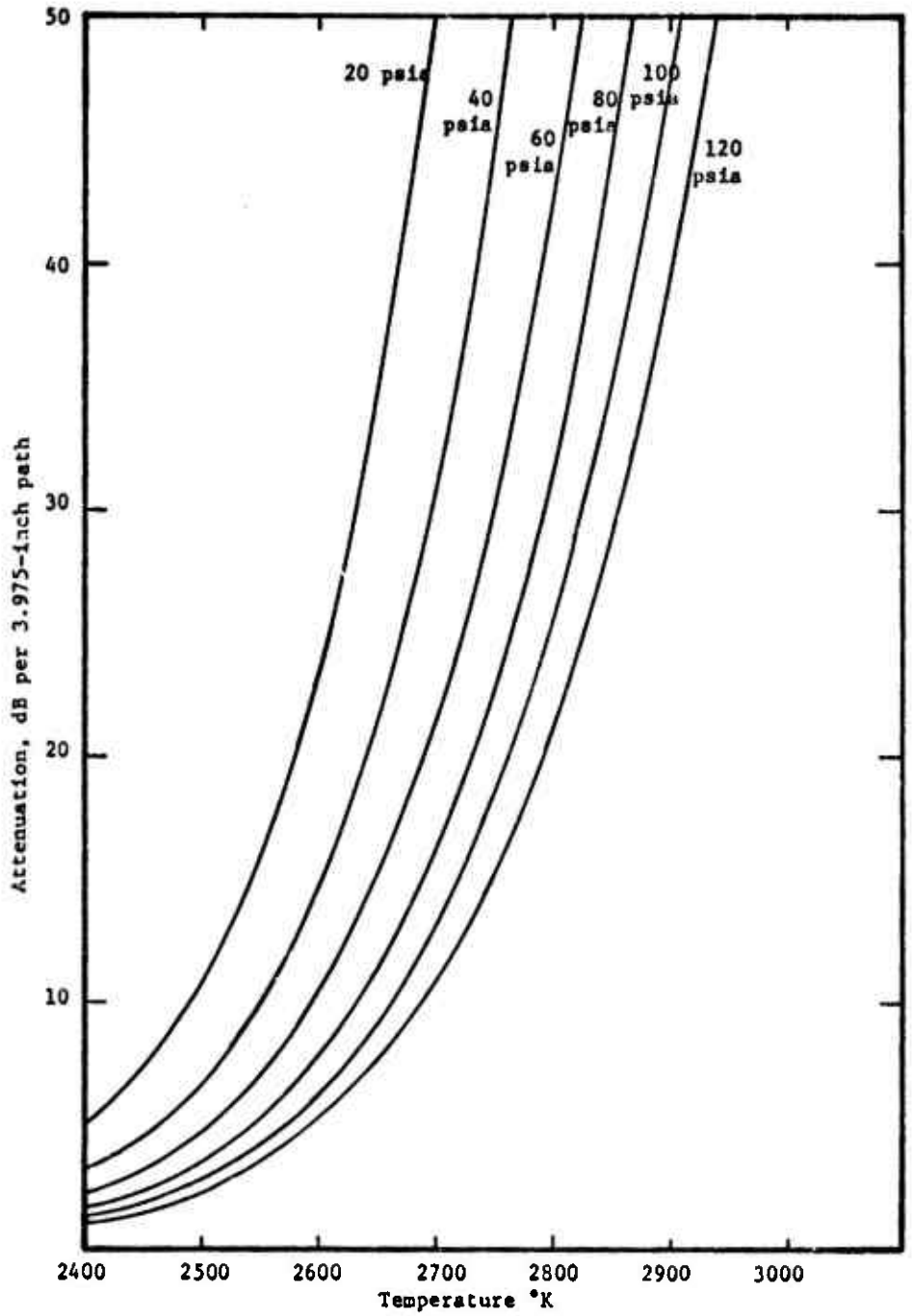

Fig. 5.9. Theoretical attenuation versus temperature and pressure for a seeding of 5 percent potassium perchlorate and 15 percent aluminum.

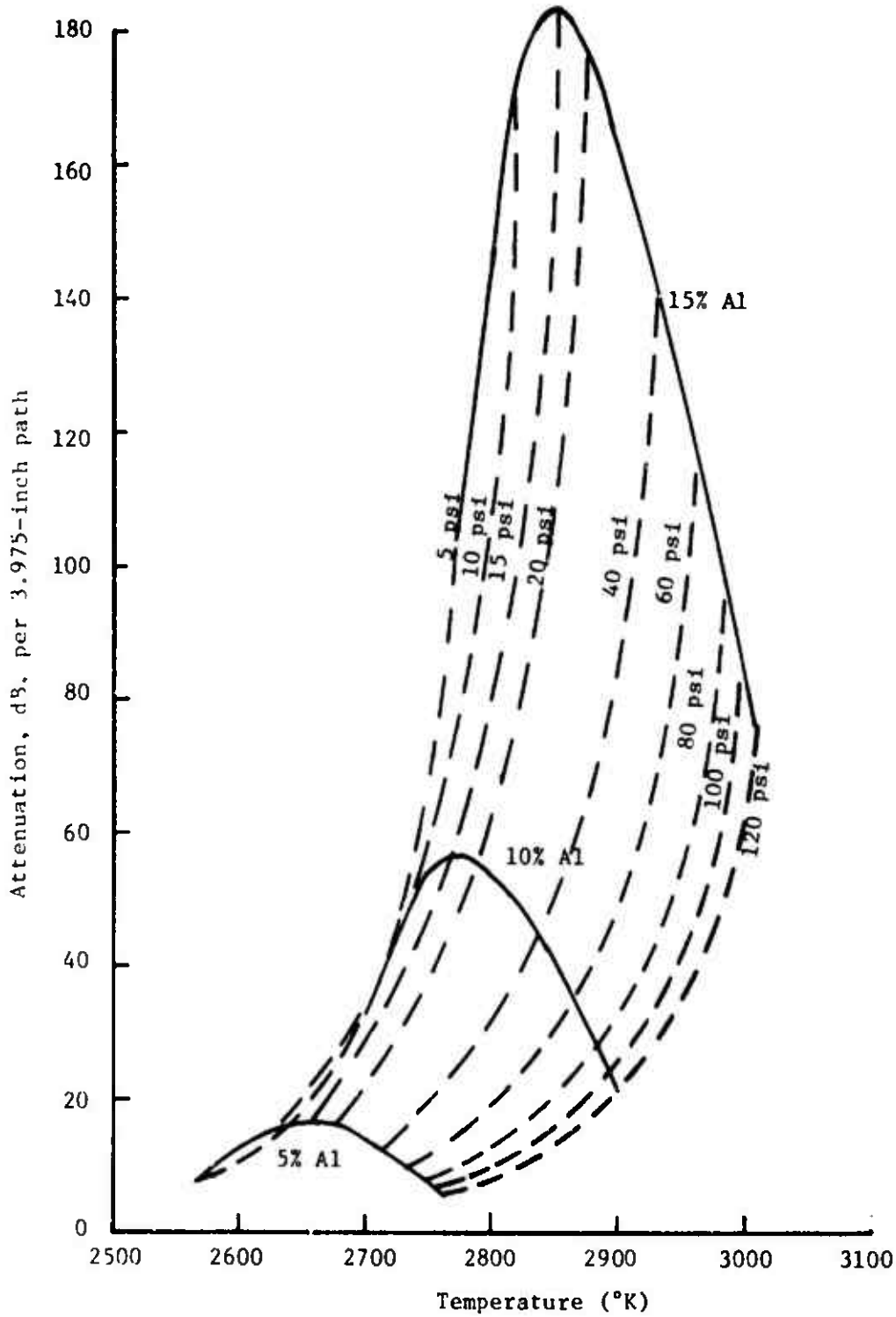

Fig. 5.10. Theoretical attenuation versus temperature for equilibrium condition.

pressure range. This is true for all three kinds of propellants considered. Figure 5.11 shows this result more clearly where wave attenuation is plotted versus pressure at equilibrium condition. Also from the computer printout, we found the electron drift velocity peaks up at one atmosphere vicinity which is the direct result of maximum wave attenuation.

The experimental results will be presented in the next chapter.

5.4 Calculation of Acoustic Gain and Loss

In this section both acoustic gain and loss will be calculated according to the equations derived in Chapter III. For the two firings picked for this calculation, both show that the loss is greater than the gain when only the fundamental mode is considered for pressure wave and only nozzle and p. .le damping loss are considered for loss mechanism. These calculations practically predicted the burning is stable.

5.4.1 Acoustic Gain

The acoustic gain expression for fundamental mode pressure waves was given by Eq. 3.94. Rewriting this equation, we have

$$\Lambda_{gain} = \frac{\nu R}{L}\left(\underline{M}\cdot\hat{n} - A_b^r\right)\cos^2\left(\frac{\pi R}{L}z\right) \qquad (3.94)$$

Recall that R/L is a dimensionless quantity.

For the firing dated April 24, 1973, a 10 percent aluminum propellant, the acoustic gain is calculated and plotted as a function

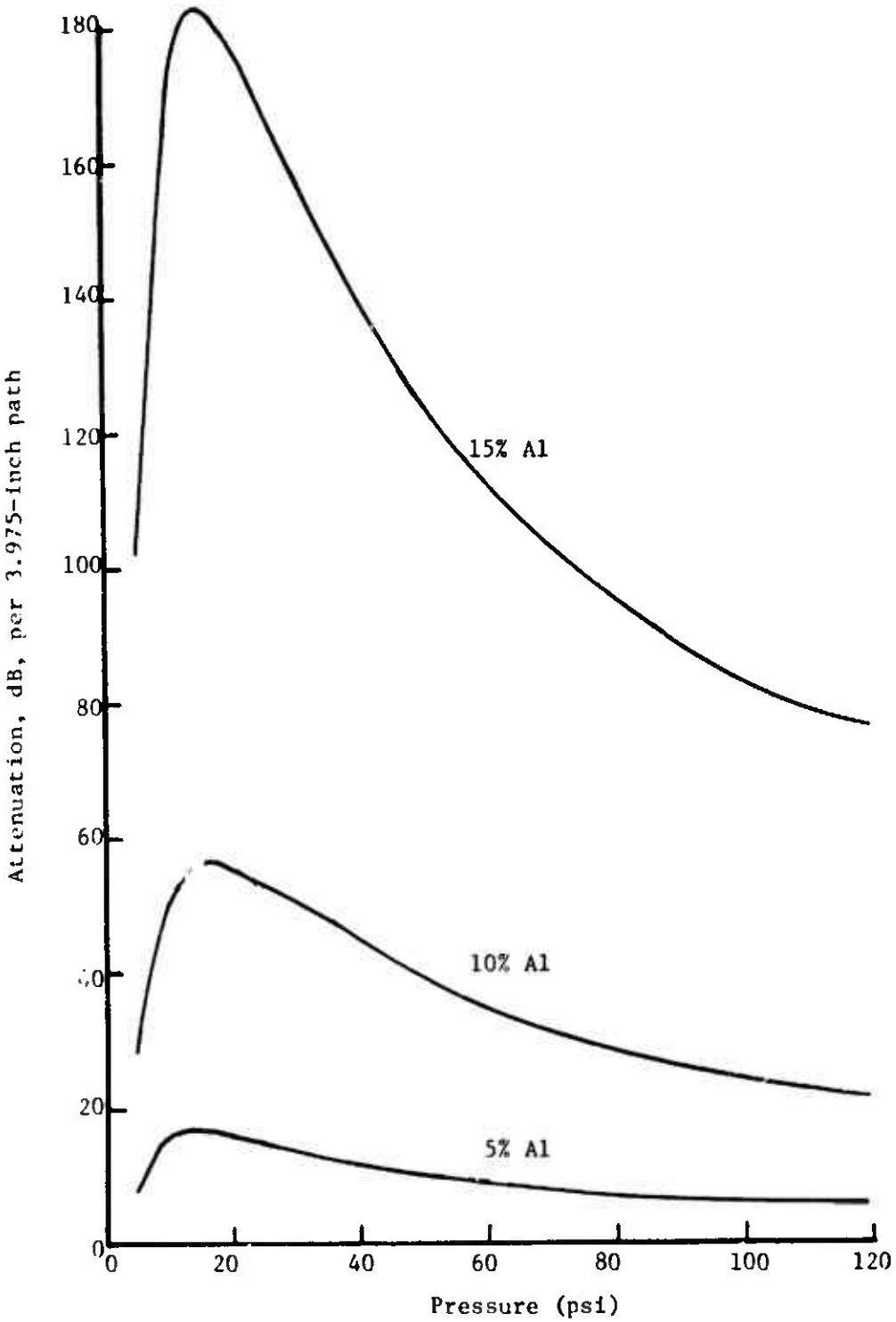

Fig. 5.11. Theoretical attenuation versus pressure for equilibrium condition.

of A_b^r. This is shown in Fig. 5.12. For this firing the total burning time was 3.8 seconds.

Figure 5.13 shows the results of the firing dated March 15, 1973, a 5 percent aluminum propellant. The total burning time was 3.3 seconds.

5.4.2 Acoustic Loss

In this section, only the nozzle loss will be considered since the particle damping loss is generally one order of magnitude less than nozzle loss. From Eq. 3.96, the nozzle loss is a function of the square of nozzle diameter for a given combustion chamber. Calculations are made for April 24, 1973 and March 15, 1973 firings and the results are 0.1320 and 0.0903, respectively. These results are plotted on Figs. 5.12 and 5.13.

Referring to Fig. 5.12, a stable system obtained experimentally, if $A_b^r < 0$ for a 10 percent aluminized propellant, the acoustic loss will exceed the acoustic gain. Figure 5.14 shows the firing data of June 20, 1972 where the high chamber pressure caused the failure of the quartz window. This window failure may have resulted from the high mean chamber pressure and/or the acoustic oscillation may have caused the build up of chamber pressure. Figure 5.15 shows the acoustic gain and loss calculated according to Eqs. 3.94 and 3.96. The acoustic loss shown is much less than acoustic gain even when $A_b^r = -0.5$.

5.5 Theoretical Calculation of Temperature Change Inside the Combustion Chamber

Although the heat loss equation has been derived in Chapter IV,

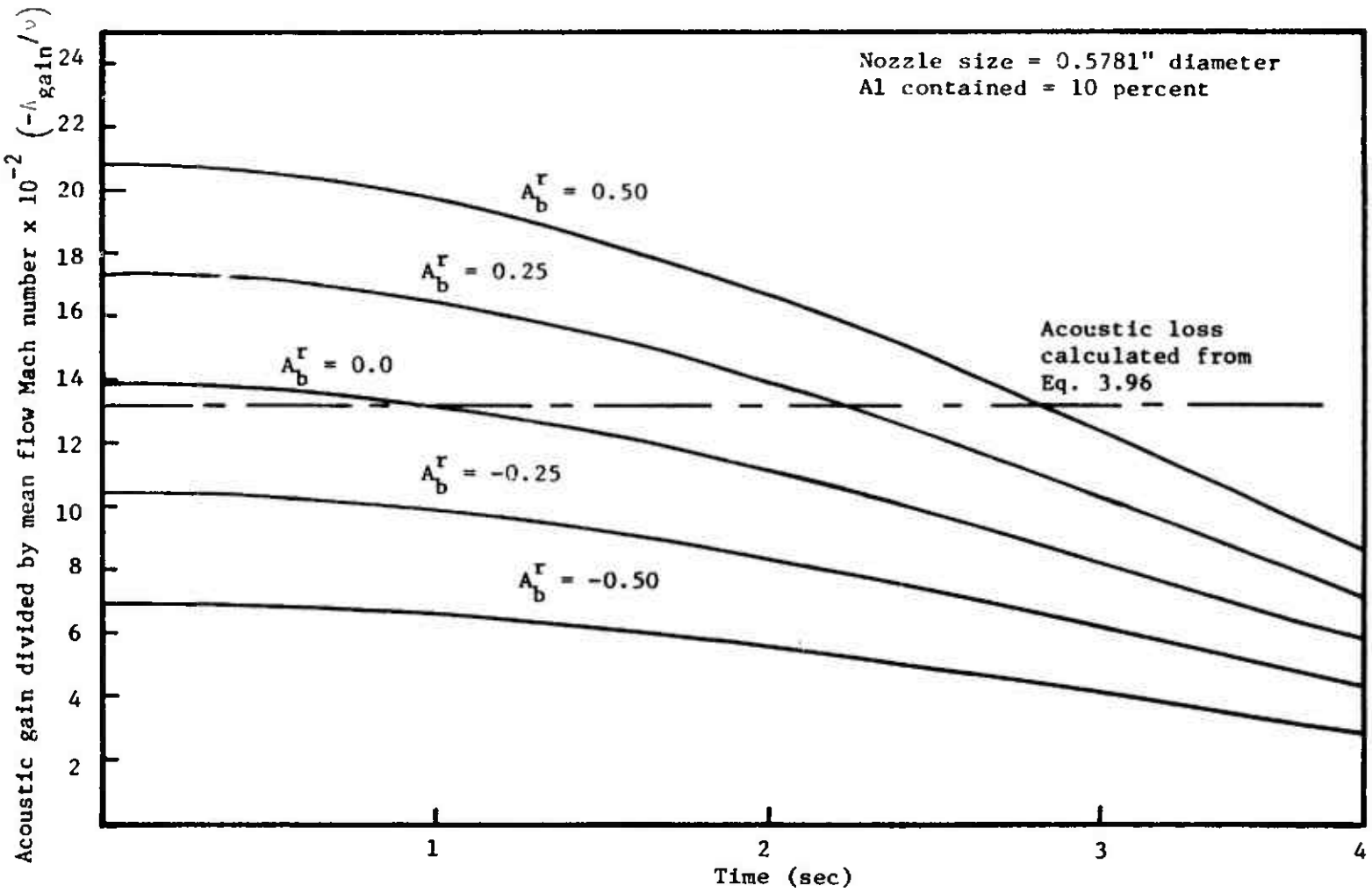

Fig. 5.12. Acoustic gain for April 24, 1973 firing.

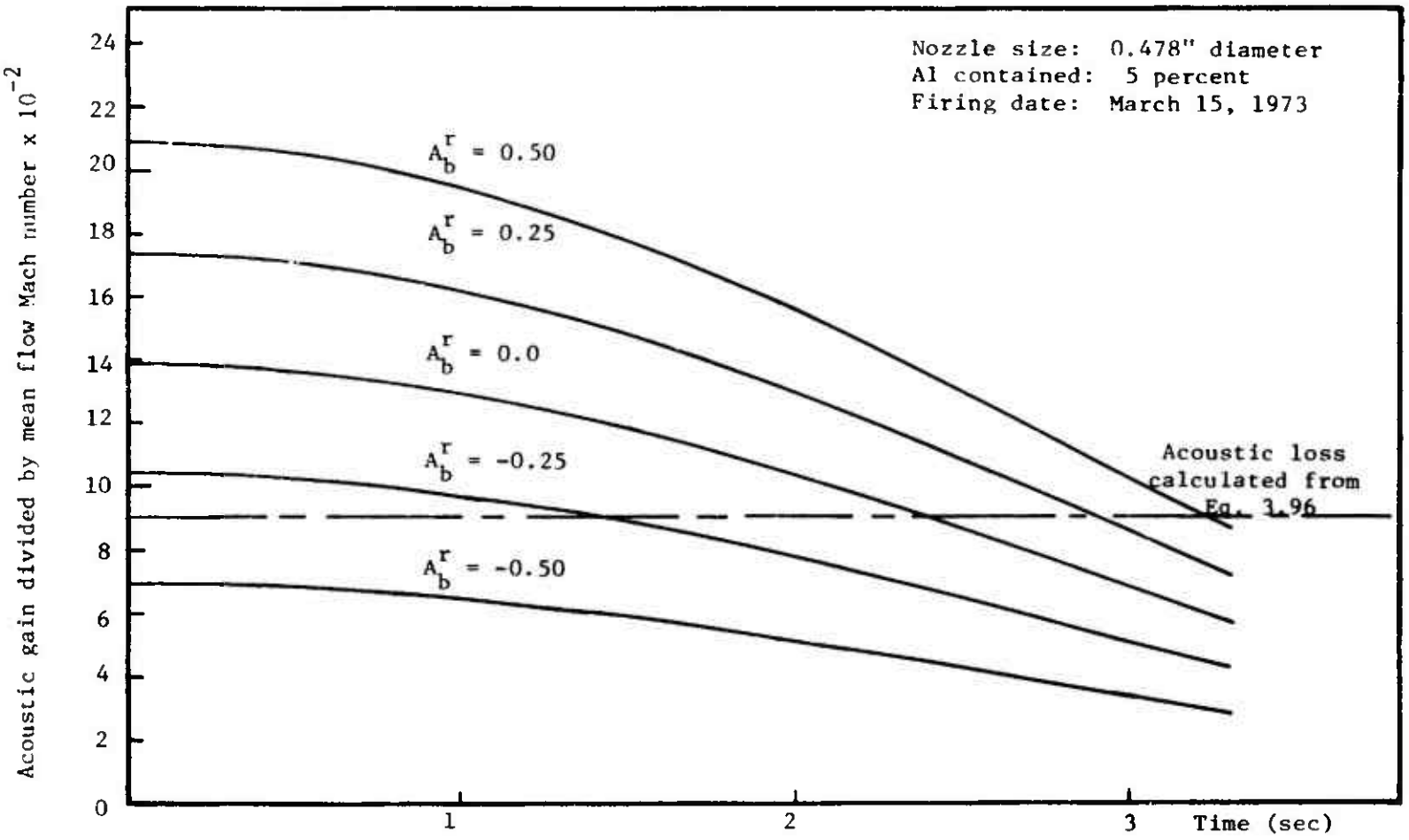

Fig. 5.13. Acoustic gain for March 15, 1973 firing.

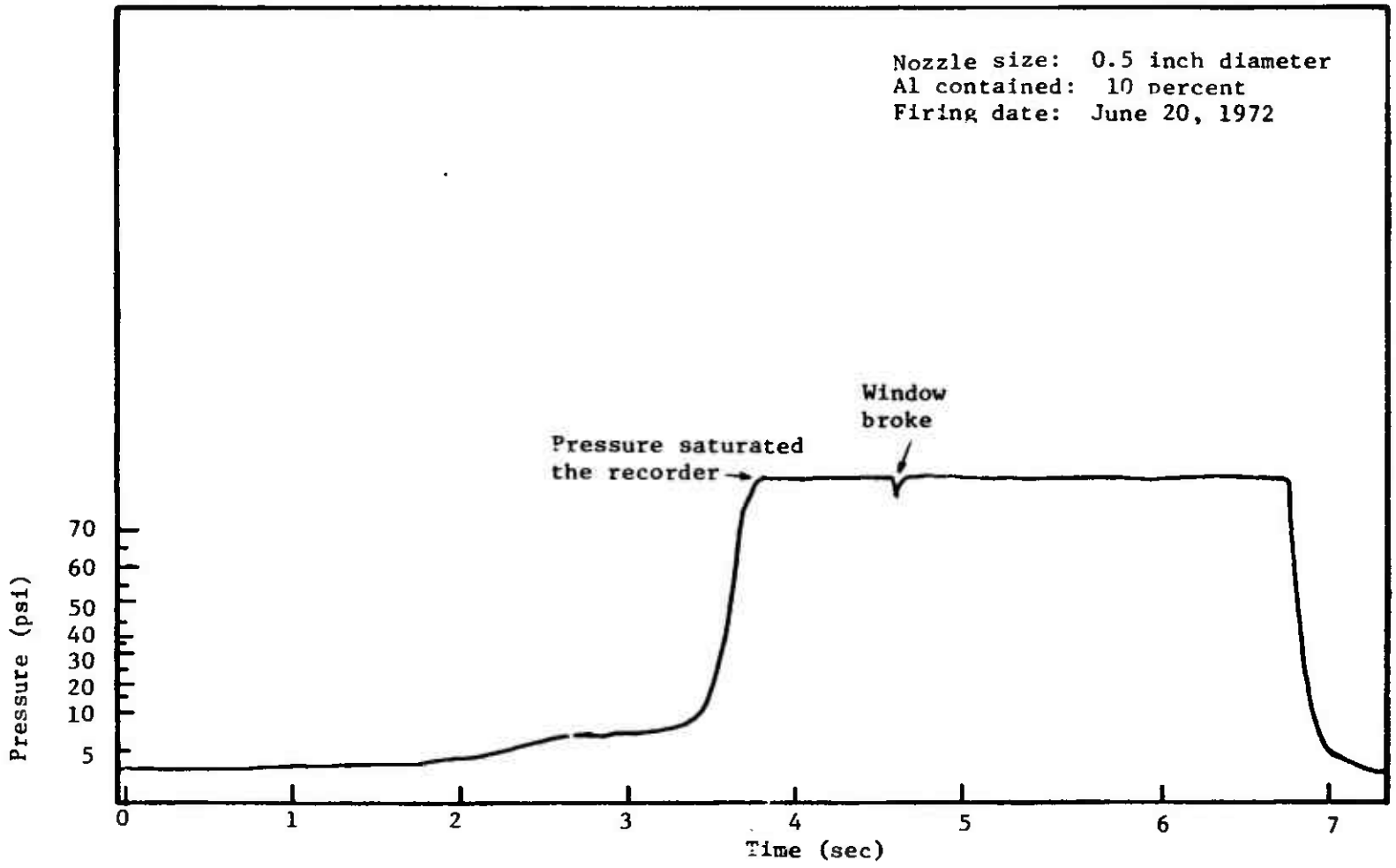

Fig. 5.14. Pressure wave of firing dated June 20, 1972.

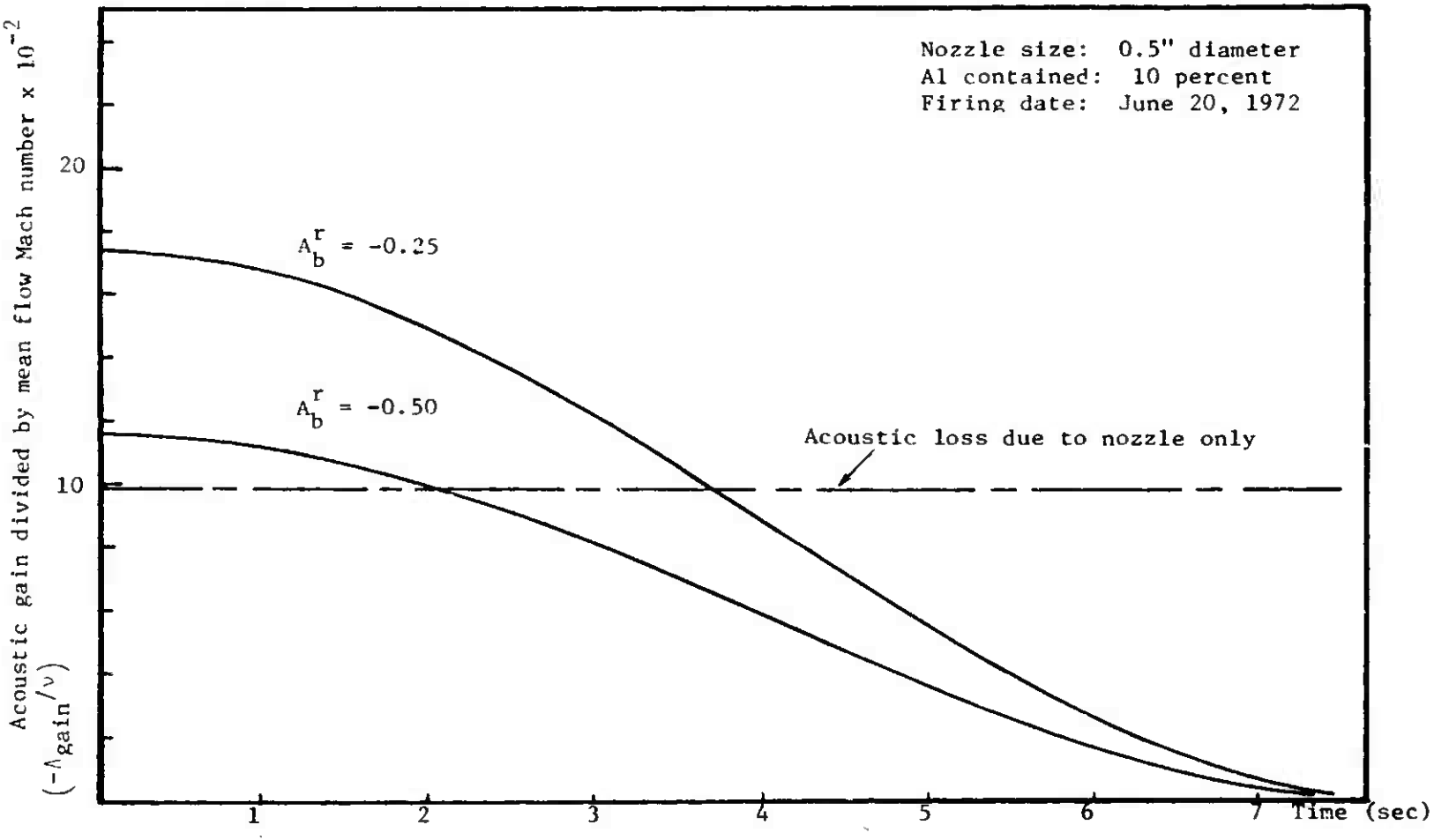

Fig. 5.15. Acoustic gain for June 20, 1972 firing.

It is still very difficult to carry out the calculation. The main problem is that there is not enough information about the gaa property inside the combuation chamber. These properties include gas viscosity, flow apeed, emisaivity, and the thermal conductivity of the motor. Using some of the "guesaed" numbers, Eqa. 4.10 and 4.11 were calculated for both ten and five percent aluminum propellant.

For all calculations emissivity is chosen to be 0.5. Viscosity of the gas is 0.17 $lb_m/ft\ hr$. For specific heat the value given by the computer program from Edwards Air Force Base was adopted. These values are listed in Appendix I.

For each kind of propellant, only one value of gas density was used since the gas composition as a whole does not vary too much in the pressure range of interest.

The results of the calculation are listed in Table 5.3.

Table 5.3. Calculated temperature change inside the combustion chamber in one inch distance.

Type of Propellant	From Eq. 4.10	From Eq. 4.11
5% Al	76.5° C	45.1° C
10% Al	77.2° C	45.1° C

VI. EXPERIMENTAL RESULTS

In this chapter, the experimental results are presented to support the theoretical predictions in Chapters II, III, and IV. First, it will be shown that the rocket chamber temperature can be measured by microwave technique accurately, even when the solid propellant was seeded with as much as ten percent aluminum by weight. Then, the combustion chamber temperature profile is plotted as a function of distance relative to an initial point away from the burning surface. The oscillation of acoustic waves was observed by pressure wave detection and microwave attenuation measurement, and the oscillation frequency is compared with theoretical calculation. Finally, the growth of acoustic waves is presented as a function of burning surface admittance.

6.1 Chamber Temperature Measurement

As mentioned previously, the temperature measurements are based on the assumption that both electron sources and sinks are present in the plasma. Since the experimental setup was discussed in Chapter V, only the results will be presented here.

Figure 6.1 shows the firing data of a 5 percent aluminum propellant with low chamber pressure. The length of the propellant was 1.6 inches long, 2 inches in diameter, and the nozzle was 0.484 inch in diameter. Sample points were taken and plotted as shown in Fig. 6.2. The dashed line shown is the equilibrium temperature for various pressure ranges. From this figure, the equilibrium temperature detected

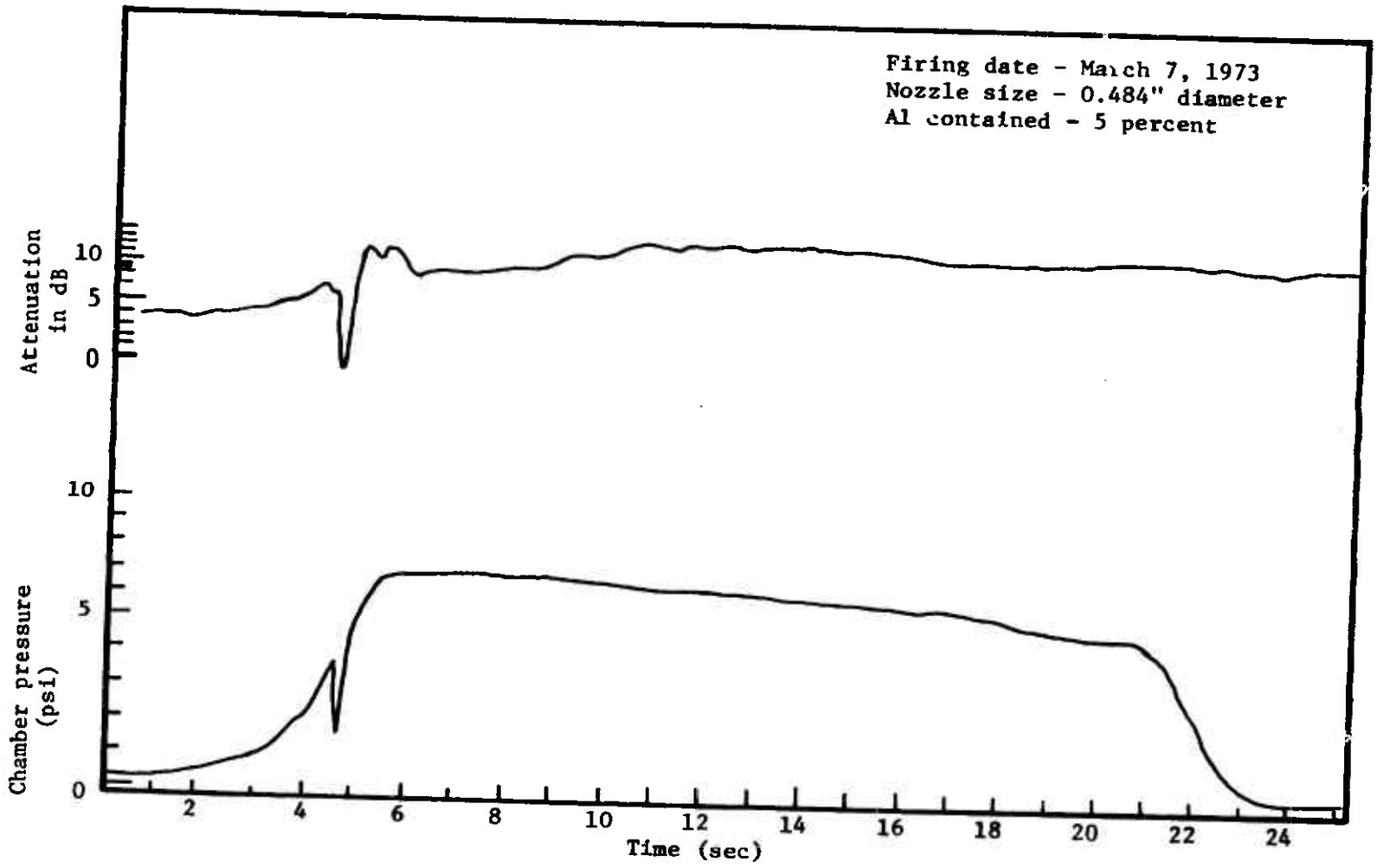

Fig. 6.1. Experimental data for March 7, 1973 firing.

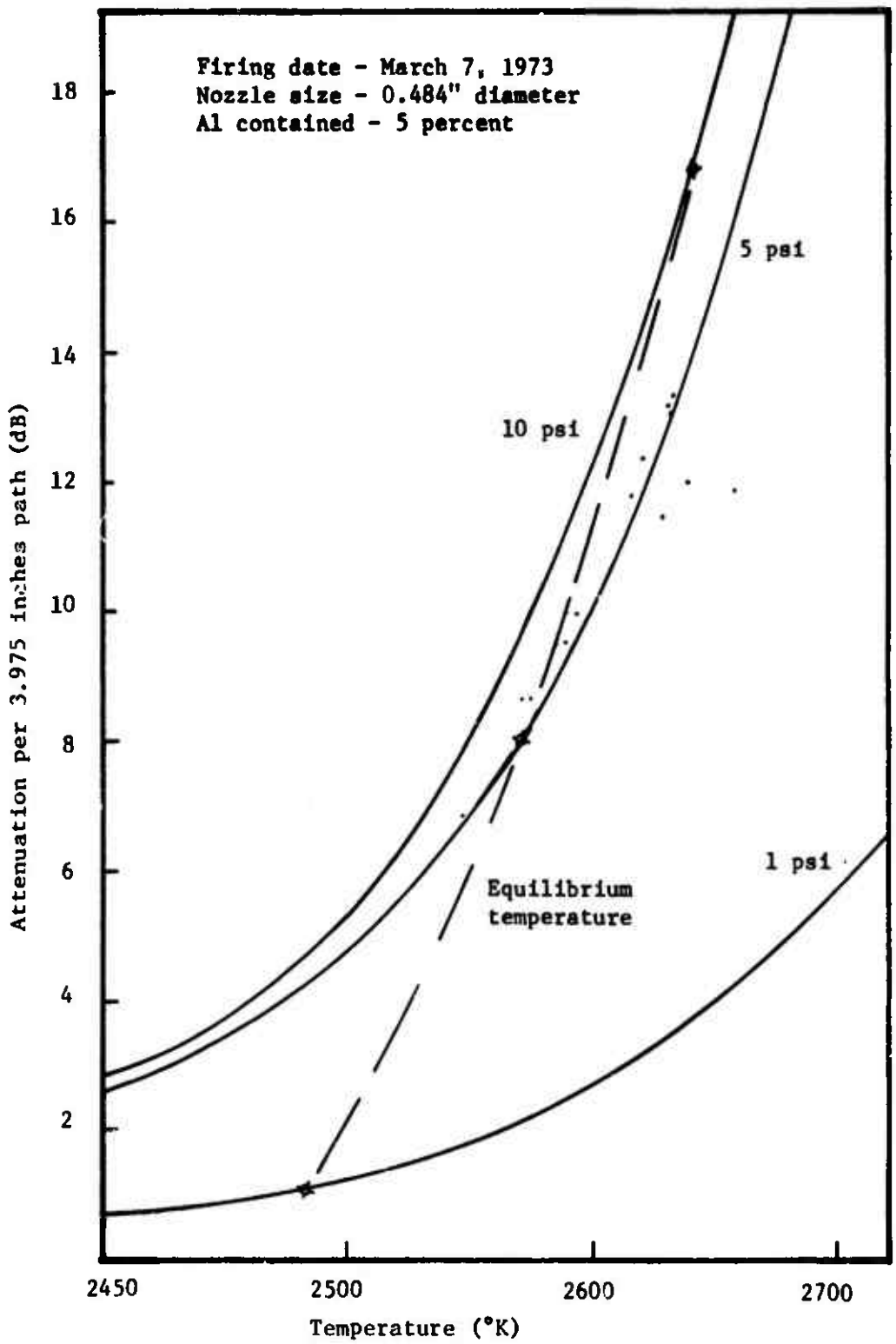

Fig. 6.2. Plotted data corresponding to Fig. 6.1.

experimentally for 5 percent aluminum at 5 psi is 2637° K. Figure 6.3 shows the firing data of a ten percent propellant with the chamber pressure of 40 pai in its equilibrium condition. The propellant is 2 inches long and 2 inches in diameter. This will be the case unless otherwise noted. Figure 6.4 shows the sample points plotted on the theoretically calculated curves. From this figure, the equilibrium temperature of the combustion chamber is determined to be 2770° K. Both results are compared with the values listed in Table 5.2. This is shown in Table 6.1.

Table 6.1. Equilibrium temperature comparison for microwave measured value and Air Force theoretical specific impulse (ISP) computer program predicted value.

Aluminum Contained	Calculated Value Using Microwave Measurement Results	Predicted Value by Air Force ISP Computer Program	Difference
5%	2637° K	2569° K	2.65%
10%	2770° K	2841° K	2.50%

Several attempts were made to detect the chamber temperature propellant, and the results are very poor. The main problem involved is the accumulation of residue around the nozzle entrance. This accumulation shrinks the nozzle passage considerably, and causes the pressure buildup inside the combustion chamber, which results in the opening of the relief valve or the breaking of the quartz window or both. Figure 6.5 shows the end piece of the rocket motor after firing. The propellant used was a 10 percent one and the nozzle size was 5/8 inch in diameter before firing. In order to compensate for the clogging effect, larger nozzles were used. But for low pressure measure-

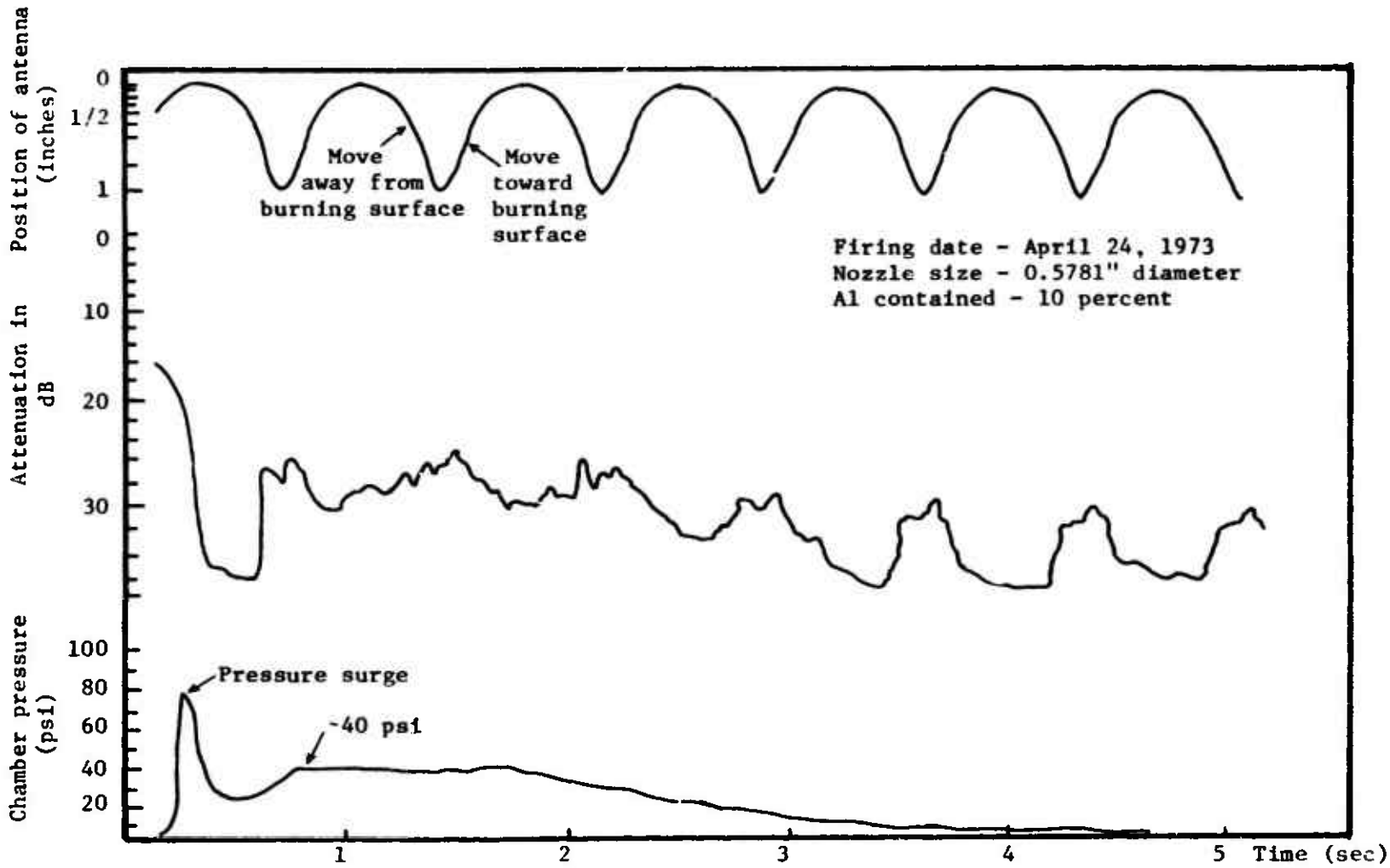

Fig. 6.3. Experimental result for April 24, 1973 firing.

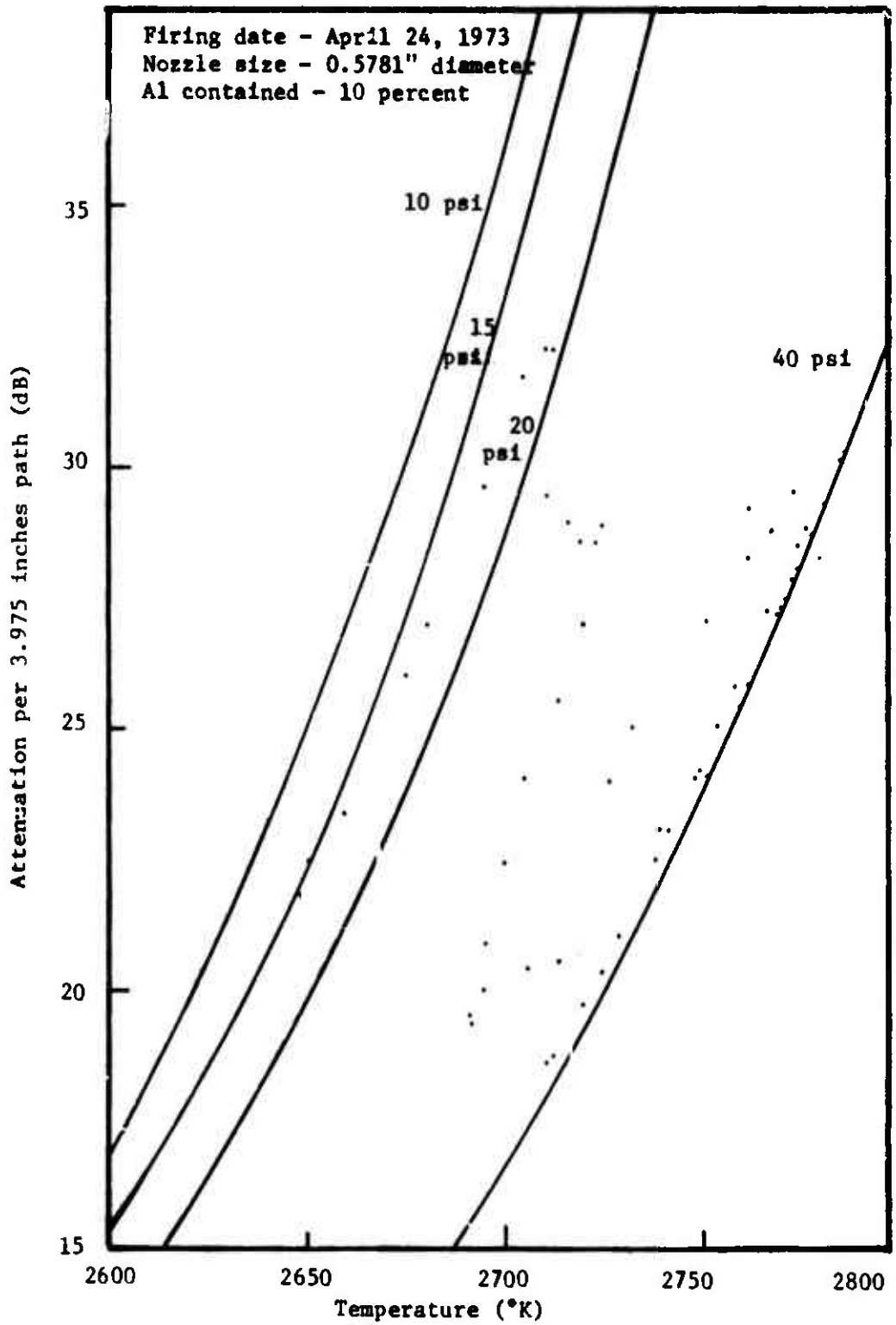

Fig. 6.4. Plotted data corresponding to Fig. 6.3.

Fig. 6.5. End piece of rocket motor after firing.

ments, the microwave attenuation went beyond the capacity of present equipment. When the pressure is extremely low, it is hard to decide just exactly what the pressure was. This situation can be seen more clearly from Fig. 5.11.

More experimental determination of the equilibrium temperature can also be obtained from the data shown in the next section.

6.2 Temperature Profile Measurements

For this part of the experiments, the antennas were scanned simultaneously across the window during the firing process. The microwave attenuation measurements made cover a horizontal distance range inside the combustion chamber away from the burning surface of the propellant. During the data reduction process, the position of the antenna and the location of the burning surface are carefully calculated from the burning rate of the propellant for each datum point, so the measured value is the true value. The first datum point was chosen on

the basis that the propellant was ignited and the equilibrium condition is, or is nearly, reached. Referring back to Fig. 6.4, the numbered data points represent the time sequence of each point. (Later this will be indicated by arrow marks with only point 1 identified.) Including the effects of antenna position and the burning of propellant, the temperature profile was plotted as shown in Fig. 6.6. Point 1 was chosen as a starting point and all the distances between points from there on were calculated relative to this starting point.

Theoretically predicted results from Eqs. 4.10 and 4.11 were also shown in Fig. 6.6 for comparison purpose. For 10 percent propellant, the results are extremely close. However, it should be noted that in the results from Eqs. 4.10 and 4.11, only the slope of the line is important.

Figure 6.7 shows other 10 percent propellant firing data. In similar fashion, sampling points were plotted in Fig. 6.8 and the temperature profile is shown in Fig. 6.9. For 5 percent propellant, the firing data are shown in Figs. 6.10 and 6.11, and the profile is shown in Fig. 6.12. More data for 5 percent aluminum propellant are shown in Figs. 6.13 and 6.14.

6.3 Oscillation of Acoustic Wave Measurements

In this section, the oscillation of acoustic waves inside the cylindrical end burner will be shown, and the oscillation frequency will also be calculated accordingly. The theoretical prediction about oscillation frequency is calculated from Eq. 3.79 and listed in Table 6.2 for several modes and chamber lengths for comparison.

Fig. 6.6. Plotted data corresponding to Fig. 6.5.

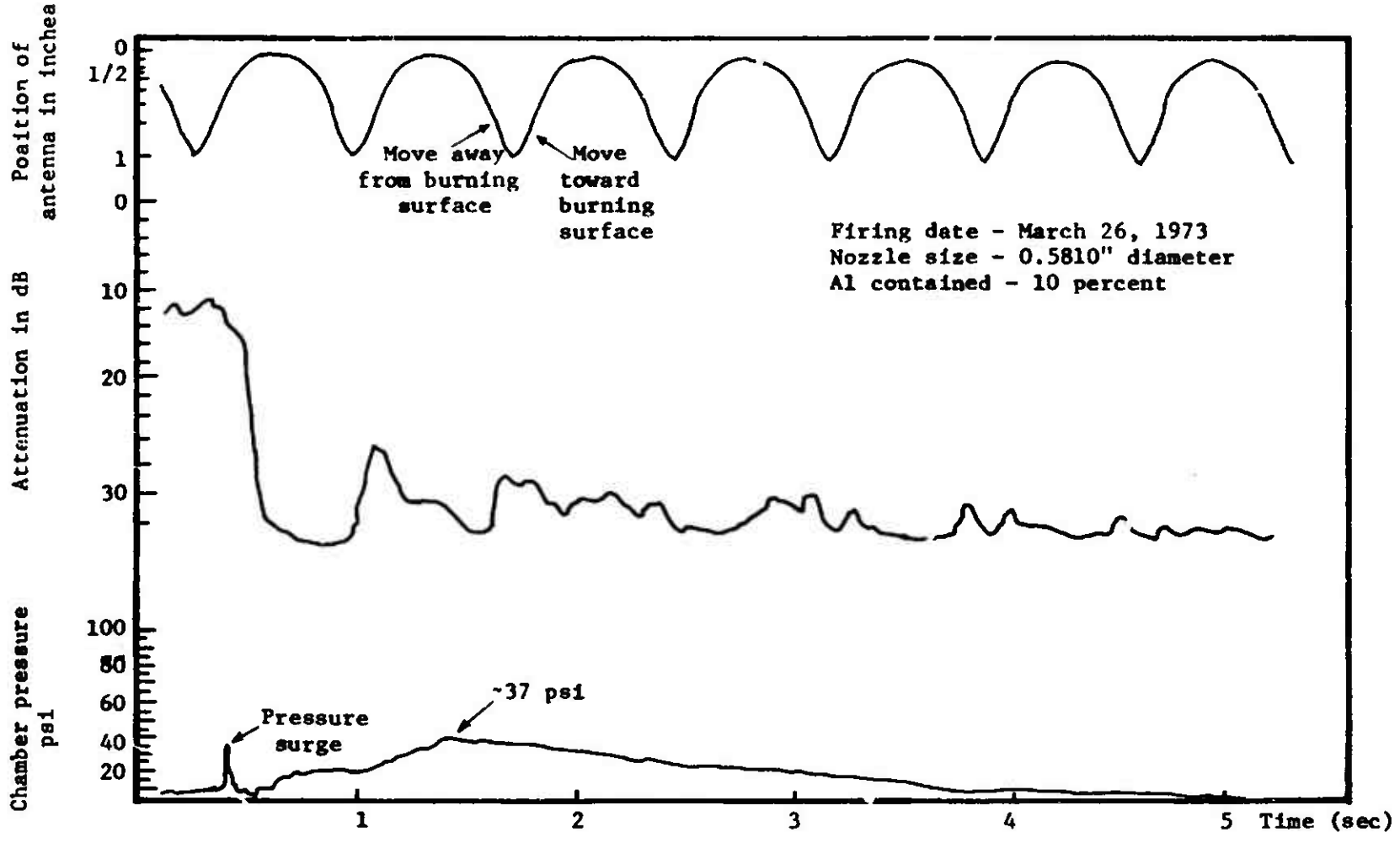

Fig. 6.7. Experimental data for March 26, 1973 firing.

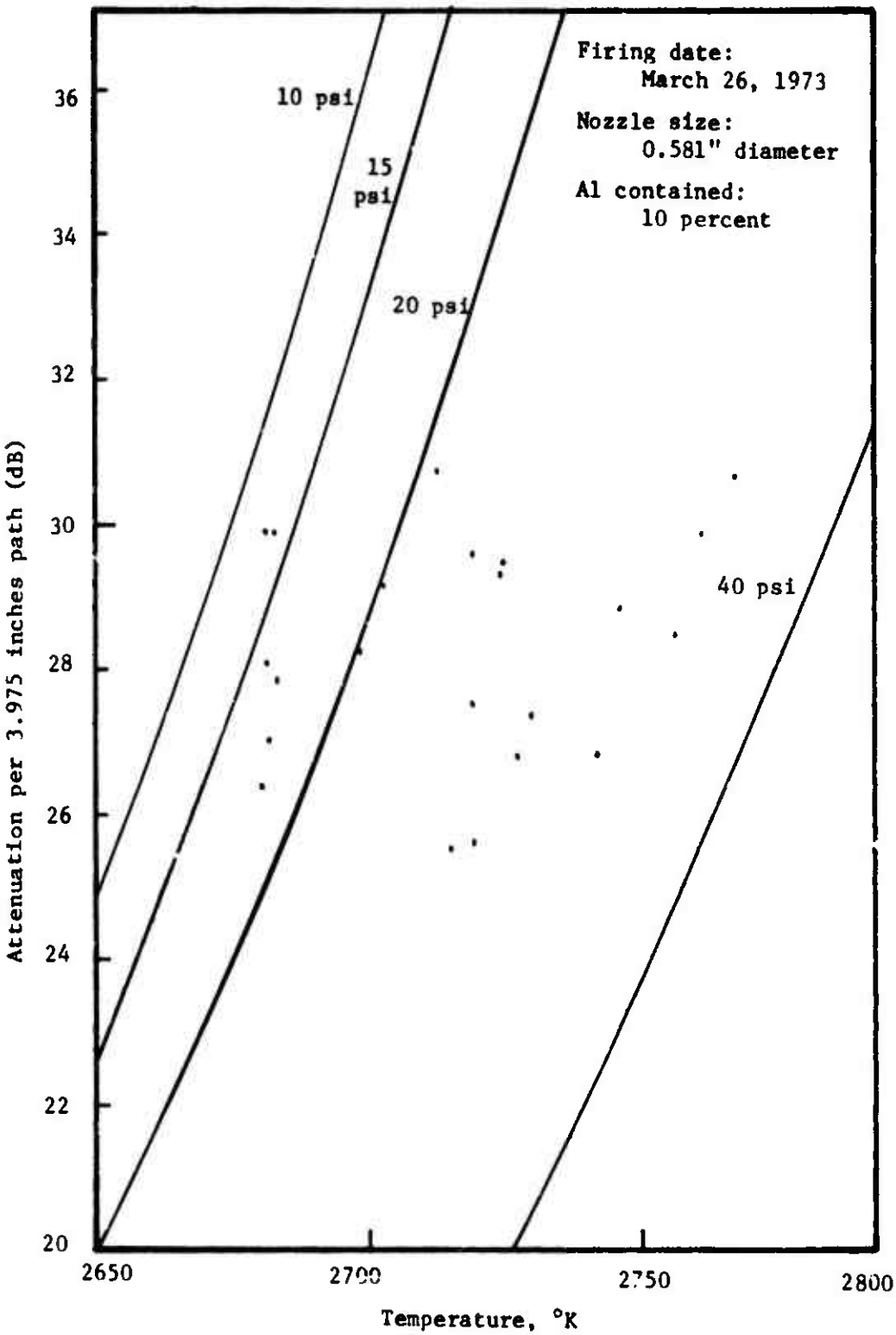

Fig. 6.8. Plotted data corresponding to Fig. 6.7.

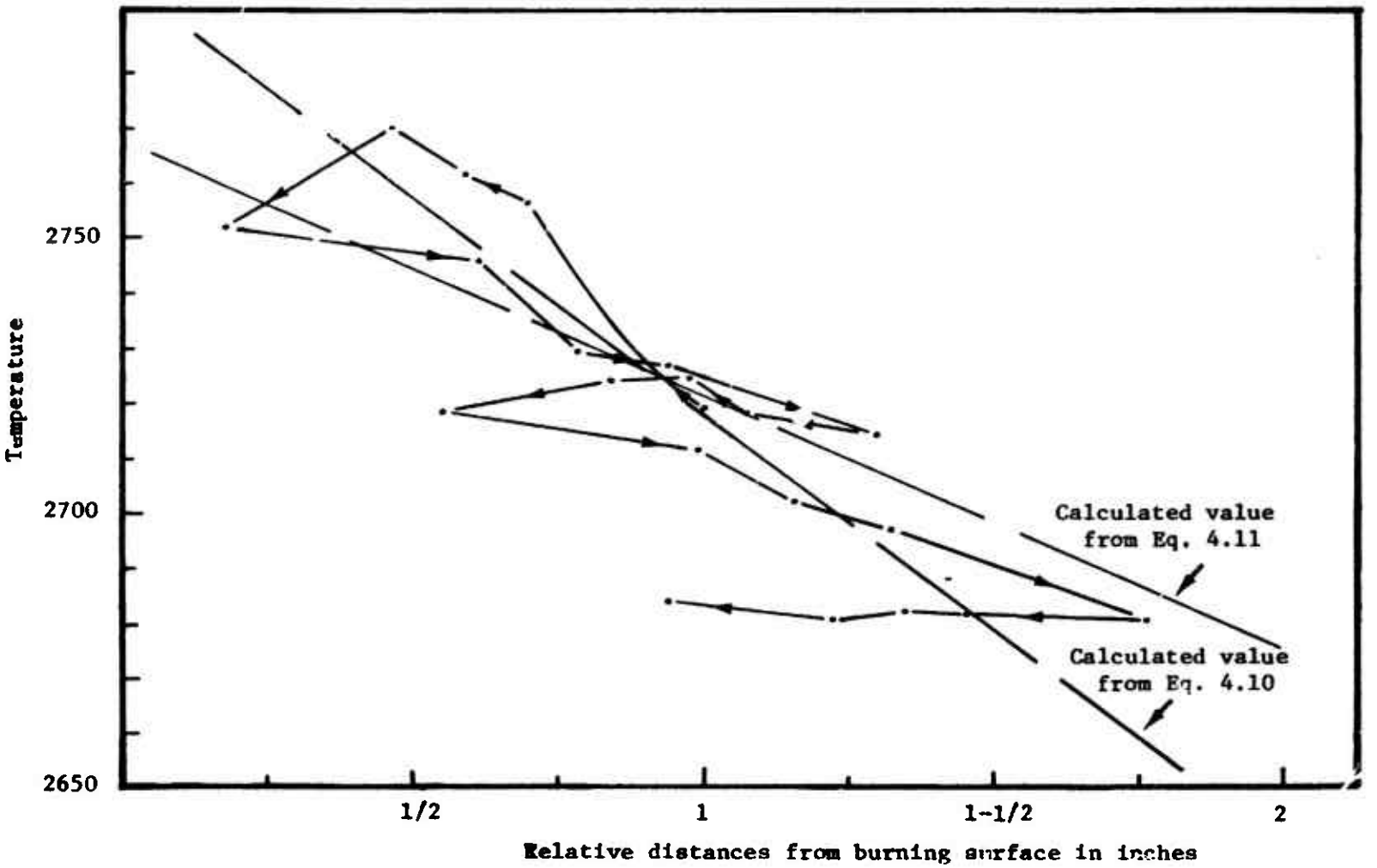

Fig. 6.9. Plotted data corresponding to Fig. 6.8.

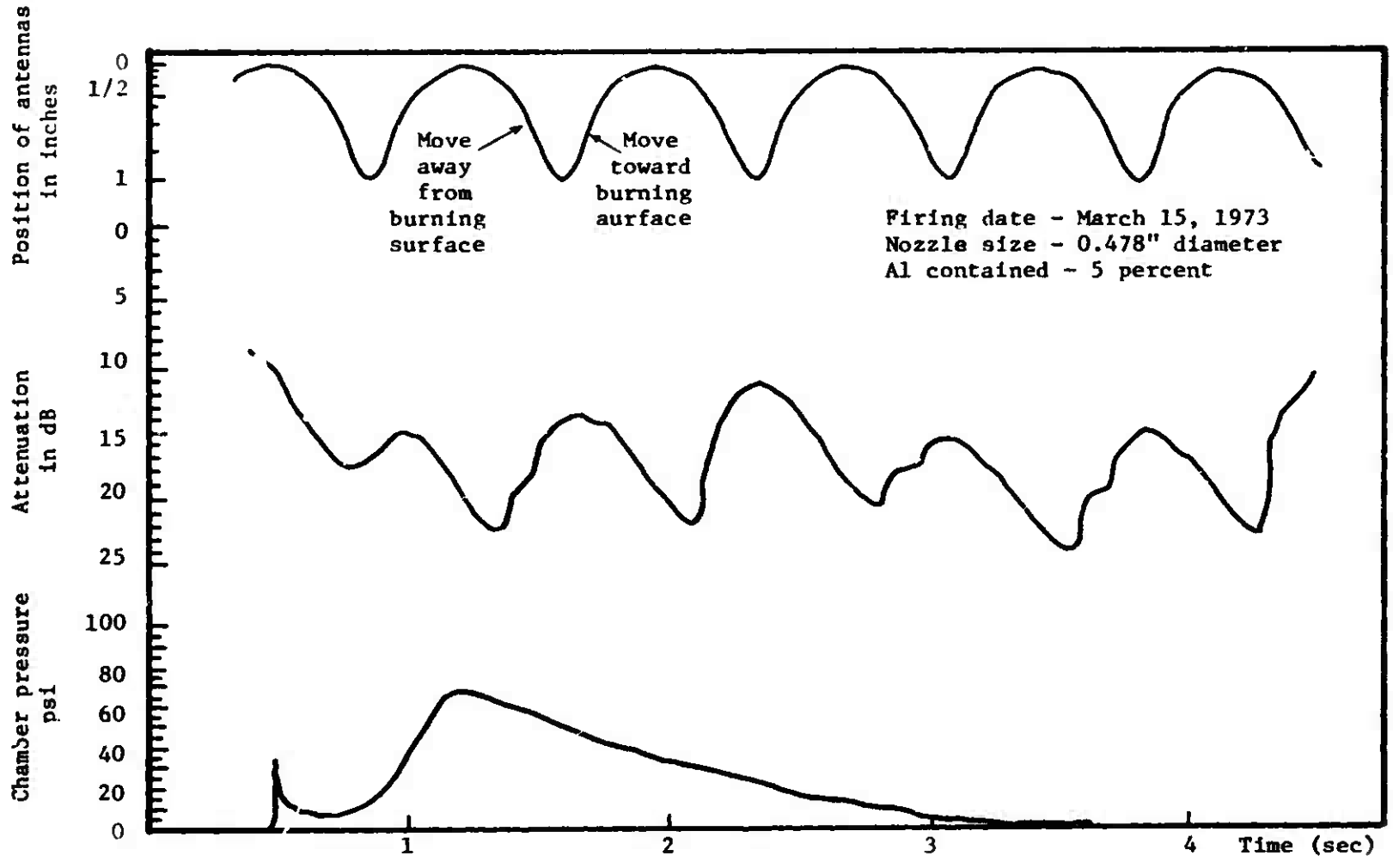

Fig. 6.10. Experimental results for March 15, 1973 firing.

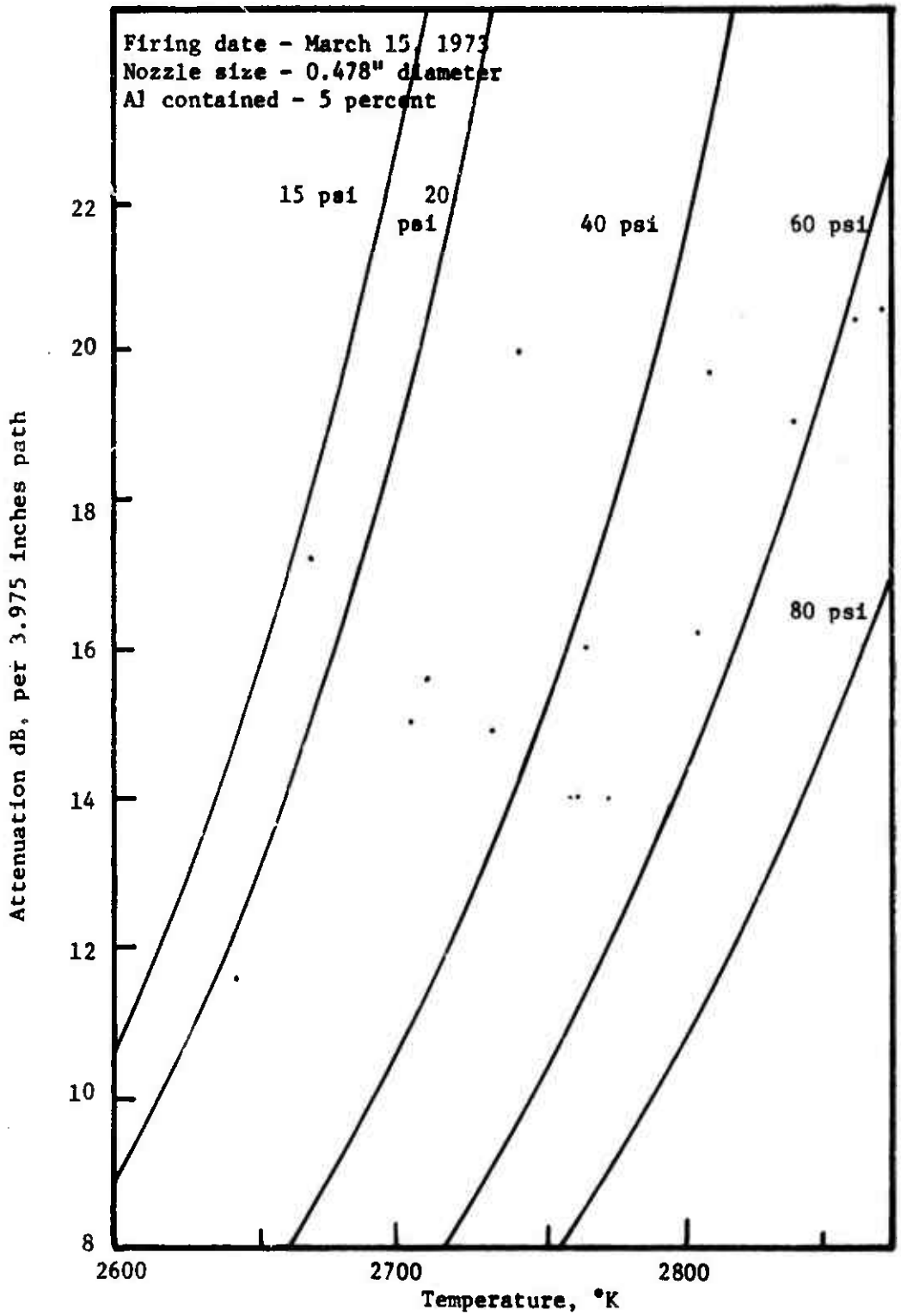

Fig. 6.11. Plotted data corresponding to Fig. 6.10.

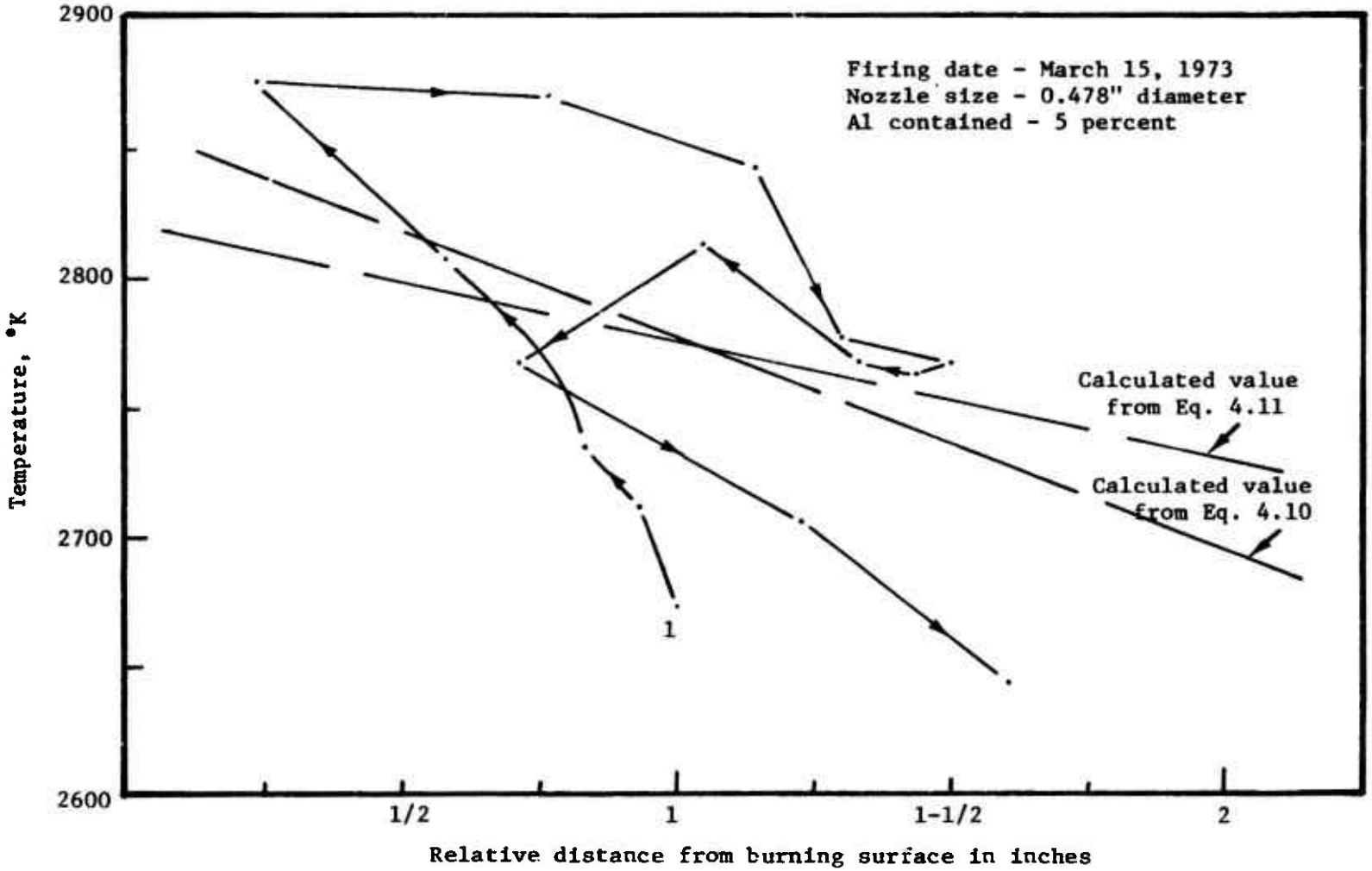

Fig. 6.12. Plotted data corresponding to Fig. 6.11.

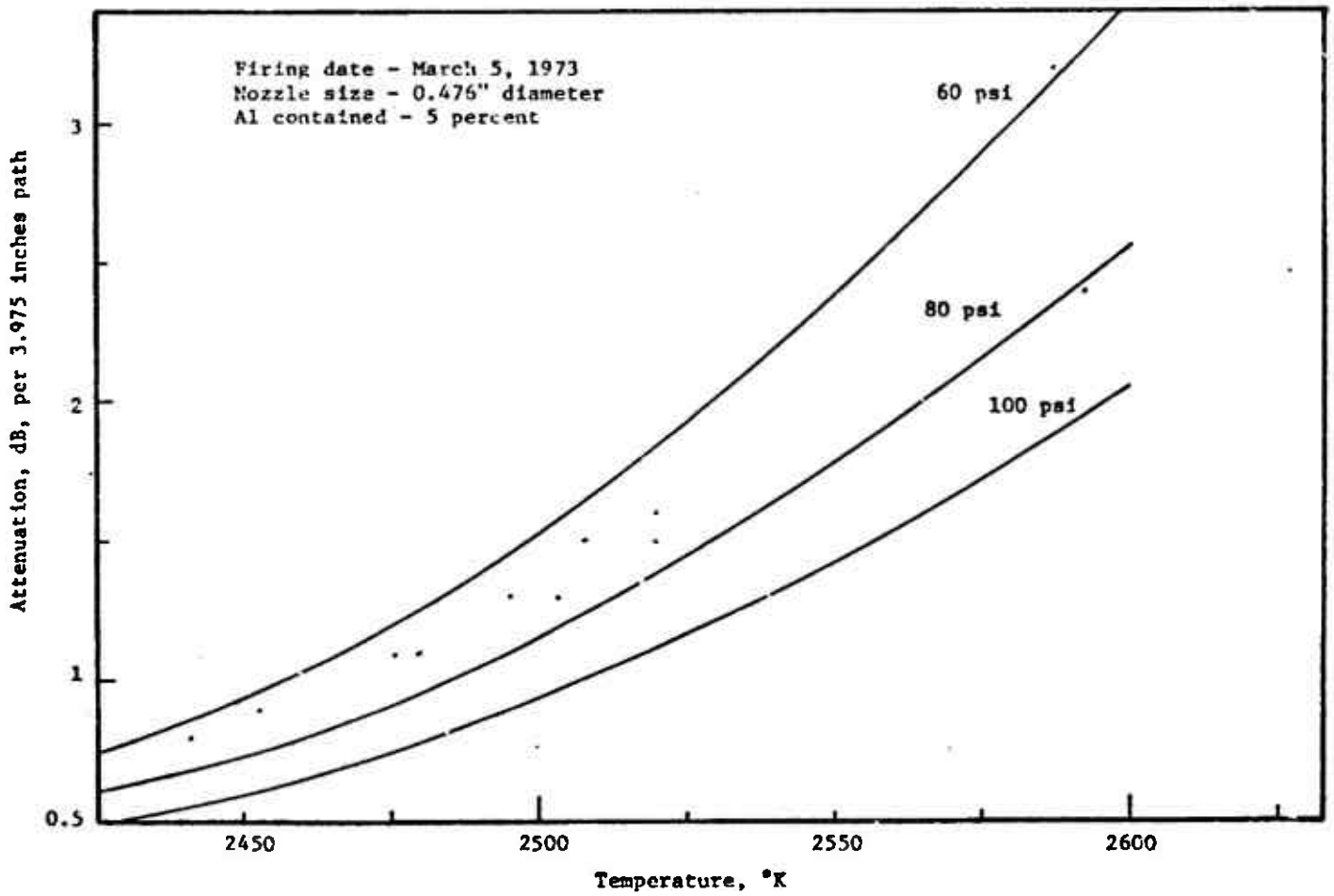

Fig. 6.13. Experimental data for March 5, 1973 firing.

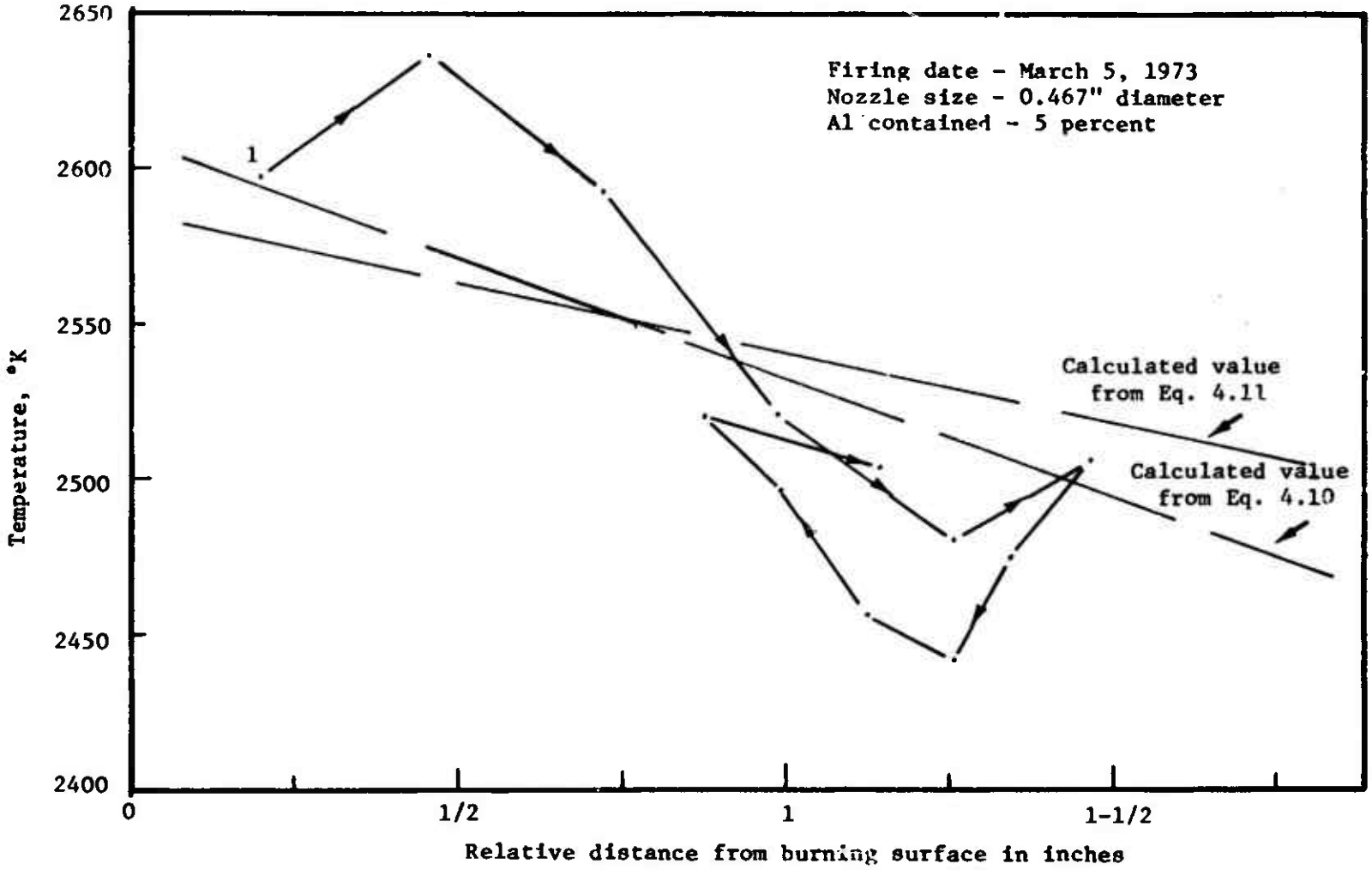

Fig. 6.14. Plotted data corresponding to Fig. 6.13.

Table 6.2. Theoretically predicted oscillation frequency. All frequencies are in kHz.

Chamber Length	Mode				
	(0, 0, 1)	(1, 0, 1)	(2, 0, 1)	(0, 1, 1)	(1, 1, 1)
$5\frac{3}{16}$	4.1381	4.2686	4,4877	4.6775	5.1316
$6\frac{3}{16}$	3.4691	3.6240	3.8796	4.0977	4.6094
$7\frac{3}{16}$	2.9867	3.1651	3.4548	3.6982	4.2581

For this part of the experiments, the combustion chamber was increased to 5-3/16 inches. For the firing dated November 27, 1973, two pressure transducers were used as before. One of them was fed into the four-channel Sanborn recorder, and the other was connected to a Hewlett-Packard model 3960 instrumentation recorder. The data registered on the Sanborn is shown in Fig. 6.15. Notice the pressure wave saturated the recorder. Figure 6.16 shows the pressure wave registered on the tape recorder and played back at the recording speed to a storage scope. Figure 6.17 through Fig. 6.21 are some segments of the pressure wave shown in Fig. 6.16 played back at a speed sixteen times slower than the recording speed. There is time separation between pictures. Figure 6.19 is the more often shown waveform and the oscillation frequency calculated from this picture is 4.39 kHz.

For the firing dated December 8, 1973, three pressure transducers were used. The additional one was mounted at the end of the rocket motor opposite the nozzle. The signal detected by this transducer was

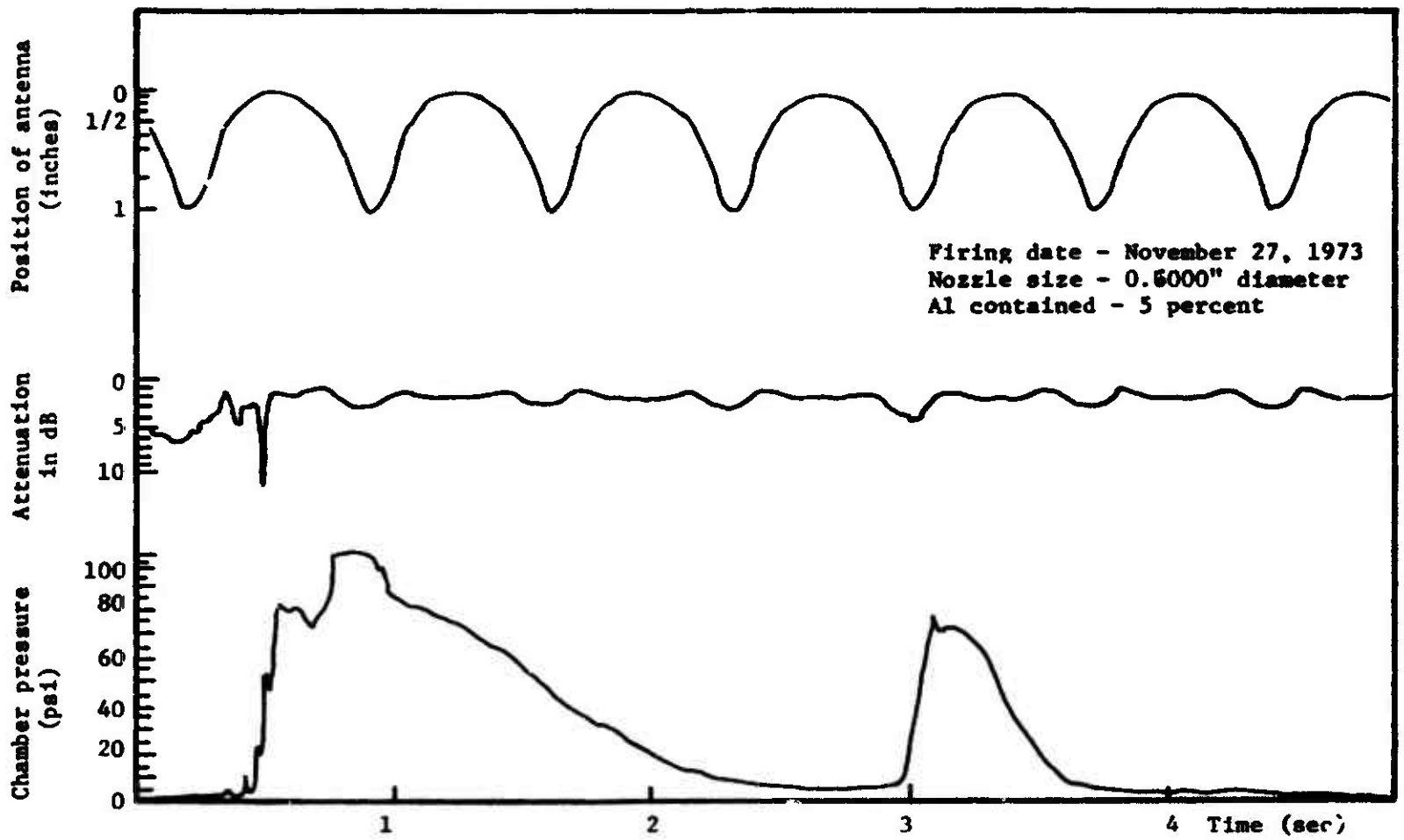

Fig. 6.15. Experimental result for November 27, 1973 firing.

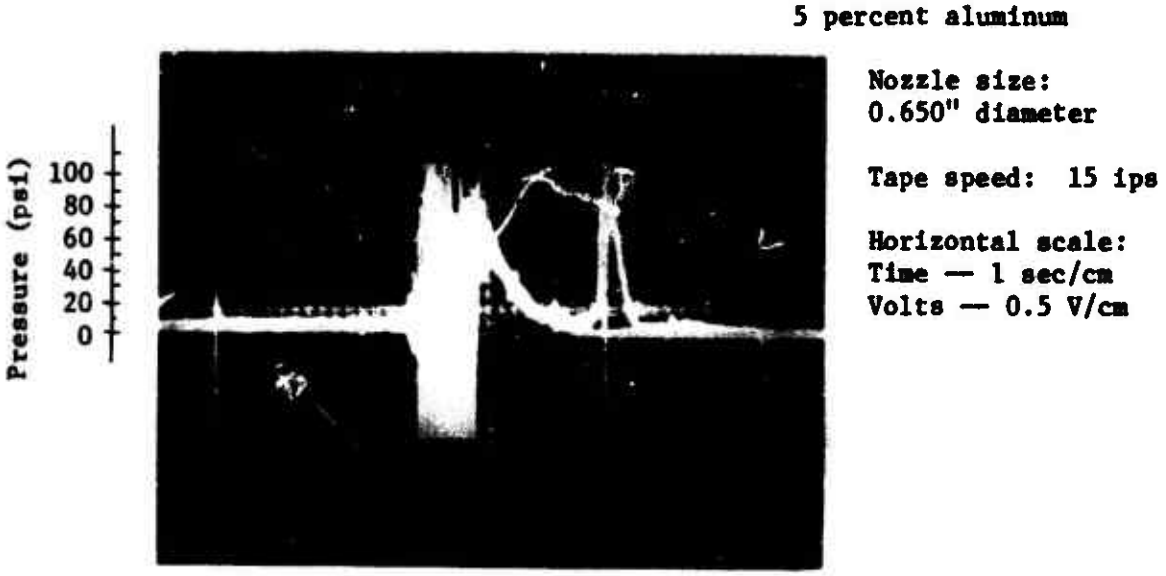

Fig. 6.16. Pressure wave of firing dated November 27, 1973.

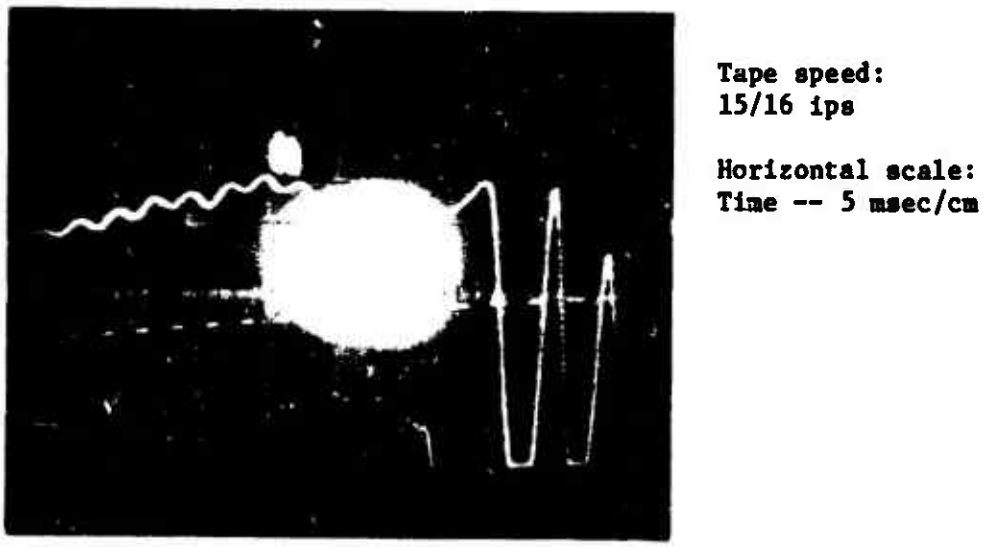

Fig. 6.17. Detail of Fig. 6.16 (one of five).

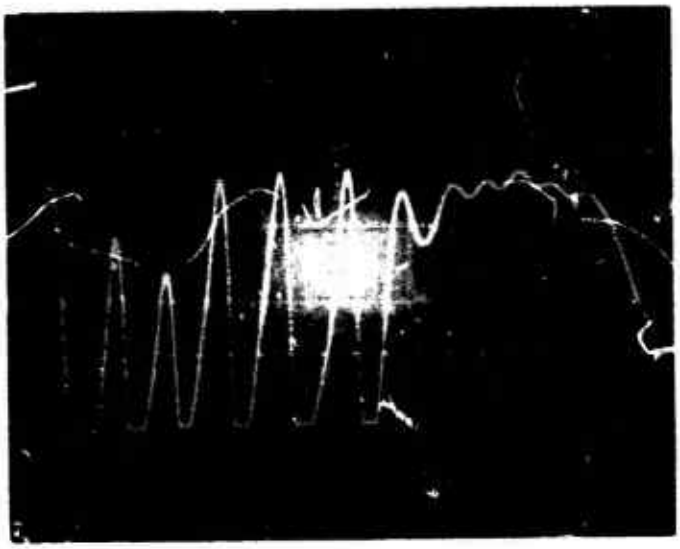

Tape speed:
15/16 ips

Time scale:
5 msec/cm

Fig. 6.18. Detail of Fig. 6.16 (two of five).

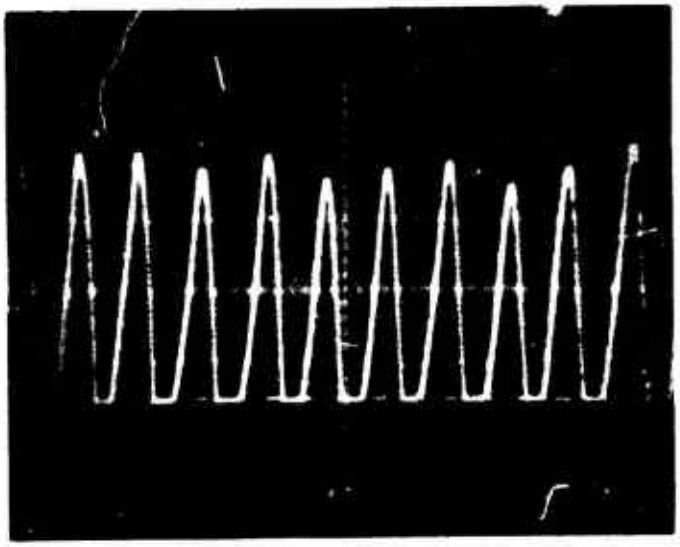

Tape speed:
15/16 ips

Time scale:
5 msec/cm

Oscillation frequency: 4.39 kHz

Fig. 6.19. Detail of Fig. 6.16 (three of five).

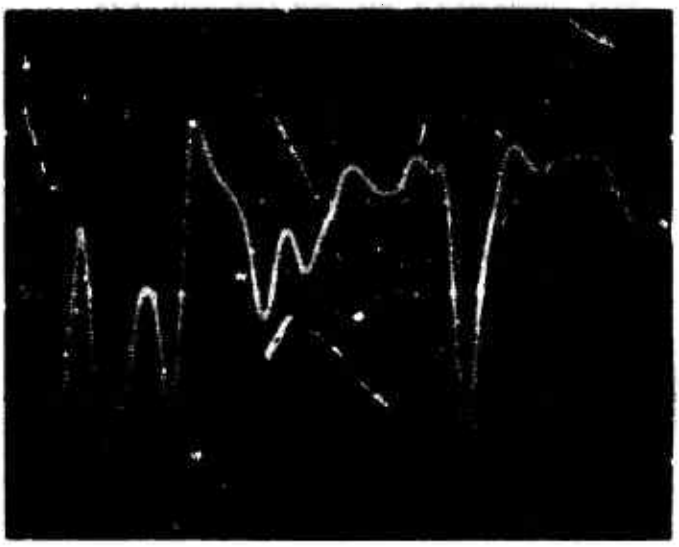

Tape speed:
15/16 ips

Time scale:
5 msec/cm

Fig. 6.20. Detail of Fig. 6.16 (four of five).

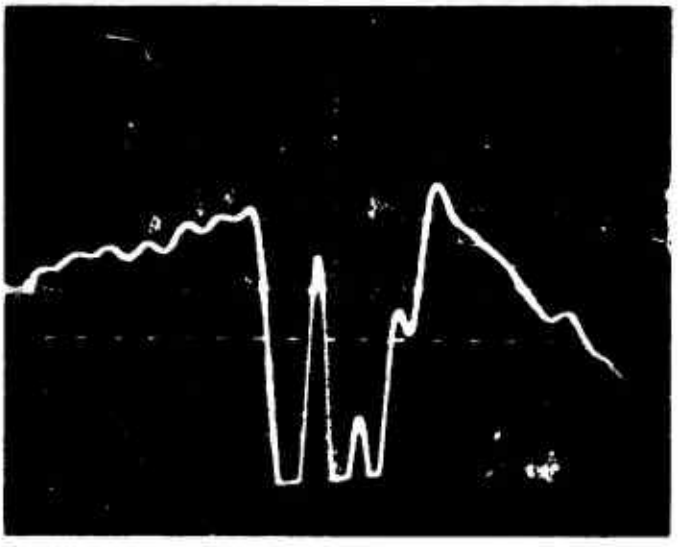

Tape speed:
15/16 ips

Time scale:
5 msec/cm

Fig. 6.21. Detail of Fig. 6.16 (five of five).

then fed into the tape recorder channel No. 2. This is shown in the lower part of Fig. 6.23. It is apparent that the oscillation was not seen at the end. Figure 6.22 shows the data obtained by the Sanborn recorder. On the upper half of Fig. 6.23 is the signal taken from the other transducer which was mounted on the top of the rocket motor about the center of the window. The signal on this picture was played back from the tape channel No. 1 at a speed two and a half times slower than the original recording speed. Figures 6.24 through 6.32 are segments of the signal registered on the upper half of Fig. 6.23 played back at sixteen times slower speed. The oscillation frequency calculated from Fig. 6.28 is 4.272 kHz, and the frequency calculated from Fig. 6.32 decreased to 3.66 kHz. This could be for one or both of the following two reasons:

1. The increase of chamber length.
2. Different mode dominates.

For the following two firings, both 5 percent propellant, two pressure transducers, one at the center and one at the end, were used. Together with the wave attenuation measurements, all signals were fed into the HP tape recorder. Figure 6.33 is the attenuation measurement of the January 18, 1974, No. 1 firing. The burning time of this and the next firing are considerably longer than all the previous propellants for some unknown reason. The only explanation is that this is a different batch.

Figures 6.34 and 6.35 are two waveforms of the microwave signal registered at different times of Fig. 6.33 as indicated. The microwave signal remains in its undistorted original waveform. This shows

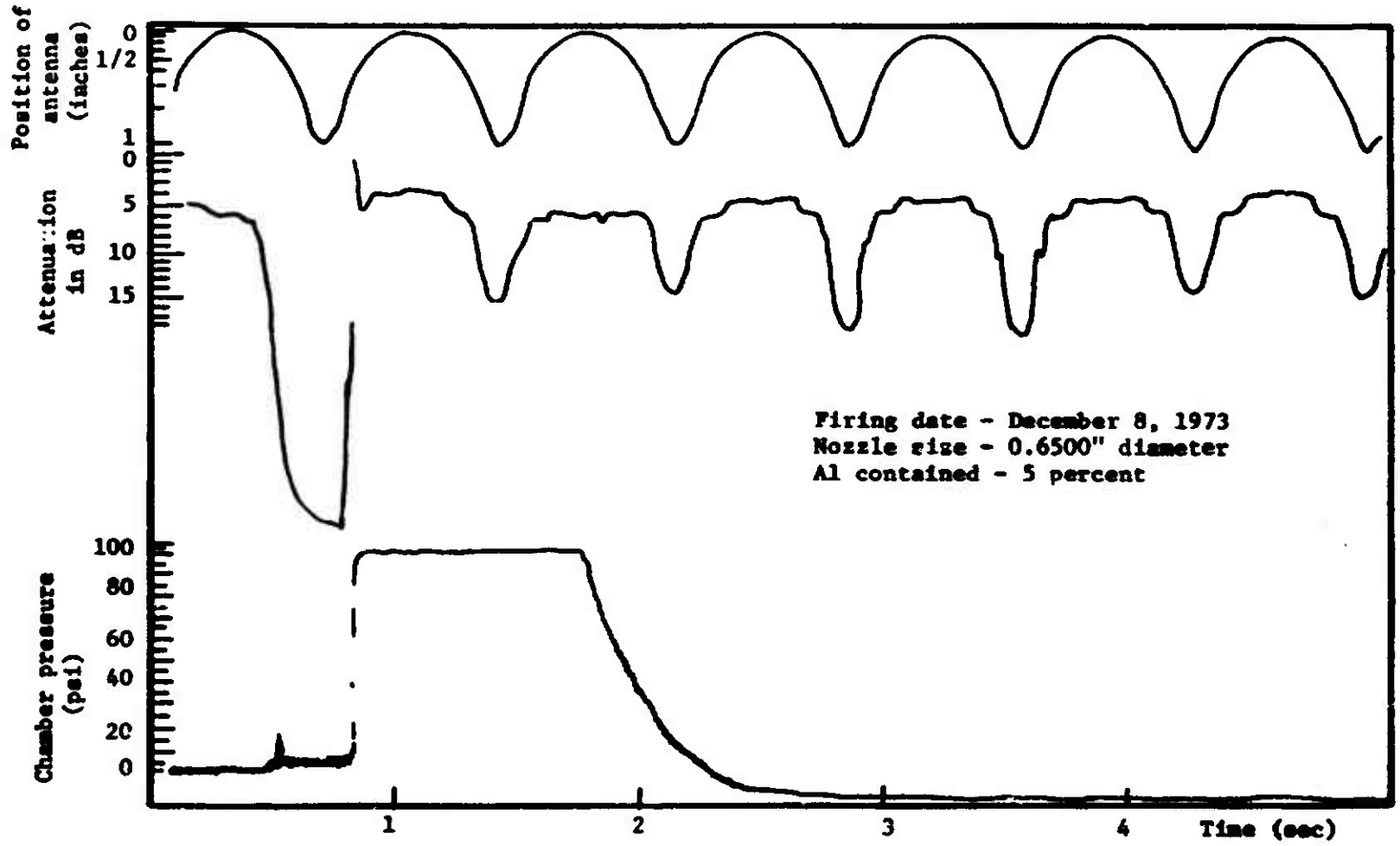

Fig. 6.22. Experimental result for December 8, 1973 firing.

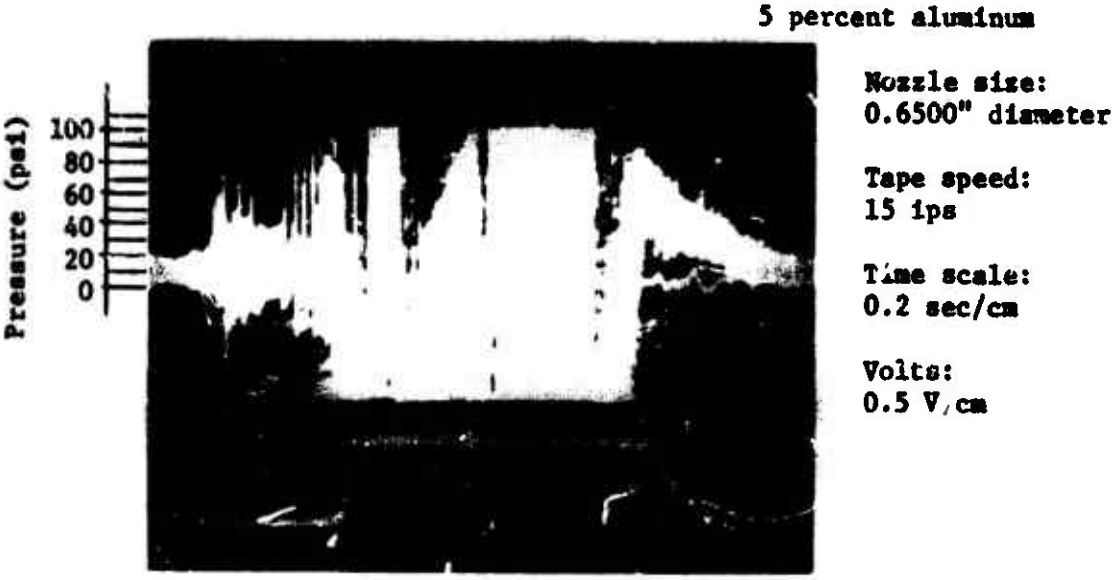

Fig. 6.23. Pressure wave of firing dated December 8, 1973.

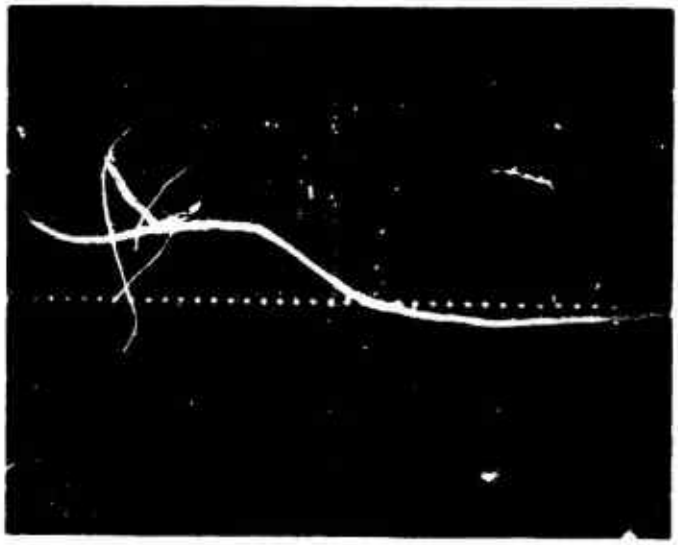

Fig. 6.24. Detail of upper waveform of Fig. 6.23 (one of nine).

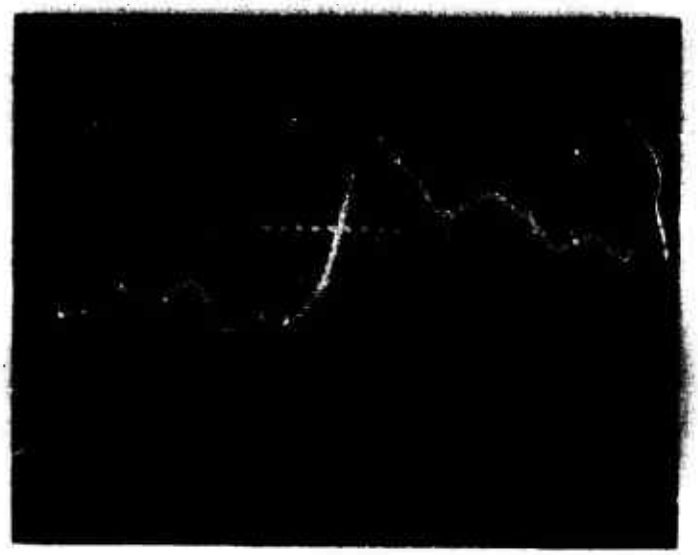

Tape speed:
15/16 ips

Time scale:
5 msec/cm

Fig. 6.25. Detail of upper waveform of Fig. 6.23 (two of nine).

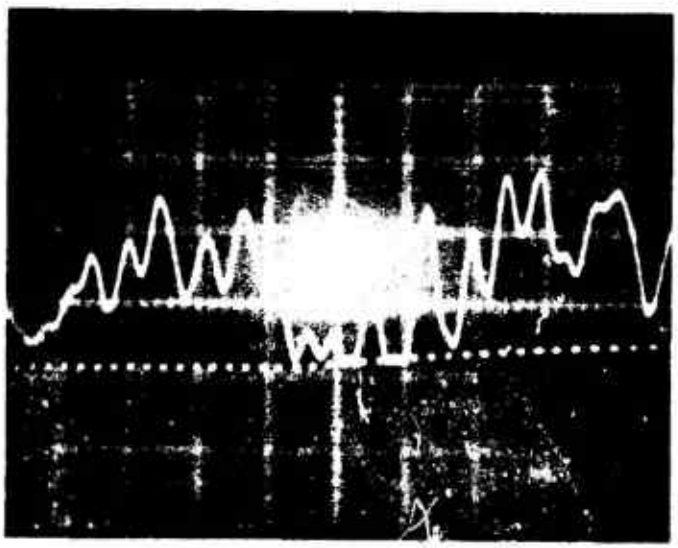

Tape speed:
15/16 ips

Time scale:
5 msec/cm

Fig. 6.26. Detail of upper waveform of Fig. 6.23 (three of nine).

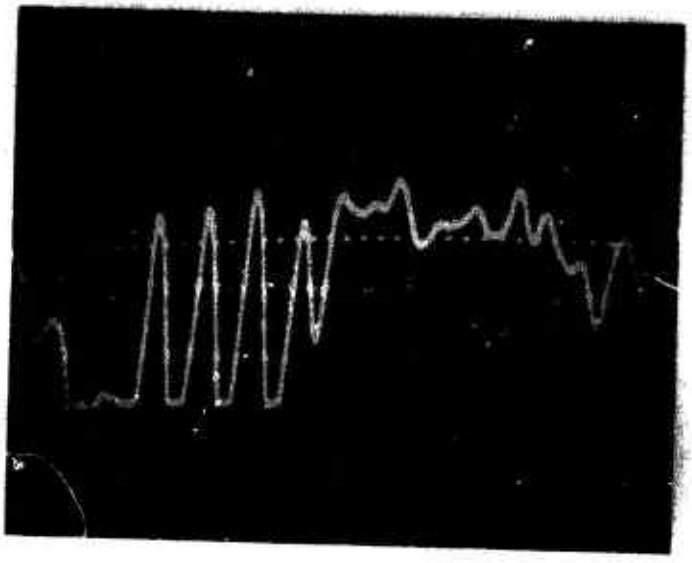

Tape speed:
15/16 ips

Time scale:
5 msec/cm

Fig. 6.27. Detail of upper waveform of Fig. 6.23 (four of nine).

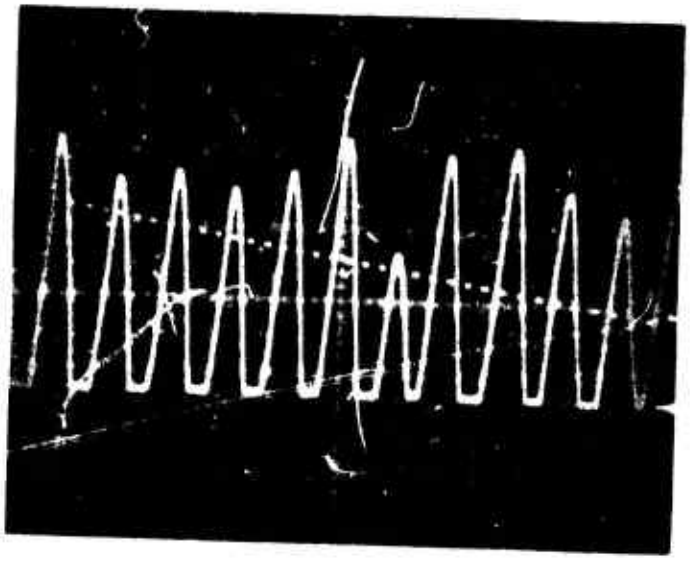

Tape speed:
15/16 ips

Time scale:
5 msec/cm

Oscillation frequency: 4.272 kHz

Fig. 6.28. Detail of upper waveform of Fig. 6.23 (five of nine).

Tape speed:
15/16 ips

Time scale:
5 msec/cm

Fig. 6.29. Detail of upper waveform of Fig. 6.23 (six of nine).

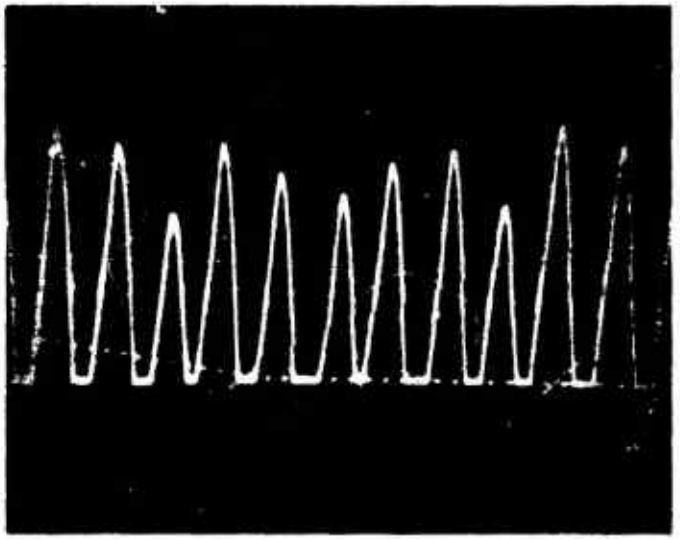

Tape speed:
15/16 ips

Time scale:
5 msec/cm

Fig. 6.30. Detail of upper waveform of Fig. 6.23 (seven of nine).

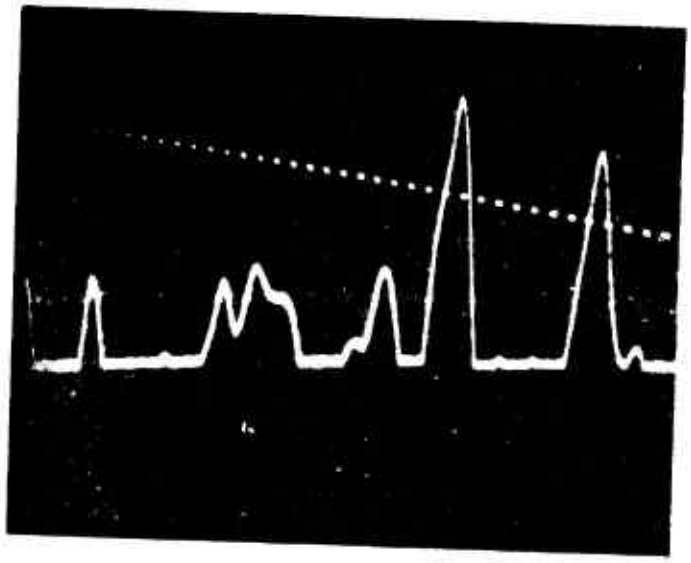

Tape speed:
15/16 ips

Time scale:
5 msec/cm

Fig. 6.31. Detail of upper waveform of Fig. 6.23 (eight of nine).

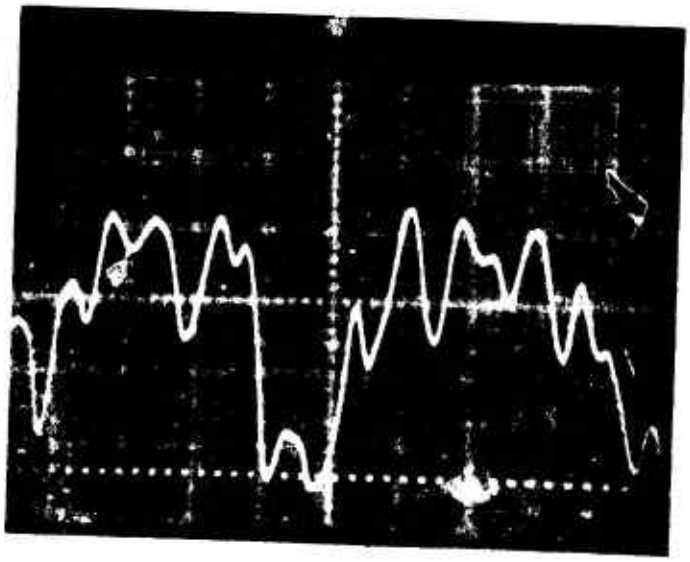

Tape speed:
15/16 ips

Time scale:
5 msec/sec

Oscillation
frequency:
3.66 kHz

Fig. 6.32. Detail of upper waveform of Fig. 6.23 (nine of nine).

5 percent Al propellant

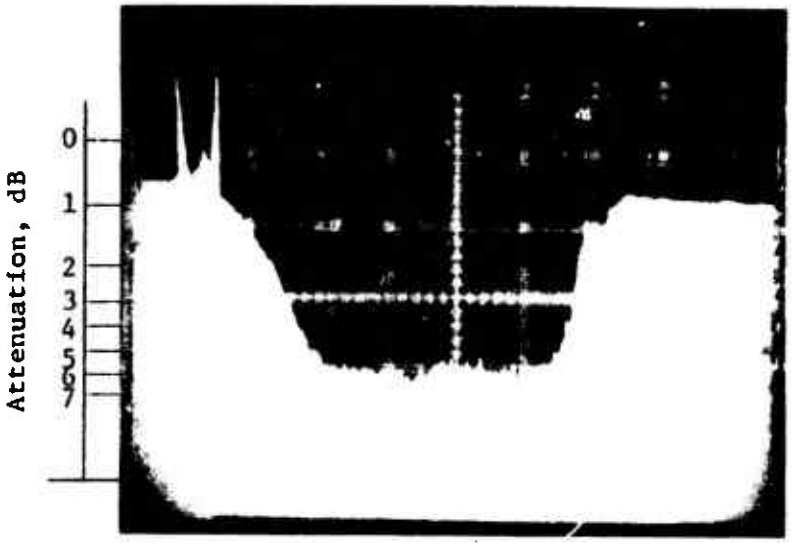

Nozzle size:
0.640" diameter

Tape speed:
15 ips

Time scale:
5 sec/cm

Fig. 6.33. Attenuation measurements of firing dated January 18, 1974, No. 1.

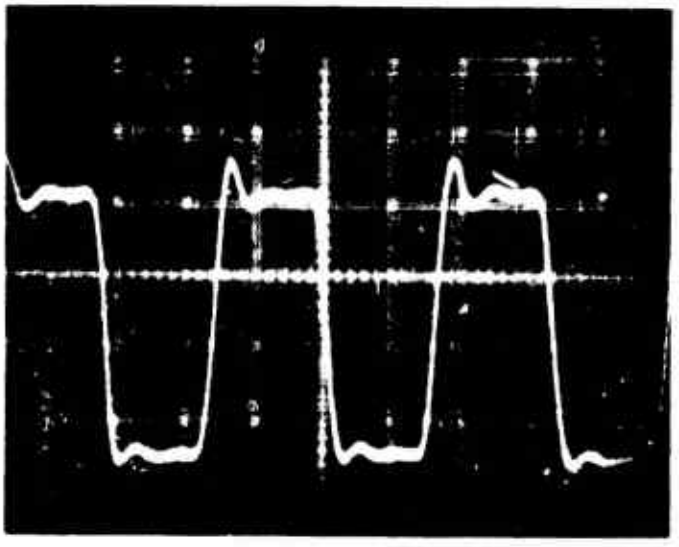

Tape speed:
15/16 ips

Time scale:
5 msec/cm

Fig. 6.34. Waveform of Fig. 6.33.

that pressure wave oscillation does not affect the microwave signal. Figure 6.36 is the pressure wave registered by the center transducer. By slowing down the playback tape speed sixteen times, the oscillation of acoustic waves can be shown clearly. Figure 6.37 shows the early part of the pressure wave and the oscillation frequency is 3.90 kHz. Figures 6.38 shows the latter part of the firing and the oscillation frequency is 4.11 kHz. Between these two high pressure peaks is a region of lower pressure. Figure 6.39 tells the detail of this region where the oscillatory curve is the sixty cycle noise. If we take this period as equilibrium situation, the temperature predicted by Fig. 5.7 is 2500 k. Compared with the value listed in Table 5.2, the error is 6.12 percent.

For the first time pressure wave oscillation was also observed by the transducer at the end. Figure 6.40 shows the signal recorded on the tape and Fig. 6.41 shows the oscillation waveform. Although both magnitudes are considerably lower than the center one, the oscillation of acoustic waves is clearly displayed. The oscillation frequency shown in Fig. 6.41 is 4.4 kHz which is higher than the center one observed.

The results of this firing are quite "different" from all the other firings. This is also the first and only time that the oscillation of acoustic waves "disappears" during the burning process. This "transition" period takes approximately five seconds, which is longer than the initial or the final oscillation period.

Figure 6.42 shows the attenuation of microwave signals for the

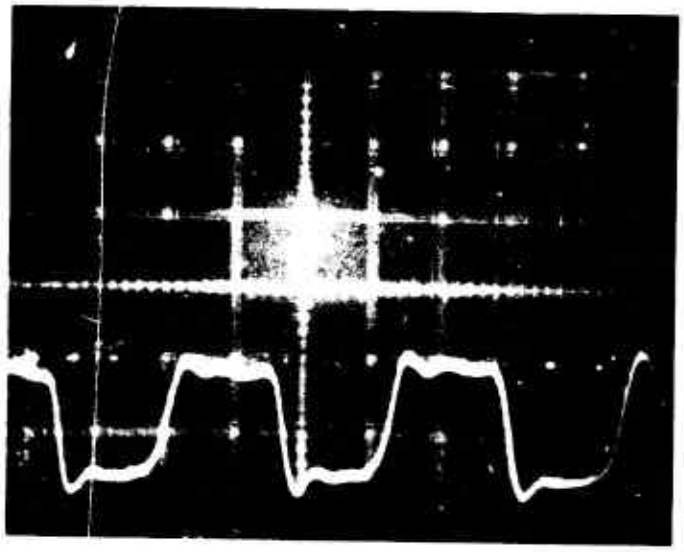

Tape speed:
15/16 ips

Time scale:
5 msec/cm

Fig. 6.35. Waveform of Fig. 6.33.

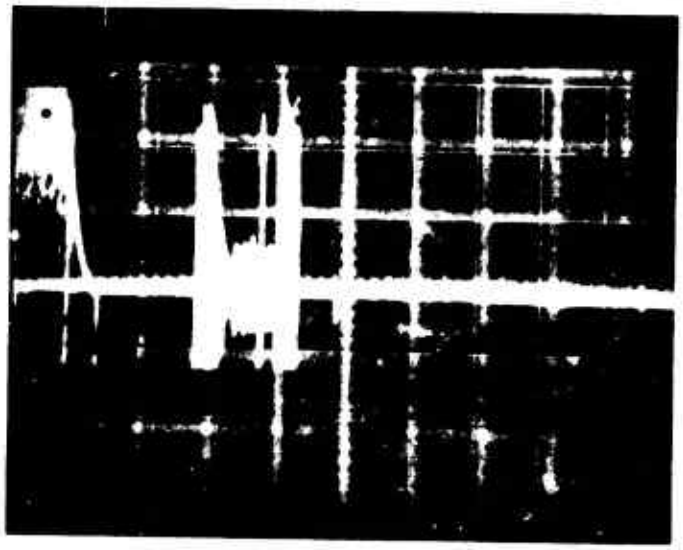

5 percent Al propellant

Nozzle size:
0.640" diameter

Tape speed:
15 ips

Time scale:
5 sec/cm

Fig. 6.36. Pressure wave of firing dated January 18, 1974, No. 1.

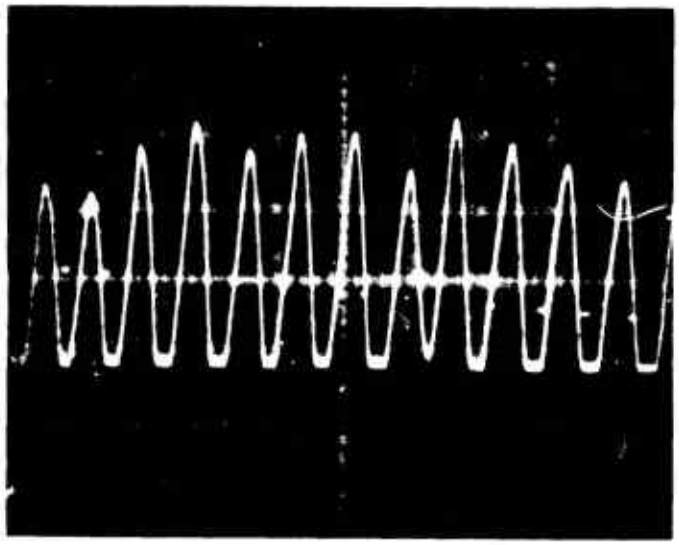

Tape speed:
15/16 ips

Time scale:
5 msec/cm

Oscillation frequency: 390 kHz

Fig. 6.37. Pressure waveform of Fig. 6.36.

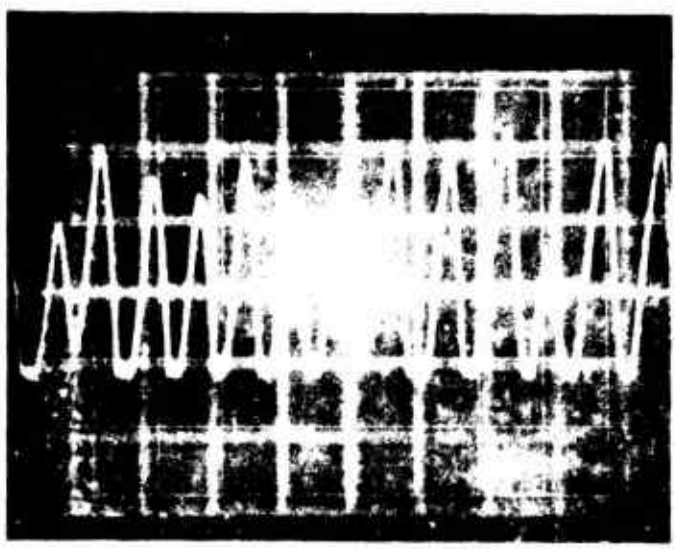

Tape speed:
15/16 ips

Time scale:
5 msec/cm

Oscillation frequency: 4.11 kHz

Fig. 6.38. Pressure waveform of Fig. 6.36.

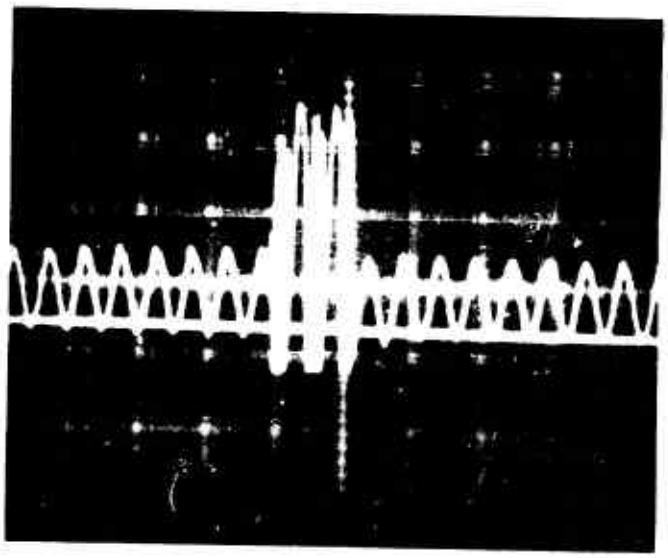

Tape speed:
15/16 ips

Time scale:
5 msec/cm

Fig. 6.39. Pressure waveform of Fig. 6.36.

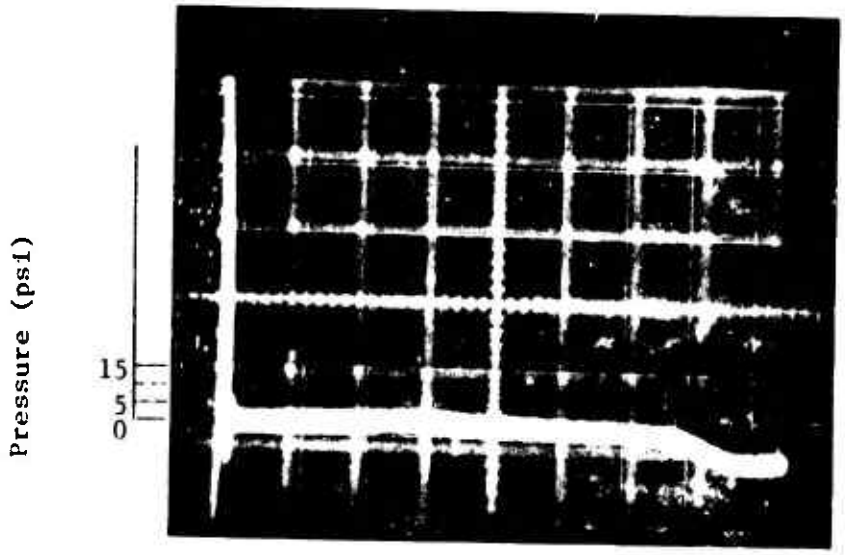

Tape speed:
15 ips

Time: 5 sec/cm

Vertical scale:
0.05 V/cm

Fig. 6.40. Pressure wave observed by the end transducer for January 18, 1974, No. 1 firing.

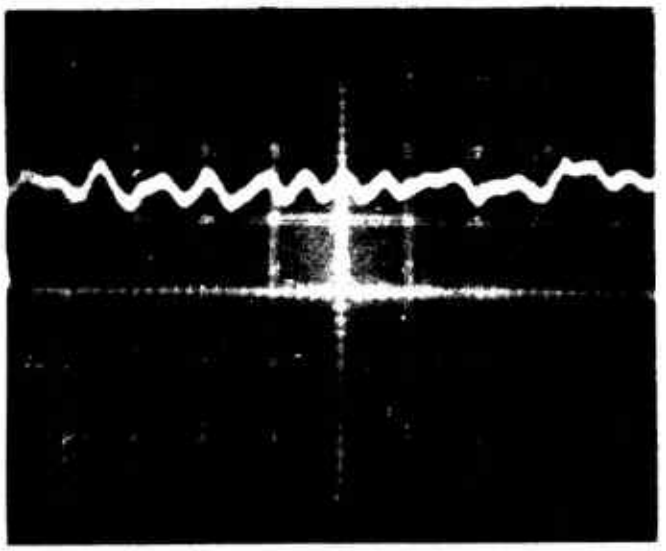

Tape speed:
15/16 ipa

Time scale:
5 msec/cm

Vertical scale:
0.01 V/cm

Oscillation frequency: 4.4 kHz

Fig. 6.41. Oscillation waveform of Fig. 6.40.

5 percent Al propellant

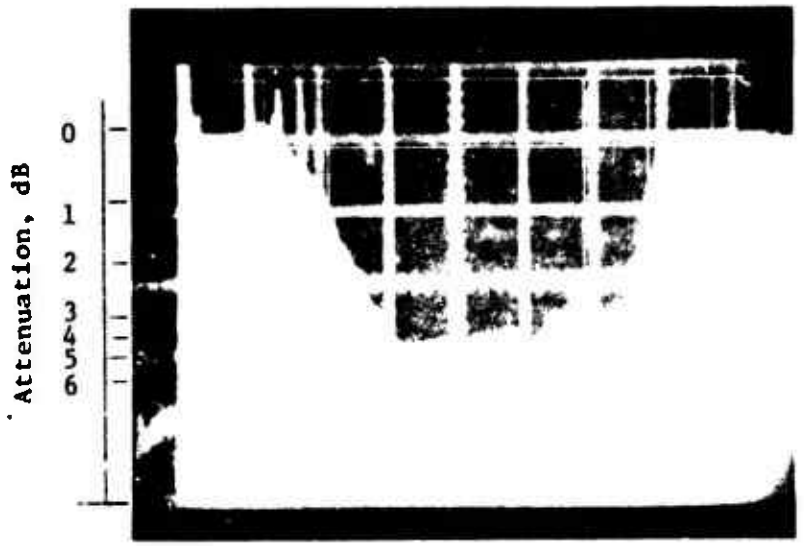

Nozzle size:
0.575" diameter

Tape speed:
15 ips

Time scale:
5 sec/cm

Fig. 6.42. Microwave attenuation for the January 18, 1974 firing No. 2.

Jsnuary 18, 1974 firing No. 2. At the center part, the attenustion is about 4 dB down. Figure 6.43 shows the puzzling pressure wsve registered on the tape by the center transducer. This could be a result of the malfunctioning of the trsnsducer. Figure 6.44 is the signal obtained by the end one. The oscillation phenomenon was again observed. This is displayed in Fig. 6.45, and the oscillation frequency is 4 kHz. This is very close to the result of the No. 1 firing. Assuming Fig. 6.43 is the true pressure wsve. the oscillation frequency obtsined from Fig. 6.46, the slowing down segment of Fig. 6.41, is 3.2 kHz.

From the two firing results mentioned above, it is obvious that at different points of the combustion chamber, different modes of acoustic wave oscillation will be observed.

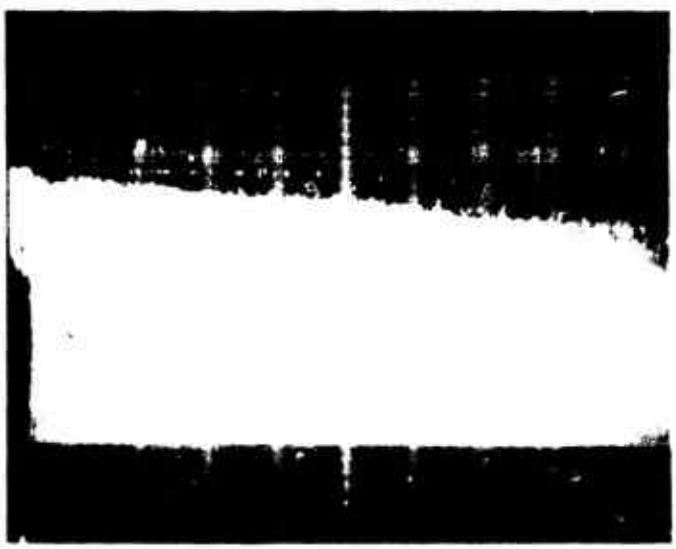

Fig. 6.4?. Pressure wave for January 18, 1974 firing No. 2.

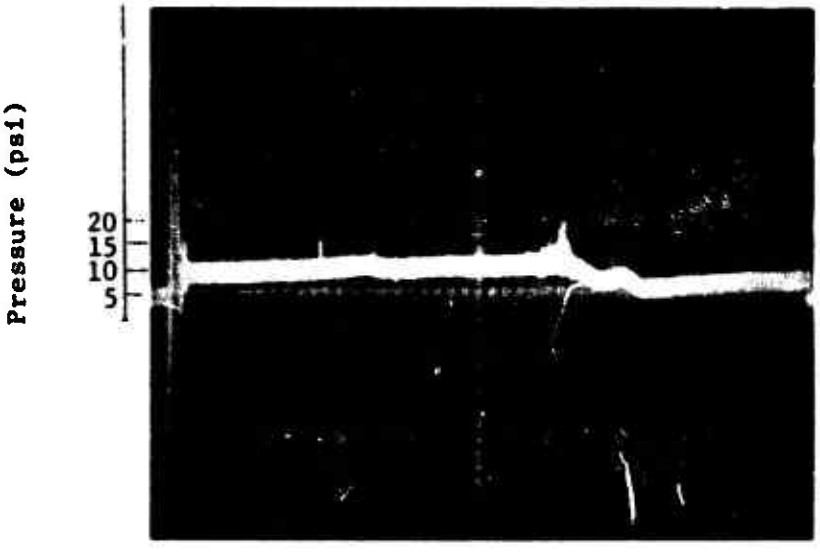

Fig. 6.44. Pressure wave recorded by the end transducer for the January 18, 1974, No. 2, firing.

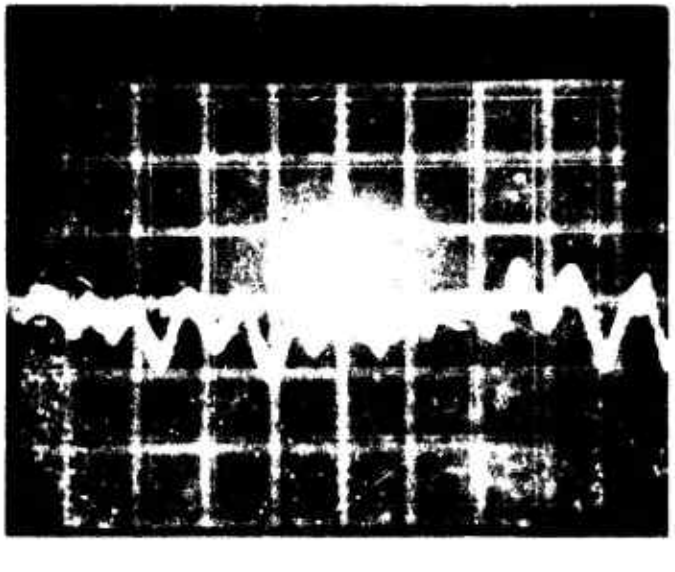

Fig. 6.45. Pressure oscillation seen by the end pressure transducer.

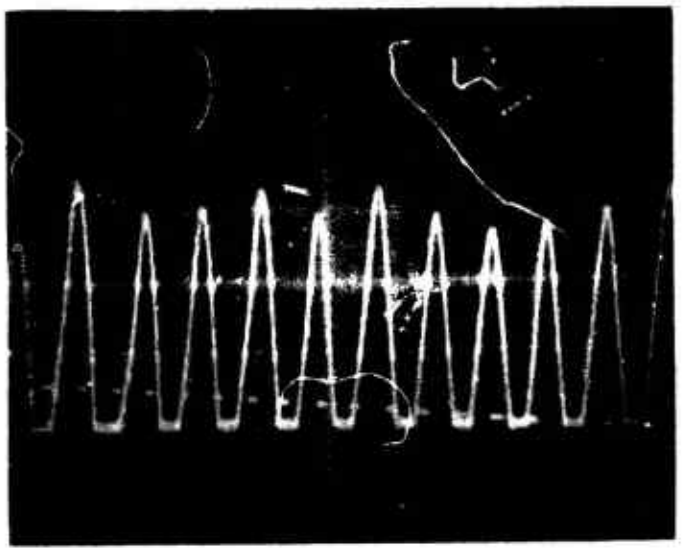

Tape speed:
15/16 ips

Time scale:
5 msec/cm

Fig. 6.46. Pressure oscillation corresponding to Fig. 6.41.

VII. SUMMARY AND CONCLUSIONS

On previous pages, the theory of using microwave attenuation measurement techniques as a plasma diagnostic tool was discussed, and the experimental results proved its accuracy and effectiveness even when the plasma is clouded with metallic particles. The results in Table 6.1 show that the experimental values are within three percent of the predicted theoretical values. This means that a temperature change of several degrees out of several thousand degrees can be measured.

The advantages of microwave attenuation measurement techniques are as follows:

1. Relatively simple equipment is needed as compared to the equipment for optical methods.
2. Measurements are made directly on any internal part of the plasma. This is done by focusing the microwave radiation to a few millimeters in radius, as described in Chapter V. The two-color method is presently the most common method used to measure the rocket combustion chamber temperature with suspended metallic particles. This technique is a measurement made of the flame radiance without penetrating the flame. The flame temperature is determined by comparing the ratio of the measured spectral radiances at two wavelengths with the ratio of the known blackbody spectral radiances at the two wavelengths. This technique also assumes that the spectral absorptance at the two wavelengths

is equal. The temperature gradients inside the flame are not detectable by this method and the spectral absorptance at two wavelengths is not always the same.

3. Measurements are made of the instantaneous and continuous response of the system.

4. Results are easy to interpret.

The conditions for the microwave attenuation measurement technique to be applicable are:

1. Plane wave assumption is justified.

2. A known number of free electrons are present to cause measurable attenuation.

3. The composition of combustion chamber gas is known.

4. The chamber pressure is measured.

The temperature profile away from the burning surface of the solid propellant was measured by the combination of the scan of the microwave signal across the rocket chamber, a scan distance of one inch, and by the motion of the burning surface, a distance of one inch, as produced by the burning itself. Figures 6.6, 6.9, 6.12, and 6.14 show some of the experimental results and the calculated values obtained from Eqs. 4.10 and 4.11 for the temperature profiles. The slopes have an angular difference of a maximum of 25 degrees for 5 percent aluminized propellant and 18.5 degrees for 10 percent aluminized propellant.

The oscillation of acoustic waves inside the combustion chamber is theoretically explored and experimentally observed. For a cylindrical end burner, the oscillation phenomenon is displayed in Figs. 6.19 to 6.46, and the oscillation frequencies obtained experimentally range from

3.2 to 4.4 kHz, whereas the calculated values listed in Table 6.2 range from 2.98 to 5.13 kHz for various oscillation modes.

The analysis of acoustic stability of a rocket motor requires the understanding of the acoustic gain and loss mechanisms. The acoustic gain and loss expressions are discussed in Chapter III and applied to the cylindrical rocket motor in Chapter V. Figures 5.12 and 5.13 show the application of the theory to the firing data for two firings where the systems are stable and the acoustic loss exceeded the gain ($A_b^r < 0$) in Fig. 5.12 and ($A_b^r < -0.25$) in Fig. 5.13. When the chamber pressure was extremely high and exceeded the quartz window strength, the windows failed as a result of one or both of the following possible conditions:

1. The chamber mean pressure was too high.
2. Acoustic oscillation caused the pressure buildup.

Figure 5.15 shows a case of failure where the acoustic loss was much less than the acoustic gain ($A_b^r = -0.5$) and failure could have resulted from the acoustic oscillation.

This investigation shows that microwave attenuation measurement techniques can be used to analyze the thermodynamic properties of a combustion plasma containing suspended metallic particles in a solid propellant rocket motor. The acoustic oscillation phenomenon of an end burner was also investigated theoretically and experimentally.

APPENDIX I

COMBUSTION CHAMBER GAS PROPERTIES

COMBUSTION CHAMBER PRESSURE 5 PSI

Propellant Al Contained	0 Percent	5 Percent	10 Percent	15 Percent
Density		1.714	1.735	1.756
Heat Cap. (cal.)		43.526	43.732	43.770
Entropy (cal.)		280.692	275.736	269.927
Molecular Weight		24.325	24.836	25.346
Total Moles of Gas		4.111	4.026	3.945
Moles of H_2		0.82705	1.07610	1.32189
Moles of H_2O		0.93208	0.58817	0.25539
Moles of N_2		0.32037	0.29922	0.27824
Moles of CO_2		0.18379	0.09346	0.03393
Moles of HCl		0.55497	0.49985	0.42980
Moles of CO		1.03658	1.12690	1.18641
Moles of K		0.00155	0.00267	0.00417
Moles of Cl		0.05649	0.06403	0.06381
Moles of Al		0.00001	0.00011	0.00109
Moles of Al_2O_3		0.09133	0.18119	0.26014

COMBUSTION CHAMBER PRESSURE 70 PSI

Propellant Al Contained	0 Percent	5 Percent	10 Percent	15 Percent
Density		1.714	1.735	1.756
Heat Cap. (cal.)		43.589	43.787	43.811
Entropy (cal.)		275.042	270.205	264.509
Molecular Weight		24.426	24.966	25.502
Total Moles of Gas		4.094	4.006	3.921
Moles of H_2		0.82727	1.08163	1.33370
Moles of H_2O		0.93898	0.59376	0.25956
Moles of N_2		0.32042	0.29925	0.27825
Moles of CO_2		0.18229	0.09228	0.03356
Moles of HCl		0.56305	0.50751	0.43492
Moles of CO		1.03808	1.12806	1.18677
Moles of K		0.00128	0.00225	0.00359
Moles of Cl		0.04797	0.05533	0.05545
Moles of Al		0.00001	0.00009	0.00099
Moles of Al_2O_3		0.09132	0.18105	0.25950

COMBUSTION CHAMBER PRESSURE 15 PSI

Propellant Al Contained	0 Percent	5 Percent	10 Percent	15 Percent
Density		1.714	1.735	1.756
Heat Cap. (cal.)		43.623	43.817	43.835
Entropy (cal.)		271.747	266.982	261.355
Molecular Weight		24.482	25.039	25.591
Total Moles of Gas		4.085	3.994	3.908
Moles of H_2		0.82732	1.08466	1.34046
Moles of H_2O		0.94284	0.59696	0.26180
Moles of N_2		0.32046	0.29927	0.27825
Moles of CO_2		0.18153	0.09166	0.03334
Moles of HCl		0.56755	0.51183	0.43783
Moles of CO		1.03883	1.12867	1.18697
Moles of K		0.00113	0.00202	0.00327
Moles of Cl		0.04326	0.05044	0.05077
Moles of Al		0.00001	0.00008	0.00092
Moles of Al_2O_3		0.09133	0.18101	0.25923

COMBUSTION CHAMBER PRESSURE 20 PSI

Propellant Al Contained	0 Percent	5 Percent	10 Percent	15 Percent
Density	1.694	1.714	1.735	1.756
Heat Cap. (cal.)	43.405	43.646	43.839	43.852
Entropy (cal.)	273.398	269.413	264.701	259.124
Molecular Weight	23.936	24.520	25.090	25.654
Total Moles of Gas	4.178	4.078	3.986	3.898
Moles of H_2	0.59052	0.82732	1.08670	1.34517
Moles of H_2O	1.26316	0.94552	0.59918	0.26328
Moles of N_2	0.34183	0.32049	0.29929	0.27826
Moles of CO_2	0.31150	0.18105	0.09126	0.03318
Moles of HCl	0.62446	0.57062	0.51482	0.43984
Moles of CO	0.90887	1.03930	1.12906	1.18711
Moles of K	0.00051	0.00103	0.00187	0.00305
Moles of Cl	0.03156	0.04004	0.04707	0.04755
Moles of Al	--	0.00001	0.00008	0.00086
Moles of Al_2O_3	--	0.09133	0.18099	0.25909

COMBUSTION CHAMBER PRESSURE 40 PSI

Propellant Al Contained	0 Percent	5 Percent	10 Percent	15 Percent
Density	1.694	1.714	1.735	1.756
Heat Cap. (cal.)	43.454	43.698	43.888	43.894
Entropy (cal.)	267.650	263.806	259.224	253.770
Molecular Weight	23.995	24.607	25.208	25.801
Total Moles of Gas	4.168	4.064	3.967	3.876
Moles of H_2	0.58803	0.82711	1.09125	1.35617
Moles of H_2O	1.26862	0.95165	0.60433	0.26648
Moles of N_2	0.34191	0.32056	0.29934	0.27828
Moles of CO_2	0.31092	0.18006	0.09039	0.03281
Moles of HCl	0.63072	0.57755	0.52169	0.44449
Moles of CO	0.90942	1.04026	1.12989	1.18743
Moles of K	0.00039	0.00082	0.00153	0.00255
Moles of Cl	0.02518	0.03281	0.03938	0.04019
Moles of Al	--	0.00001	0.00006	0.00072
Moles of Al_2O_3	--	0.09136	0.18098	0.25893

COMBUSTION CHAMBER PRESSURE 60 PSI

Propellant Al Contained	0 Percent	5 Percent	10 Percent	15 Percent
Density	1.694	1.714	1.735	1.756
Heat Cap. (cal.)	43.479	43.725	43.915	43.919
Entropy (cal.)	264.294	260.534	256.032	250.652
Molecular Weight	24.026	24.654	25.273	25.884
Total Moles of Gas	4.162	4.056	3.957	3.863
Moles of H_2	0.58669	0.82689	1.09365	1.36234
Moles of H_2O	1.27148	0.95499	0.60718	0.26810
Moles of N_2	0.34196	0.32061	0.29937	0.27830
Moles of CO_2	0.31069	0.17959	0.08995	0.03253
Moles of HCl	0.63398	0.58126	0.52544	0.44705
Moles of CO	0.90965	1.04071	1.13030	1.18761
Moles of K	0.00034	0.00072	0.00135	0.00229
Moles of Cl	0.02187	0.02894	0.03519	0.03616
Moles of Al	--	--	0.00005	0.00064
Moles of Al_2O_3	--	0.09138	0.18101	0.25894

COMBUSTION CHAMBER PRESSURE 80 PSI

Propellant Al Contained	0 Percent	5 Percent	10 Percent	15 Percent
Density	1.694	1.714	1.735	1.756
Heat Cap. (cal.)	43.496	43.745	43.933	43.936
Entropy (cal.)	261.916	258.217	253.771	248.445
Molecular Weight	24.046	24.685	25.318	25.941
Total Moles of Gas	4.159	4.051	3.950	3.855
Moles of H_2	0.58577	0.82669	1.09521	1.36657
Moles of H_2O	1.27336	0.95724	0.60914	0.26913
Moles of N_2	0.34199	0.32064	0.29940	0.27830
Moles of CO_2	0.31056	0.17930	0.08967	0.03243
Moles of HCl	0.63610	0.58372	0.52798	0.44878
Moles of CO	0.90977	1.04098	1.13056	1.18772
Moles of K	0.00030	0.00065	0.00123	0.00211
Moles of Cl	0.01972	0.02637	0.03236	0.03344
Moles of Al	--	--	0.00005	0.00058
Moles of Al_2O_3	--	0.09140	0.18104	0.25899

COMBUSTION CHAMBER PRESSURE 100 PSI

Propellant Al Contained	0 Percent	5 Percent	10 Percent	15 Percent
Density	1.694	1.714	1.735	1.756
Heat Cap. (cal.)	43.507	43.759	43.947	43.950
Entropy (cal.)	260.072	256.421	252.021	246.738
Molecular Weight	24.060	24.709	25.351	25.985
Total Moles of Gas	4.156	4.047	3.945	3.848
Moles of H_2	1.27474	0.95892	0161060	0.26986
Moles of N_2	0.34202	0.32066	0.29942	0.27830
Moles of CO_2	0.31049	0.17911	0.08947	0.03231
Moles of HCl	0.63764	0.58554	0.52987	0.45007
Moles of CO	0.90983	1.04116	1.13074	1.18781
Moles of K	0.00028	0.00060	0.00114	0.00197
Moles of Cl	0.01815	0.02448	0.03026	0.03140
Moles of Al	--	--	0.00004	0.00054
Moles of Al_2O_3	--	0.09141	0.18106	0.25906

COMBUSTION CHAMBER PRESSURE 120 PSI

Propellant Al Contained	0 Percent	5 Percent	10 Percent	15 Percent
Density	1.694	1.714	1.735	1.756
Heat Csp. (cal.)	43.517	43.769	43.958	43.961
Entropy (cal.)	258.567	254.956	250.593	245.344
Molecular Weight	24.072	24.727	25.377	26.020
Total Moles of Gas	4.154	4.044	3.941	3.843
Moles of H_2	0.58451	0.82633	1.09723	1.37231
Moles of H_2O	1.27581	0.96025	0.61176	0.27042
Molea of N_2	0.34204	0.32068	0.29943	0.27830
Molea of CO_2	0.31044	0.17896	0.08931	0.03221
Moles of HCl	0.63883	0.58695	0.53135	0.45109
Moles of CO	0.90986	1.04128	1.13088	1.18788
Molea of K	0.00026	0.00056	0.00108	0.00187
Moles of Cl	0.01694	0.02301	0.02860	0.02980
Moles of Al	--	--	0.00004	0.00050
Molea of Al_2O_3	--	0.09142	0.18109	0.25193

APPENDIX II

ATTENUATION CALCULATION COMPUTER PROGRAM

```
00100      1*    C      ATTENUATION PROGRAM                                                    000000
00101      2*           DIMENSION RHO(15),RHOE(15),BB(15),DD(15),X(15),WP(15),ATTN(15),        000000
00101      3*          1ATT,DG(15),T(15)                                                       000000
00103      4*           REAL MOFH2, MOFH20, MOFN2, MOFCO2, MOFHCL, MOFCO, MMFH2, MMFH20,       000001
00103      5*          1MMFN2,MMFCO2,MMFHCL,MMFCO,MOTOT,MMFK,MMFAL                            000001
00104      6*           COMPLEX P,Q,R,YCUBE(3)                                                 000001
00104      7*    C      READ IN ALL CONSTANTS                                                  000001
00105      8*           DATA PLANK,ZMASS,BOLTZ,ZCHARG,PI,AVOG,FREQ,QVSH20,QVSHCL,QVCO2,        000001
00105      9*          1QCO,QH2,QQVCO,QQVH2,QQVN2/6.62517E-34,9.1083E-31,1.38044E-23,          000001
00105     10*          21.6021E-19,3.141596,6.0224E23,22.725E9,5.92E-8,1.835E-8,7.16E-14,      000001
00105     11*          32.65E-20,8.92E-20,2.08E-25,1.464E-25,2.7E-25/                         000001
00125     12*           W=2.*PI*FREQ                                                          000001
00126     13*           WSQ=W**2                                                              000005
00127     14*           CLGT=2.99793E8                                                        000007
00130     15*           CK=W/CLGT                                                             000011
00131     16*           C=8./(3.*SQRT(PI))                                                    000014
00132     17*           EV=4.31                                                               000023
00133     18*           DY=0.05                                                               000025
00134     19*           JOJ=1                                                                 000027
00135     20*           PERCNT=5.0                                                            000031
00136     21*           AL=5.0                                                                000033
00137     22*       15  I=0                                                                   000035
00140     23*           PRESP=1.0                                                             000035
00140     24*    C      READ IN MOLE FRACTION DATA                                             000035
00141     25*       48  READ 60, MOTOT,MMFH2,MMFH20,MMFN2,MMFCO2,MMFHCL,MMFCO,MMFK,CL,       000040
00141     26*          1 MMFAL                                                                 000040
00155     27*       60  FORMAT (10F8.5)                                                      000055
00156     28*           IF(PRESP) 7,7,51                                                      000055
00161     29*       51  K=1                                                                  000060
00162     30*           PRES=PRESP/14.7                                                       000062
00163     31*           MOFH2=MMFH2/MOTOT                                                     000064
00164     32*           MOFH20=MMFH20/MOTOT                                                   000067
00165     33*           MOFN2=MMFN2/MOTOT                                                     000072
00166     34*           MOFCO2=MMFCO2/MOTOT                                                   000075
00167     35*           MOFHCL=MMFHCL/MOTOT                                                   000100
00170     36*           MOFCO=MMFCO/MOTOT                                                     000103
00171     37*           ZN=((MMFK+MMFAL)/MOTOT)*AVOG                                          000106
00172     38*           ZNCL=CL/MOTOT*AVOG                                                    000113
00173     39*           TEMP=2.4E3                                                            000117
00174     40*           C1=MOFCO2*QVCO2                                                       000121
00175     41*           C2=MOFH20*QVSH20+MOFHCL*QVSHCL                                        000123
00176     42*           CZ=MOFCO*QCO+MOFH2*QH2                                                000127
00177     43*           CN=MOFN2*QQVH2+MOFN2*QQVN2+MOFCO*QQVCO                                000134
00200     44*        1  IF(K-10) 69,2,2                                                       000145
```

```
00210     45*     C      CACULATE THE INTEGRAL,V BAR=B-JO                                  000145
00203     46*        69 BETA=ZMASS/(2.*BOLTZ*TEMP)                                        000150
00204     47*           RHO(K)=PRES*AVOG/(82.05*TEMP)*1.E6                                000156
00205     48*           T=4.*BETA                                                         000166
00206     49*           T1=C1*RHO(K)*BETA                                                 000170
00207     50*           T2=C2*RHO(K)*(SQRT(BETA))**3                                      000173
00210     51*           TZ=CZ*RHO(K)*SQRT(BETA)                                           000205
00211     52*           TM=CM*RHO(K)                                                      000211
00212     53*           DI=0.                                                             000214
00213     54*           BI=0.                                                             000215
00214     55*           B=0.                                                              000216
00215     56*           D=0.                                                              000217
00216     57*           Y=0.0                                                             000220
00217     58*           J=0.                                                              000221
00220     59*        30 Y=Y+DY                                                            000223
00221     60*           J=J+JJJ                                                           000225
00222     61*           IF(J-65) 70,100,100                                               000230
00225     62*        70 DENOM1=(T**Y)**2                                                  000233
00226     63*           BL=B                                                              000236
00227     64*           DL=D                                                              000240
00230     65*           YPOLY=T2+T1*Y+TZ*Y**2+TM*Y**3                                     000242
00231     66*           DENOM2=YPOLY**2                                                   000257
00232     67*           DENOM=DENOM1+DENOM2                                               000261
00233     68*           B=C*YPOLY*Y**5*EXP(-Y**2)/DENOM*BETA                              000263
00234     69*           D=C*X*BETA*Y**6*EXP(-Y**2)/DENOM*BETA                             000303
00235     70*           DB=0.5*(BL+B)*DY                                                  000315
00236     71*           DD=0.5*(DL+D)*DY                                                  000321
00237     72*           BI=BI+DB                                                          000325
00240     73*           DI=DI+DD                                                          000327
00241     74*           GO TO 30                                                          000331
00242     75*       100 BB(K)=BI                                                          000333
00243     76*           DD(K)=DI                                                          000335
00243     77*     C     DETERMINE THE IONIZATION AND PLASMA FREQUENCY                     000335
00244     78*           ZEXPK=EXP(-ZCHARG*EV/(BOLTZ*TEMP))                                000337
00245     79*           ZEXPCL=EXP(-ZCHARG*3.78/(BOLTZ*TEMP))                             000352
00246     80*           ZTEMP=TEMP*SQRT(TEMP)                                             000362
00247     81*           ZCONST=(SQRT(2.*PI*9.1083*1.38044)/6.62517)**3*1.E21              000367
00250     82*           ALPHA1=ZCONST*ZTEMP*ZEXPK*1.E-20                                  000405
00251     83*           ALPHA2=4.*ZCONST*ZTEMP*ZEXPCL*1.E-20                              000411
00252     84*           A1=ZN*1.E-20                                                      000417
00253     85*           A2=ZNCL*1.E-20                                                    000422
00254     86*           P=CMPLX(ALPHA1+ALPHA2+A2, 0.0)                                    000425
00255     87*           G=CMPLX(ALPHA1*(A2-A1+ALPHA2), 0.0)                               000431
00256     88*           R= CMPLX(-ALPHA1*ALPHA2*A1, 0.0)                                  000436
```

```
00257     89*           CALL CUBIC(P,Q,R,YCUBE)                                          000444
00260     90*           DO 500 LL=1,3                                                    000455
00263     91*           LZ=LL                                                            000455
00264     92*           IF(REAL(YCUBE(LZ))) 500,500,502                                  000460
00267     93*       500 CONTINUE                                                         000465
00271     94*           PRINT 99, TEMP                                                   000465
00274     95*        99 FORMAT(5X,'NO SOLUTIONS ARE FOUND FOR A TEMPERATURE OF  ',F6.1//) 000472
00275     96*           X(K)=0.                                                          000472
00276     97*           RHOE(K)=0.                                                       000473
00277     98*           WP(K)=0.                                                         000474
00300     99*           ATTN(K)=0.                                                       000475
00301    100*           ATTNDB(K)=0.                                                     000476
00302    101*           GO TO 37                                                         000477
00303    102*       502 RHOE(K)=REAL(YCUBE(LZ))*1.E20*ZCHARG                             000501
00303    103*     C     X(K) IS THE NUMBER DENSITY OF ELECTRONS                          000501
00304    104*           X(K)=REAL(YCUBE(LZ))*1.E20                                       000510
00305    105*           ZNE=RHOE(K)                                                      000512
00306    106*           WPSQ=ZNE*1.602/9.1083*36.*PI*1.E21                               000513
00306    107*     C     WP(K) IS THE PLASMA FREQUENCY                                    000513
00307    108*           WP(K)=SQRT(ABS(WPSQ))                                            000521
00310    109*           T(K)=TEMP                                                        000527
00310    110*     C     USING B, D, WP, AND TEMP, CALCULATE THE ATTENUATION              000527
00311    111*           TERM1=WPSQ/4.5Q*W*DD(K)-1.                                       000531
00312    112*           TERM2=SQRT(TERM1**2+(WPSQ/W5Q*W*BB(K))**2)                       000540
00312    113*     C     ATTN(K) IS IN NEPERS/METER                                       000540
00313    114*           IF(TERM1+TERM2) 505,510,510                                      000552
00316    115*       505 PRINT 606,TEMP                                                   000555
00321    116*       606 FORMAT(5X,'ATTENUATION TERM IS NEGATIVE FOR A TEMPERATURE OF  ', 000562
00321    117*          1F6.1//)                                                          000562
00322    118*           ATTN(K)=0.                                                       000562
00323    119*           ATTNDB(K)=0.                                                     000563
00324    120*           GO TO 37                                                         000564
00325    121*       510 ATTN(K)=SQRT(TERM1+TERM2)*CK/SQRT(2.)                            000566
00325    122*     C     ATTNDB IS DB ATTENUATION PER 2.20 INCH ATTENUATION PATH          000566
00326    123*           ATTNDB(K)=20.*0.4342948*2.54E-2*2.9375*ATTN(K)                   000603
00327    124*        37 T(K)=TEMP                                                        000606
00330    125*           TEMP=TEMP+50.0                                                   000610
00331    126*           K=K+1                                                            000612
00332    127*           GO TO 1                                                          000615
00333    128*        2  PRINT 3, PRESP, PERCNT, AL                                     000617
00340    129*           PRINT 4                                                          000625
00342    130*           PRINT5                                                           000631
00344    131*           PRINT 6,(T(J),RHO(J),RHOE(J),BB(J),DD(J),X(J),WP(J),ATTN(J),ATTNDB 000635
00344    132*          1(J),J=1,15)                                                      000635
```

```
00362    133*        25 PRINT 10                                                                    000656
00364    134*           IF (I-1) 11, 12, 12                                                         000662
00367    135*        11 PRESP=PRESP+4.0                                                             000666
00370    136*           I=I+1                                                                       000671
00371    137*           GO TO 48                                                                    000674
00372    138*        12 PRESP=PRESP+5.0                                                             000676
00373    139*           IF (PRESP-20.0) 48, 48, 77                                                  000700
00376    140*        77 PRESP=PRESP+15.0                                                            000703
00377    141*           IF (PRESP-120.0) 48, 48, 7                                                  000706
00402    142*         7 CONTINUE                                                                    000712
00403    143*           AL=AL+5.0                                                                   000712
00404    144*           IF (AL-15.0) 13, 13, 14                                                     000714
00407    145*        13 GO TO 15                                                                    000717
00410    146*        14 CONTINUE                                                                    000722
00411    147*        10 FORMAT(1H1)                                                                 000722
00412    148*         3 FORMAT(2X,'CALCULATED ATTENUATION PARAMETERS FOR ',F5.1,' PSIA WIT          000722
00412    149*          1H ',F4.1,' PERCENT POTASSIUM PERCHLORATE AND ',F4.1,' PERCENT ALUM         000722
00412    150*          2INUM'///)                                                                  000722
00413    151*         4 FORMAT(1X,'TEMP',' GAS ',' CHARGE ',' V BA                                 000722
00413    152*          1R INTEGRATION ',' ELECTRON',' PLASMA ',                                    000722
00413    153*          2ATTENUATION ')                                                             000722
00414    154*         5 FORMAT(5X,' DENSITY ',' DENSITY ',9X,'B',13X,'D',6X,'                      000722
00414    155*          1 DENSITY ',' FREQUENCY ',' NEPERS/METER DB',//)                            000722
00415    156*         6 FORMAT(1X,F7.1,E12.7,6E15.7,F10.3//)                                       000722
00416    157*           END                                                                         000722

END OF COMPILATION:        NO  DIAGNOSTICS.
```

```
00101      1*            SUBROUTINE CUBIC(P,Q,R,Y)                                  CUBIC  1    000000
00101      2*      C     *ROUTINE TO SOLVE A CUBIC EQUTION.                         CUBIC  2    000000
00103      3*            COMPLEX P,Q,R,Y(3),A,B,W,PO,Z1,CCBRT,CSQRT,T               CUBIC  3    000000
00104      4*            DATA W/(-0.5,0.866025404)/                                 CUBIC  4    000000
00105      5*            PO=P/3.0                                                   CUBIC  5    000000
00107      6*            A=Q/3.0-PO**2                                              CUBIC  6    000005
00110      7*            B=PO**3+0.5*(R-PO*Q)                                       CUBIC  7    000033
00111      8*            Z1=-B                                                      CUBIC  8    000105
00112      9*            IF(ABS(REAL(A))+ABS(AIMAG(A))) 1,3,1                       CUBIC  9    000106
00115     10*          1 T=CSORT(A**3+B**2)                                         CUBIC 10    000113
00116     11*            Z1=-B+T                                                    CUBIC 11    000166
00117     12*            IF(REAL(B)) 3,3,2                                          CUBIC 12    000173
00122     13*          2 Z1=-B-T                                                    CUBIC 13    000176
00123     14*          3 IF(AIMAG(Z1))5,4,5                                         CUBIC 14    000206
00126     15*          4 Z1=CMPLX(CBRT(REAL(Z1)),0.0)                               CUBIC 15    000207
00127     16*            GO TO 6                                                    CUBIC 16    000216
00130     17*          5 Z1=CCBRT(Z1)                                               CUBIC 17    000220
00131     18*          6 DO 7 K=1,3                                                 CUBIC 18    000227
00134     19*            Y(K)=Z1-A/Z1-PO                                            CUBIC 19    000227
00135     20*          7 Z1=W*Z1                                                    CUBIC 20    000244
00137     21*            RETURN                                                     CUBIC 21    000264
00140     22*            END                                                        CUBIC 22    000313

      END OF COMPILATION:        NO  DIAGNOSTICS.
```

APPENDIX III

COMPARISON OF WAVE TRANSMISSIONS BETWEEN HORN ANTENNAS WITH DIRECT WAVEGUIDE CONNECTIONS

Measurements of the transmission characteristics of the horn antenna were made* and the results are given in the following table for the various cases:

1. Free space between antennas
2. Transmission through rocket motor with quartz window
3. Rocket motor in place but with quartz window blocked

	Without Dielectric Lens	With Dielectric Lens	Difference
Free space between antennas	- 3.7 dB	- 0.6 dB	3.1 dB
Through rocket motor with quartz window	-10.6 dB	- 1.6 dB	9.0 dB
Rocket motor in place but with quartz windows blocked	-19.0 dB	-25.5 dB	-6.5 dB

The insertion loss was compared to a direct connection of waveguide, and the measurements of horn without lenses and with lenses were made.

---

* H. S. Hwang, C. H. Durney, and R. W. Grow, "Final Report on the Study of Dielectric Insert Horn Antennas", unpublished memorandum.

It is apparent that the insertion loss of the lens-fitted horn antennas was 0.6 dB without the motor in place and 1.6 dB with the motor in place with transmission through the quartz windows of the motor.

BIBLIOGRAPHY

1. F. Kurlbaum, *Physik, Z.*, Vol. 3, 1902, p. 187.

2. W. W. Coblentz, *Investigations of Infrared Spectra*, Part I, Carnegie Institute of Washington, 1905, reprinted by the Coblentz Society, 1962, p. 122.

3. H. Schmidt, *Ann. Physik*, Vol. 29, 1909, p. 971.

4. P. J. Dickerman, editor, *Optical Spectrometric Measurements of High Temperatures*, University of Chicago Press, Chicago, 1961.

5. A. G. Gaydon, *The Spectroscopy of Flames*, John Wiley and Sons, Inc., New York, 1957, Chapter VIII.

6. A. G. Gaydon and H. G. Wolfhard, *Flames, Their Structure, Radiation, and Temperature*, Chapman and Hall, London, 1953, Chapters X and XI.

7. H. C. Hottel, G. C. Williams, and W. P. Jensen, "Optical Methods of Measuring Plasma Jet Temperatures", WADD TR 60-676, Part II, Air Force Systems Command, Wright-Patterson Air Force Base, Ohio, 1961.

8. R. H. Tourin, *Spectroscopic Gas Temperature Measurement*, Elsevier Publishing Company, New York, 1966, p. 1.

9. A. S. Jones, C. C. Johnson, and R. W. Grow, *IEEE Transactions, Nuclear Science*, Vol. NS-11, January 1964, p. 277.

10. R. G. Olsen and R. W. Grow, "Investigation of the Feasibility of Measuring the Chamber Temperature of Solid Propellant Rocket Motors by Using Microwave Attenuation Measurements", Technical Report TH-2, Microwave Device and Physical Electronics Laboratory, University of Utah, Salt Lake City, Utah, June 1970.

11. R. H. Tourin, *Spectroscopic Gas Temperature Measurement*, Elsevier Publishing Company, New York, 1966, p. 103.

12. R. H. Tourin, *Spectroscopic Gas Temperature Measurement*, Elsevier Publishing Company, New York, 1966, p. 39.

13. C. C. Johnson, *Fields and Wave Electromagnetics*, McGraw-Hill Book Company, New York, 1969, p. 10.

14. C. C. Johnson, *Fields and Wave Electromagnetics*, McGraw-Hill Book Company, New York, 1969, p. 394.

15. M. A. Uman, *Introduction to Plasma Physics*, McGraw-Hill Book Company, New York, 1964, p. 42.

16. P. Molmud, "Langevin Equation and the AC Conductivity of Non-Maxwellian Plasma", *Physical Review*, Vol. 114, April 1, 1959, pp. 29-32.

17. M. A. Uman, *Introduction to Plasma Physics*, McGraw-Hill Book Company, New York, 1964, pp. 33-36.

18. H. Margenau, "Conduction and Dispersion of Ionized Gases at High Frequency", *Physical Review*, Vol. 69, May 1964, pp. 575-585.

19. I. P. Shkarofsky, T. W. Johnson, and M. P. Bachynski, *The Particle Kinetics of Plasmas*, Addison-Wesley Publishing Company, Inc., Reading, Pennsylvania, 1966, pp. 175-184.

20. H. S. W. Massey and E. H. S. Burkop, *Electronic and Ionic Impact Phenomena*, Oxford University Press, London, England, 1952, pp. 205-210.

21. S. Altschuler, "Theory of Low-Energy Electron Scattering by Polar Molecules", *Physical Review*, Vol. 107, July 1957, pp. 114-117.

22. S. Altschuler, P. Molmud, and M. Moe, "The Electromagnetics of the Rocket Exhaust", Space Technology Laboratory Report, GM TR 0165-00397, June 1958, p. 130.

23. S. Glasstone, *Textbook of Physical Chemistry*, Van Nostrand Company, New York, 1947, p. 882.

24. O. W. Richardson, *Emission of Electricity from Hot Bodies*, Longmann, Green and Company, London, England, 1921, p. 47.

25. A. S. Jones, "Microwave Diagnostics of Nonideal Plasma", Ph.D. dissertation, Department of Electrical Engineering, University of Utah, August 1963 (Confidential).

26. C. C. Johnson and C. K. Bullock, "Thermionic Emission from Hot Particles in a Plasma", *Journal of Applied Physics*, Vol. 35, October 1964.

27. F. E. C. Culick, "Acoustic Oscillations in Solid Propellant Rocket Chamber", *Astronautica Acta*, Vol. 12, 1966, p. 116.

28. For more information, see F. E. C. Culick, "Calculation of the Admittance Function for a Burning Surface", *Astronautica Acta*, Vol. 13, June 1967, p. 221.

29. T. A. Angelus, "Unstable Burning Phenomenon in Doublebase Propellants", *Progress in Astronautics and Rocketry*, Academic Press, 1960, Vol. 1, *Solid Propellant Rocket Research*, pp. 527-559.

30. H. Margenau, "Conduction and Dispersion of Ionized Gases at High Frequency", *Physical Review*, Vol. 69, May 1964, p. 123.

31. F. G. Buffman, Jr., G. L. Dehoritz, R. O. Slater, and E. W. Price, "Acoustic Attenuation Experiments on Subscale, Cold-Flow Rocket Motors", *AIAA Journal*, Vol. 5, February 1967, pp. 272-280.

32. P. S. Epstein and R. R. Carhart, "The Absorption of Sound in Suspensions and Emulsion", *Journal of the Acoustical Society of America*, Vol. 25:3, May 1953.

33. F. T. McClure, R. W. Hart, and J. F. Bird, "Acoustic Resonance in Solid Propellant Rocket Chambers", *Journal of Applied Physics*, Vol. 31, 1960, p. 5.

34. R. W. Hart and R. H. Cantrell, "Amplification and Attenuation of Sound by Burning Propellant", *AIAA Journal*, Vol. 1, 1963, p. 398.

35. B. H. Nall, "Acoustic Attenuation in a Solid Propellsnt", *AIAA Journal*, Vol. 1, January 1963, p. 76.

36. Private communication with Dr. A. D. Baer, Department of Chemical Engineering, University of Utah, Salt Lake City, Utsh; also see W. H. McAdams, *Heat Transmission*, McGraw-Hill Book Company, New York, 1954, p. 221.

37. R. B. Bird, W. E. Stewart, and E. N. Lightfoot, *Transport Phenomena*, John Wiley and Sons, Inc., New York, 1962, pp. 432-433.

38. G. J. Van Wylen and R. E. Sonntag, *Fundamentals of Classical Thermodynamics*, John Wiley and Sons, Inc., New York, 1965, p. 532.

39. H. S. Hwang and R. W. Grow, Technical Report MDL-Q26, Microwave Device and Physical Electronics Laboratory, University of Utah, Salt Lake City, Utah, September 30, 1968, p. 216.

40. H. S. Hwang and R. W. Grow, Technical Report MDL-Q30, Microwsve Oevice and Physical Electronics Laboratory, University of Utah, Salt Lake City, Utah, September 30, 1969, pp. 126-129.

41. R. L. Coates, "A Quantitative Experimental Study of the Oscillatory Combustion of Solid Rocket Propellsnts", Ph.D. disaertation, Department of Chemical Engineering, University of Utah, 1962.

42. H. S. Hwang, J. L. Hou, and R. W. Grow, Technical Report MDL-Q29, Microwave Device and Physical Electronics Laboratory, University of Utah, Salt Lake City, Utah, June 30, 1969, pp. 129-132.